SKELETAL IMPACTS OF CONTINUOUS LOW-DOSE-RATE GAMMA RADIATION EXPOSURE DURING SIMULATED MICROGRAVITY

A Dissertation

by

RIHANA BOKHARI

Submitted to the Office of Graduate and Professional Studies of
Texas A&M University
in partial fulfillment of the requirements for the degree of

DOCTOR OF PHILOSOPHY

Chair of Committee,	Susan A. Bloomfield
Committee Members,	John Ford
	Harry A. Hogan
	Michael Massett
	Nancy Turner
Head of Department,	Melinda Sheffield-Moore

August 2018

Major Subject: Kinesiology

ABSTRACT

One of the greatest unknowns in human spaceflight is the effects of low-dose-rate galactic cosmic radiation (GCR). The majority of radiation studies deliver the total radiation dose expected on a 2-3 year mission in minutes. However, timing of radiation delivery is known to be biologically relevant. Very few studies have attempted to assess an appropriate timing, or dose-rate, of GCR exposure.

We tested the effects of continuous low-dose-rate radiation (CIRR, dose rate of 6.25 mGy/day for 28 days) in combination with a slightly interrupted hindlimb unloading (iHU), simulated microgravity, and exercise treatments. CIRR alone led to few changes compared to the non-irradiated group. CIRR+iHU led to reductions in total body bone mineral density, lean mass, fat mass, cancellous bone volume and microarchitecture, and femoral neck ultimate load. Although exercise led to improvements in bone mass it was not able to mitigate losses when combined with CIRR and iHU. This indicates a differential response of bone to CIRR in combination with iHU. CIRR may not be detrimental to bone alone but further study is needed to understand the negative effects during iHU, which may not be rescuable by exercise.

In the second experiment, we sought to assess how aging may affect the response to CIRR and HU in adult and middle-aged (astronaut aged) mice. Astronaut aged animals responded differently to CIRR and HU alone compared to adult animals. CIRR+HU diminished bone parameters beyond HU alone in both ages. Finally we conclude that young, skeletally mature animals may not be a good model for middle-aged crew members.

Our results show that CIRR alone is not detrimental to bone, unlike what is normally found with acute radiation. Care on future missions should be taken to counter the combined

detrimental effect of CIRR and unloading on bone. Our findings in different ages of mice suggest that the response to the combination of unloading and CIRR is conserved regardless of age and is therefore a continued life-long concern. The effects of space relevant radiation on bone continue to be a concern for future spaceflight missions, especially exploration class missions to the moon and Mars.

ACKNOWLEDGEMENTS

I'm am very grateful for all of the wonderful people I have met at Texas A&M and the opportunities presented during my time here. I am grateful to Dr. Bloomfield for supporting me and all of my side project endeavors and for all of your guidance and support through them. Dr. Hogan, thank you for always being willing to teach me and make complicated mechanical concepts easy to understand. Dr. Ford, thank you for teaching me everything I know about radiation. Your class sparked my interest in the complex and ever-evolving field of radiation biology. Dr. Massett, your class was one of the first I took upon coming to Texas. I want to thank you for continuing to teach me to be an exercise physiologist. Dr. Turner, thank you for believing in me as a Space Life Scientist and supporting all of my side project endeavors.

Thank you to all of the Bone Biology/Bone Mechanics lab members that I have become close to throughout the years! All of you have been a great support system through the process of my PhD; I wouldn't be here without you. Especially I would like to thank Corinne Metzger for teaching me how to do lab work and always being there to help me when it is needed. I would definitely not be here without you.

I would like to thank the NSBRI Space Life Sciences program for supporting me for two years and getting me very involved in space research. It has been the most terrific fun. I would like to thank all of the wonderful people at the Physical Education and Activity Program and especially Frank Thomas, Melinda Grant and Jorge Granados. Additionally, I am grateful for funding support from NSBRI, ACSM, TACSM, CEHD and the Huffines Institute for Sports Medicine and Human Performance.

Finally, I would like to thank my wonderful family for always being there to support and love me. Thank you, Mom and Dad, for always standing by me, especially during the tough times. Thank you, Shaun and Jarid, for always keeping my life interesting! I would not be here without the support and love of my wonderful boyfriend, Connor Dolan. You will forever be my science buddy and no matter where we go next I know we will conquer it together. When 3 different people told me that I needed to meet the guy who liked space and studies bones named Connor, I knew we would be friends. When I first met you I knew that I wanted to be more than friends; thank you, Diarra Williams, for making that happen. You always bring intelligence, fun and happiness to my life and I would not be where I am without your love and support. I want to thank the two furbabies in my life, Thor and Annabelle; you bring a smile to my face and love to my heart. I want to thank my emotional support system here at Texas A&M, Erica Renfrew; you are the sweetest person made of sunshine and your presence always makes my day better. I want to thank my adventure buddies, the Gal Pals, you are always there for a good time and a break from the stress of PhD life. I want to thank Mee-a and Sean, my Taekwondo buddies, as well as the rest of the team members over my five years here for being wonderful supports. It always makes my day better if I can kick something at the end of it. I know that having you all in my life and being a part of the team kept me sane during the insanity of doing a PhD. Finally, I want to thank the rest of my lovely friends over the years I have been here; you have all played an important part in my journey!

CONTRIBUTORS AND FUNDING SOURCES

This work was supervised by a dissertation committee consisting of Dr. Susan A. Bloomfield, Dr. Harry A. Hogan, Dr. John Ford and Dr. Nancy Turner and Dr. Melinda Sheffield-Moore, Department Head of the Department of Health and Kinesiology.

Tissues utilized in Chapter 2 were generated in a small add-on experiment embedded within Dr. Bloomfield's larger NASA Space Biology funded grant (NNX13AL25G). All hypothesis, study designs and animal protocols were developed jointly by R.S. Bokhari, C. Metzger and Dr. Susan Bloomfield. All analyses were completed by R.S. Bokhari. Additional funding for these studies comes from the Texas American College of Sports Medicine, the College of Education and Human Development, and the Huffines Institutefor Sports Medicine and Human Performance in the form of student grants on which R.S. Bokhari was the PI.

Tissues utilized in Chapter 3 were generated in a second add-on experiment embedded within Dr. Bloomfield's larger NASA Space Biology funded grant (NNX13AL25G). Animals were donated courtesy of Dr. Nancy Turner's breeding colony at Texas A&M University, as funded by her NASA project. All hypotheses, study designs and animal protocols were developed jointly by R.S. Bokhari, C. Metzger and Dr. Susan Bloomfield. All analyses were completed by R.S. Bokhari. Additional funding for these studies comes from the American College of Sports Medicine Research Foundation in the form of a student grant on which R.S. Bokhari was the PI.

TABLE OF CONTENTS

LIST OF FIGURES

Page

LIST OF TABLES

1. INTRODUCTION AND LITERATURE REVIEW

1.1 Introduction

Astronauts traveling to Mars will undoubtedly be exposed to both microgravity and radiation. Microgravity effects on bone tissue have been extensively studied and though there are still questions to ask, NASA's more immediate concern is the effects of space relevant radiation. The radiation that future space travelers will encounter is difficult to study due to practical difficulties with the cost of conducting radiation exposure experiments at particle accelerator facilities at national laboratory facilities and hence experimenter's ability to deliver simulated galactic cosmic radiation (GCR) at proper dose rates. It is, therefore, imperative that a better understanding of space-relevant radiation impacts on physiology be gained through animal studies. There are no approved countermeasures for GCR, in large part because it is not possible to shield GCR and the effects of GCR on mammalian physiology are not well understood as the longest mammalian experience with it is a 12 day Apollo mission to the moon. The studies conducted for this dissertation using a continuous low-dose-rate radiation field present an opportunity to study total radiation doses at realistic dose rates for what would be experienced by humans on exploration missions beyond low Earth orbit. Although we cannot perfectly replicate GCR, it is imperative that more studies attempt to understand the effects of an appropriate dose rate incurred over prolonged periods of time on mammalian physiology.

In this dissertation the first objective was to assess the effects of spaceflight relevant dose rates of total body radiation exposure and hindlimb unloading on bone and how an exercise trained state can alter these effects. We first aimed to determine the impact of continuous radiation

exposure on oxidative status, measures of bone quantity, structural integrity and cell activity. We expected to find that continuous radiation will cause oxidative damage, diminish bone quantity, bone structural integrity and stimulate an increase in osteoclast presence while decreasing osteoblast presence. We also aimed to determine the impact of hindlimb unloading on bone quantity, structural integrity and cell activity of mice exposed to continuous radiation. We expect to find that continuous radiation along with hindlimb unloading will further diminish bone quantity, bone structural integrity and increase osteoclast presence while decreasing osteoblast presence. We also aimed to determine the impact of an exercise trained state on mitigating decrements in measures of bone quantity, bone structural integrity, bone cell activity and oxidative status during continuous radiation exposure with and without hindlimb unloading. We expected to find that exercising mice exposed to continuous radiation with and without hindlimb unloading would have less oxidative damage as well as improved bone quantity, bone structural integrity, lower osteoclast presence and increased osteoblast presence versus sedentary mice exposed to the same radiation. The second objective of this dissertation was to assess how the impact of spaceflight relevant rates of total body radiation exposure and hindlimb unloading on bone differ between adult and middle-aged mice. First we aimed to compare the impact of continuous low-dose radiation exposure on oxidative status, bone quantity, structural integrity and cell activity in aged and mature female mice. We expected to find that aging along with continuous radiation will increase oxidative damage, further diminish bone quantity and bone structural integrity, increase osteoclast presence and lower osteoblast presence in middle-aged female animals comparison to adult female animals. The last aim was to compare the impact of hindlimb unloading during continuous low-dose radiation exposure on bone quantity, structural integrity and cell activity in old and mature female mice. We expected to find that aging along with hindlimb unloading and

continuous radiation would further diminish bone quantity, bone structural integrity, increase osteoclast presence and lower osteoblast presence osteoclast in comparison to mature females.

1.2 Bone Biology Overview

Bone is an organ that plays a part in mechanical support. There are 2 basic structures, cortical and cancellous bone. Cortical bone serves the function of mechanical support but in different ways. Cancellous bone, a lattice structure made of trabecula found in bone which support load as well as redistribute stresses to the stronger cortical shell allowing the structure some ductility to resist fracture. Cortical bone, which is the primary form of bone throughout the skeleton, takes on the role of loading. Because of the structural difference in these 2 structures of bone, being that the cancellous bone has significantly more surface area, there is often a differential in response to stressors (S. A. Bloomfield, Martinez, Boudreaux, & Mantri, 2016; Burr & Allen, 2013). For example, bone exposed to disuse will experience greater losses in the cancellous bone than the cortical bone (Li et al., 2012; Shirazi-Fard et al., 2013; Zerath et al., 2000).

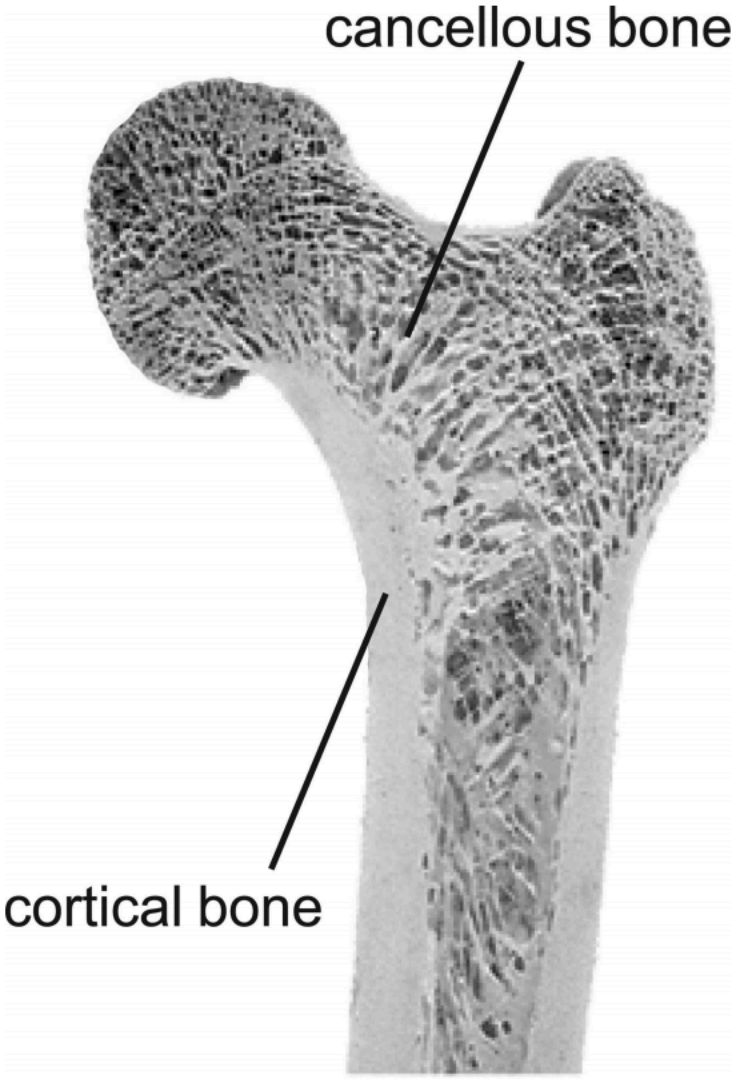

Figure 1.1 Image of cortical and cancellous regions of a long bone. (Reprinted from Willems, Langenbach, Everts, & Zentner, 2013 [Willems, N. M., Langenbach, G. E., Everts, V., & Zentner, A. (2013). The microstructural and biomechanical development of the condylar bone: a review. *European journal of orthodontics, 36*(4), 479-485.]).

Bone itself is made of 10% water, 25% organic material and 65% mineral (Burr & Allen, 2013). Although bone is 65% mineral, there are 3 kinds of cells that function on the surfaces or

within the bone (Dempster et al., 2013). The first of these cells are osteoclasts, multinucleated bone resorbing cells, containing lysosomes and tartrate-resistant acid phosphatase the main function of which is to dissolve bone. Osteoclasts are found on the surfaces of bone and it is from here that they resorb bone. Osteoclasts are multinucleated due to the fusion of mononuclear precursor cells. The multinucleated nature of osteoclasts is one of the primary ways in which these cells are identified histologically; namely, an osteoclast is a cell on the bones surface that is multinucleated and surrounded by a cytoplasm. Osteoclasts begin as monocytes and then transition into preosteoclasts. At this point macrophage colony-stimulating factor and receptor activator of the nuclear factor NFkB ligand (RANKL) stimulate preosteoclasts to commit to the osteoclast lineage and fuse. Osteoprotegerin inhibits the fusion of preosteoclsts. Osteoclasts mature and become polarized which enables them to adhere to the bone and allow them to acidify and degrade the mineral matrix of bone. Finally, after their role in bone resorption is complete, osteoclasts undergo apoptosis, a process that is not currently well understood (Burr & Allen, 2013).

The second of these cells are osteoblasts, bone forming cells, whose main function is to create new bone matrix on the surface of the bone which can later be mineralized (Dempster et al., 2013). Both bone morphogenic protiens and canonical Wnt signaling are important for osteoblastogenesis. Osteoblasts begin as mesenchymal progenetors, cells which also give rise to chondrocytes, muscle cells and adipocytes. For these mesenchymal progenetors to commit to becoming preosteoblasts Runx2 and β–catenin signals in addition to an inhibition of the Rbp-jk (Burr & Allen, 2013). Preosteoblasts then have continued signals from Runx2, β–catenin and Rbp-jk to result in an immature osteoblast which then matures into a mature osteoblast. Osteoblasts function on the surface of the bone by producing matrix and mineralizing it. It is at

this point that we can identify osteoid, in a Von Kossa stain with a tetrachrome counterstain, which is found when osteoblasts produce matrix but before it is mineralized. Once osteoblasts are mature they can either surround themselves with bone matrix and become terminally differentiated into mature osteocytes or they can undergo apoptosis and die (Burr & Allen, 2013).

The last bone cell, the osteocyte, is found embedded in the bone matrix and is responsible for signaling to osteoclasts and osteoblasts. Until recently osteocytes were thought to have very little function but now they are thought to perform endocrine signaling functions throughout the body and also respond to mechanical cues. Osteocytes are encased in lacunae and have dendritic like processes and are connected by gap junctions which allow communication between surface cells, osteoclasts and osteoblasts. Osteocytes are mechanosensing and one way in which they respond to loads is through the production of sclerostin, a Wnt signaling antagonist. Osteocytes also influence osteoclast and osteoblast cells by secreting factors such as osteoprotegerin and receptor activator of the nuclear factor NFkB ligand. Osteocytes influence bone formation by increasing Wnt signaling and influence bone resorption by increasing or decreasing osteoclasts, as well controlling osteoclast recruitment. Eventually, all osteocytes, long lived as they are, will undergo apoptosis (L. Bonewald, 2004; L. F. Bonewald, 2011; Burr & Allen, 2013).

Bone modeling is either the formation or resorption of bone during growth and development. Bone remodeling is sequential bone resorption followed by bone formation at the same location. Over time the skeleton is repaired by a replacement of bone matrix and a repair of microdamage (Burr & Allen, 2013). In this process, osteoclasts and osteoblast form a basic multicellular unit (BMU) whose function is to remodel the skeleton throughout life (Burr & Allen, 2013). Remodeling takes place in 5 stages; activation, resorption, reversal, formation and

quiescence. Activation involves the recruitment of osteoclast precursors to become osteoclasts. Resorption involves the dissolving of mineral and liberation of collagen fragments. Reversal is the succession of resorption and the start of formation. Formation is the laying down of bone matrix followed by mineralization. Finally, quiescence is the resting phase of the remodeling process.

Any imbalance in this process, coined bone turnover, can lead to bone loss or bone gain. This can be a good thing, for example, following exercise training, after which greater amounts of bone formation take place with increased mechanical loads placed on the skeleton (Hoshi, Watanabe, Chiba, & Inaba, 1998; Ju, Sone, Ohnaru, Choi, & Fukunaga, 2012). It can also be very deleterious for bone, for example, after prolonged spaceflight where the lack of gravity gives rise to more resorption than formation and great losses in bone mass (Shirazi-Fard et al., 2013; Sibonga, 2013; Zerath et al., 2000).

1.3 Spaceflight Environment and Ground-Based Simulations

The spaceflight environment presents many challenges to humans. The first is lack of gravity. It is nearly impossible to understand the mechanism of this bone loss using human subjects, since this would require invasive bone biopsies; therefore, rodent models are often used so that more invasive measures of bone may be utilized. Many inflight animal experiments have been performed throughout the history of the space program. One such study in young rodents found a 12% decrease in bone mineral density in the cancellous region of the pelvis in rats (Zerath et al., 2000). Another study found a 26% decrease in cancellous bone volume of the proximal tibia of animals which have experienced microgravity (Shane A Lloyd et al., 2015).

Unfortunately, flying animals into space is extremely expensive and can only be done for some experiments. As a result a ground based model has been designed, hindlimb unloading, where the tail of the rodents are harnessed so that the animal's hindlimbs do not touch the ground, to simulate microgravity (Ferreira, Crissey, & Brown, 2011; Globus & Morey-Holton, 2016; Li et al., 2012; Morey-Holton & Globus, 2002). Traditionally hindlimb unloading has been achieved in rats and mice by adhering a harness to the sides of the tail and, by attaching that harness to a rod or wire across the top of the cage, raising the animal's hindquarters off the ground with the body at approximately 30° off the horizontal to simulate weightlessness as well as the cephalic fluid shift effect found in space, pictured in Figure 1.2 (Globus & Morey-Holton, 2016; Morey-Holton & Globus, 2002). Another accepted method of hindlimb unloading employs a tail-ring surgically inserted between the 4^{th} and 6^{th} caudal vertebra which is then twisted so that it can hang from a hanging apparatus, pictured in Figure 1.2 (Ferreira et al., 2011). Both of these hindlimb unloading methods have been used to successfully simulate microgravity effects in the hindlimbs in countless studies.

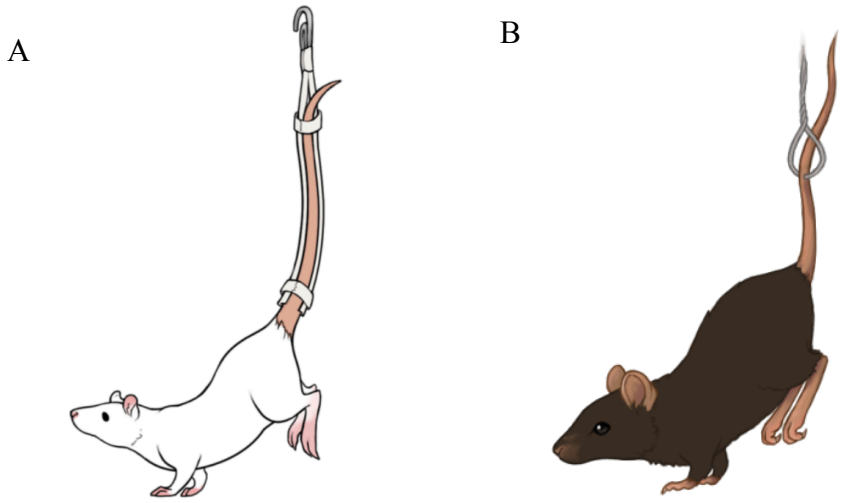

Figure 1.2 Cartoon representations of unloading. A) Cartoon representation of traditional rat hindlimb unloading consistent with the model designed by Morey-Holton *et al* (Morey-Holton & Globus, 2002). Artwork by Jennifer Kosniewski; (Kosniewski, 2017). B) Cartoon representation of tail-ring insertion hindlimb unloading method (Artwork printed with permission from Jennifer Kosniewski)

The second major challenge the space environment presents is radiation exposure. There are two kinds of radiation that astronauts may experience on long-duration missions to celestial bodies. The first kind of radiation is solar particle events (SPE) which are easily detected, giving time for crew to seek effective shielding. Although SPEs are extremely dangerous, there are approved and acceptable shielding and drug countermeasures for this kind of radiation. The second kind of radiation exposure is galactic cosmic radiation (GCR), comprised of a spectrum of radiation species; 98% nuclei comprised of 87% hydrogen ions, 12% helium ions, and 1% heavy nuclei, and 2% electrons and positrons (Simpson, 1983). GCR, though very high in energy, is extremely low dose and constant; therefore, astronauts will be exposed to a continuous

low dose of radiation spread over a period of nearly 3 years for missions to Mars (Hassler et al., 2014; McGirl et al., 2015). Future missions will expand outside of the safety of the Van Allen belts, magnetic fields protecting the Earth from GCR, making radiation a greater concern for extra-planetary missions than long-duration missions to the International Space Station.

Due to the difficulty, expense and dangers of experimentation outside of low Earth orbit, experiments investigating GCR relevant radiation and influence on bone must be done using ground based analogs. There are several ways to study radiation effects on the ground that can simulate parts of the GCR spectrum. Gamma radiation can be delivered in low or high doses at radiation producing facilities around the world. Many previous studies that have examined the effects of gamma radiation in animals (Joshua S Alwood et al., 2012; Joshua S Alwood et al., 2015; Hamilton et al., 2006; Kondo et al., 2010; Sams, 1966; Willey, Lloyd, Nelson, & Bateman, 2011; Willey et al., 2008; Xu et al., 2014). In humans, specifically after the use of the atomic bombs in Japan, there is adequate knowledge of the effects of gamma radiation on humans; however, most of these studies have examined overall health of victims and cancer risk (Brenner et al., 2003; Brenner, Elliston, Hall, & Berdon, 2001; Einstein, Henzlova, & Rajagopalan, 2007; Hayashi et al., 2005; Pierce & Preston, 2000). Gamma radiation represents only a small part of the GCR spectrum. The most dangerous part of the GCR spectrum is heavy ion radiation, ions heavier than Helium. Although these represent the smallest portion of the spectrum they are very damaging. Heavy ion radiation of high energies can be produced on Earth only at particle accelerator facilities such as the NASA Space Radiation Laboratory at Brookhaven National Laboratory. Particle accelerator facilities provide an excellent opportunity to study the effects of appropriate energies and ions of radiation; however, they can only deliver radiation in the form of a beam (which includes many particles) delivered in minutes. These facilities are not capable

of delivering even close to the appropriate dose-rate at a manageable cost to the researcher. Although we can simulate parts of the GCR in separate experiments the field still has not found a way to simulate GCR fully in the way it exists naturally.

1.4 Bone Alterations with Chronic Disuse/Microgravity Exposure

Without mechanical stimulation and resistance to Earth's 1G force, bone mineral density of astronauts decrease 2-9% across many bone sites, particularly weight-bearing bones (Sibonga et al., 2007). This poses significant risk to astronauts traveling to low Earth orbit and beyond. One effective countermeasure to this has been exercise and proper nutrition. If exercise and proper nutrition are maintained during future interplanetary travel, humans may sufficiently reduce their risk of fracture when returned to any amount of gravity. Unfortunately, exercise demands a large portion of crew time during the day which has led NASA to seek other methods for bone maintenance during spaceflight. This has been largely unsuccessful because no treatment can match the benefit of exercise. Future missions will not have the space allotment that the International Space Station has for exercise equipment; therefore, it may be difficult to maintain exercise at the quantity and quality required to maintain bone mass, which keeps the topic of microgravity effects on bone on the list of astronaut health concerns.

Bone geometry and architecture will adapt to loads regularly imposed on the skeleton. For example, if an individual engages in weight-bearing resistance exercise their bones will adapt to support the increases in muscle mass and to resist the heavy loads being imposed on the body. With disuse, a lack of mechanical loading, bone mass is lost and cancellous microarchitecture is compromised. In space, weightlessness negates the need to walk,

diminishing mechanical loading on legs and spine greatly. A greater than 10% decrease, in some cases, in bone mineral density, was found in the lumbar spine, femoral neck and trochanter of astronauts exposed to long duration space flight (Sibonga, 2013). This bone loss can be simulated with high fidelity in rodent models exposed to hindlimb unloading (HU), especially when using skeletally mature animals (Globus & Morey-Holton, 2016; Li et al., 2012; Morey-Holton & Globus, 2002). Twenty-eight days of hindlimb unloading leads to a 31% decrease in cancellous bone volume and decrements in microarchitecture as well as in cortical bone volume parameters. Mechanical testing of bones, done to determine the force required for fracture, that have undergone hindlimb unloading reveals a 36% decrease in ultimate stress (Shirazi-Fard et al., 2013). In hindlimb unloaded animals there was a 21% reduction in cancellous bone mineral density and change in the architecture of the lattice structure following hindlimb unloading (Li et al., 2012).

Studies also have demonstrated increases in tartrate-resistant acid phosphatase (TRAP) and cathepsin K, both expressed largely by osteoclasts with hindlimb unloading. This suggests a mechanism for the loss in bone mass in that osteoclast activity and presence are increased with HU (Saxena, Pan, Dohm, & McDonald, 2011). Sclerostin, a Wnt signaling antagonist expressed by osteocytes, is increased in disuse suggesting that mechanical loading is inhibiting the Wnt pathway, a key bone formation signaling pathway (Spatz et al., 2015). It is accepted, due in part to the above literature, that disuse results in the increase in osteoclast activity and decrease in osteoblasts leading to bone loss.

1.5 Radiation Effects on Bone Structure and Bone Cell Activity

In animal models, bone loss following acute, high dose radiation exposure is largely specific to the cancellous bone (the lattice structure within the cortical bone) (Shane AJ Lloyd et al., 2008). When imaged using micro-computed tomography, the amount of cancellous bone volume (%BV/TV) was decreased in mice exposed to gamma, iron carbon or proton radiation (J. Alwood et al., 2010; Eric Ryan Bandstra, 2008; Green, Adler, Chan, & Rubin, 2012; Wright et al., 2015). Previous studies assessing the effects of radiation on bone have found decrements ranging from 14-41% compared to control in bone volume and structural quality following exposure to various doses and ions of radiation (J. Alwood et al., 2010; Joshua S Alwood et al., 2012; Eric R Bandstra et al., 2009; Boyle, Simonet, & Lacey, 2003; Green et al., 2012; Havaki et al., 2015; Shane A Lloyd et al., 2012). Bone loss in the cancellous compartment is of concern because it is essential to the mechanical integrity of long bone metaphyses and vertebral bodies and losses in this bone compartment results in bone fragility that can lead to fracture (Joshua S Alwood et al., 2012; Baxter, Habermann, Tepper, Durham, & Virnig, 2005; Mitchell & Logan, 1998; Siegel et al., 2012; Willey et al., 2011; Wright et al., 2015). The observed changes in bone volume and mass with radiation also lead to structural deficits in the tissue as a whole (J. Alwood et al., 2010; Joshua Stewart Alwood, 2009). One such study which found a 14% decrease in cancellous bone volume also found a 24% decrease in yield force at the vertebral body, a mixed bone site, with hindlimb unloading (J. Alwood et al., 2010). These hindlimb unloading driven structural changes increase the risk of fracture due to disuse induced bone loss.

The change in bone mass from radiation exposure is a result of altered responses of bone cells (osteoclasts, osteoblasts and osteocytes) (Joshua S Alwood et al., 2015; Boyle et al., 2003; Shane AJ Lloyd et al., 2008; Willey et al., 2008). Cancellous bone loss is increased in response to radiation in part by increasing osteoclast activity (Kondo et al., 2010). Osteoclast surface was increased by 46% in mice exposed to 1-2 Gy of gamma radiation (Kondo et al., 2010). Alwood *et al*. found 2 Gy of iron radiation leads to increases in the expression of key genes involved in osteoclast function in tibial bone tissue. Gene expression of osteoprogenerin (OPG) and receptor activator of nuclear factor kappa-β ligand (RANKL), proteins stimulating osteoclastogenesis, were upregulated (Joshua S Alwood et al., 2015). Studies utilizing a variety of species and doses of radiation document increases in osteoclastogenesis and osteoclast activity (Wright et al., 2015). The increased activity of osteoclasts will ultimately lead to more bone resorption and, therefore, bone loss.

Bone resorption and formation normally function in concert to maintain healthy bone tissue (Robling, Castillo, & Turner, 2006). Imbalance between osteoclast activity and osteoblast activity can lead to bone loss. Wright *et al*. found a decreased bone formation rate due to acute radiation exposure (Wright et al., 2015). To understand this reduction they studied irradiated osteoblast-like MC3T3 cells in vitro and measured for Annexin V, a marker of cellular apoptosis; it was found that Annexin V levels in MC3T3 cells were increased 24 hours after 10 Gy of exposure (Wright et al., 2015). In other studies mineralizing surface was lower in irradiated animals (Kondo et al., 2010; Macias et al., 2016). Therefore, acute high doses of radiation may increase osteoblast cell death decreasing osteoblast numbers. Bone loss may also be influenced by the action of osteocytes, mature bone cells embedded in the bone matrix which

had long been thought to be inactive cells contributing only structurally to bone. Only recently have osteocytes been shown to be mechanosensitive and responsible for much cell signaling in response to stressors in the bone (L. F. Bonewald, 2011; Burger & Klein-Nulend, 1998; Robling, Burr, & Turner, 2001; Robling et al., 2006; Robling & Turner, 2002). It has been known since the 1950s that in vivo osteocyte death is found following radiation (Vaughan, 1956). Wright *et al*. found an increase in DNA fragmentation, an early marker of apoptosis, in osteocytes of the irradiated limb (Wright et al., 2015). This group also showed an increase in Annexin V in osteocyte-like MLO-Y4 cells in vitro 24 hours following 4 Gy of radiation exposure, a large amount in terms of space radiation (Wright et al., 2015). Osteocyte apoptosis is a potent signal to increase osteoclast activity, leading to increased bone loss (Manolagas & Parfitt, 2013). Osteocytes are mechanosensing cells and responsible for much signaling within bone tissue to osteoclasts and osteoblasts. Therefore, impaired osteocyte function or cell death following radiation exposure might lead to exacerbated bone loss with microgravity exposure, further increasing risk of fracture. (L. F. Bonewald, 2011; Rabelo, Beletti, & Dechichi, 2010).

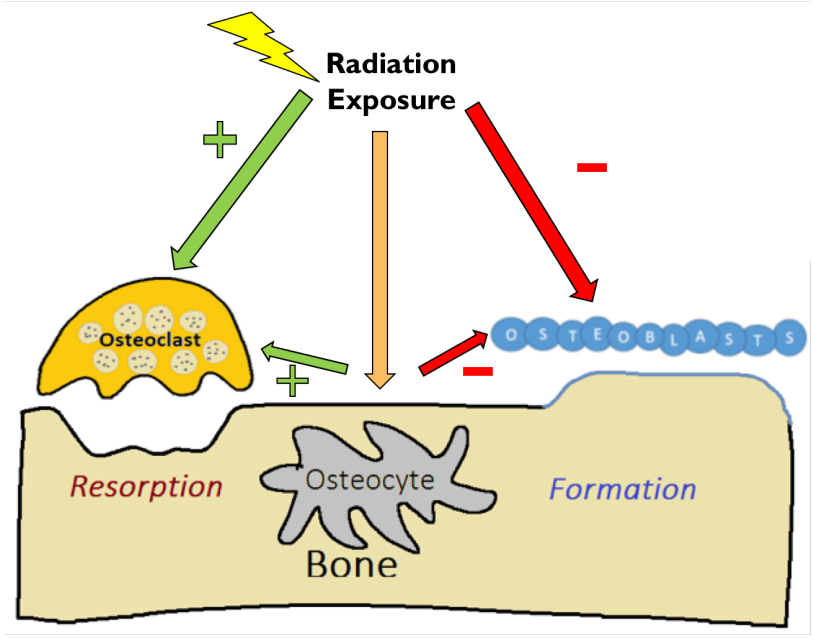

Figure 1.3 Bone cellular response to radiation exposure. Osteoclast activity is increased by radiation exposure. There are osteocyte changes with radiation exposure leading to an increase in osteoclasts and a decrease in osteoblasts. Osteoblast activity can increase slightly after radiation exposure, but the preponderance of published data indicates a negative impact on osteoblasts resulting in less bone formation. (Artwork adapted with permission from Corinne Metzger)

The above evidence supports the conclusion that radiation increases osteocyte apoptosis, increases osteoclasts and decreases osteoblasts. The cause of these changes is currently unknown, though there are three widely accepted possible mechanisms: reactive oxygen species, an inflammatory response, changes in hematopoietic tissue. Reactive oxygen species, normal biproducts of cellular metabolism, and free radicals can be produced by radiation through its interaction with water and cellular materials as it passes through organic tissue. When radiation deposits energy generating ROS if it passes through DNA this could lead to damage, resulting in cell apoptosis or mutation (Cooke, Evans, Dizdaroglu, & Lunec, 2003; Gomes, Silva, & Oliveira, 2012; Havaki et al., 2015). An increase in ROS is implicated as a factor that damages non-

irradiated tissues in response to radiation exposure (De Lisio et al., 2011). Although this has not yet been shown in bone, previous data from our laboratory and others documents oxidative damage, presumably from ROS, in bone as a result of radiation exposure, which may provide a mechanistic explanation for radiation-induced bone loss and lead to effective interventions (Yuen, 2012). Radiation is known to lead to an increase in inflammatory response. Radiation has been shown to increase TNF-α, which has been shown by our lab to decrease osteoblasts, increase osteoclasts, RANKL, OPG, sclerostin and osteocyte apoptosis, which further increases bone resorption and decreases bone formation (Hallahan, Spriggs, Beckett, Kufe, & Weichselbaum, 1989; Metzger, Narayanan, Zawieja, & Bloomfield, 2017). Therefore, a possible mechanism of radiation effects in bone could be driven by changes in inflammation. Finally, hematopoietic tissue is known to be highly affected by even low radiation doses (Hall & Giaccia, 1994). A dose of only 2 Gy is enough to severely damage the hematopoietic tissue, which is normally a source of illness in irradiated humans. Although hematopoietic tissue is one of the most sensitive to radiation induced damage, it is able to recover and therefore damage to it is generally not life threatening, though it could be physically damaging in other ways. Bone marrow contains precursors for osteoclasts and osteoblasts, among many other cell types; therefore, if hematopoietic tissue is depleted due to radiation it is possible that this contributes to changes in surface bone cells. Although there is no consensus on the mechanism of radiation effects in bone, it is likely that all of these mechanisms are working in concert or at different times during the bone response to radiation.

1.6 Achieving Low-Dose-Rate Radiation Exposures

Astronauts outside the Earth's magnetosphere will be constantly exposed to low doses of high-energy particles, key components of galactic cosmic radiation (GCR). Since GCR is impossible to shield against, understanding the effects on mammalian biology is of the utmost importance prior to extensive space travel outside of low-Earth-orbit. Low-dose-rate radiation is nearly impossible to study on Earth in the exact way it manifests in outer space. One way to study the effects of low-dose rate radiation is to expose animals continuously over an extended period of time (days to weeks). It is only possible to do this with the lower linear energy transfer (LET) radiation, hydrogen and helium ions, comprising 98% of the GCR spectrum or with gamma, which is used as the reference radiation for translating effects to human relevance (Hassler et al., 2014; McGirl et al., 2015). The best way to simulate the appropriate energy and ions, especially those with heavy nuclei, found after radiation has passed through shielding material is to use a particle accelerator facility. Unfortunately, it is impossible for these facilities to provide a realistic dose rate of radiation seen in outer space. The amount of power from the energy grids and time required at these facilities to produce a relevant dose rate would be extremely expensive if a study wanted to simulate GCR for even one day, let alone the months it would take to get a true biological understanding. However, it is not likely that these facilities could even provide a dose rate as low as what is expected on the cruise to Mars, ~0.48 mGy/day, or on the surface of the planet, 0.21 mGy/day (Hassler et al., 2014). It may be possible to build a facility that could deliver this kind of radiation but that has yet to be published.

The relevance of the use of lower LET radiation to understand GCR effects is important since radiation of a significantly lower LET comprises 98% of the GCR spectrum compared to

heavy ion radiation, comprising 1% of the spectrum (Simpson, 1983). All of these functional difficulties make the use of continuous low dose rate radiation an attractive solution for the problem of understanding biological effects of GCR spectrum relevant radiation. Even the use of gamma radiation, though not a large component of the GCR spectrum in outer space, is important to study because its function is extremely similar to what could be seen when GCR spectrum particles interact with shielding, human organic materials as they pass through and, as particle radiation, represents half of the radiation expected from heavier ions (Hall & Giaccia, 1994; Simpson, 1983).

While the energies and radiation ions of previous studies assessing the effects of radiation exposures are relevant to GCR, the dose rate is not. Fractionated radiotherapy has proven that the timing of radiation delivery is biologically relevant; therefore, it would suggest that GCR would not necessarily have the same effect as acute radiation exposures (Hall & Giaccia, 1994). In cell culture and in vivo assays, it has been demonstrated that potentially lethal radiation delivered in fractionated doses allows for DNA damage repair, further increasing the surviving fraction of cells (Hall & Giaccia, 1994). Continuous low-dose-rate radiation is considered to be "an infinite number of infinitely small doses;" therefore, functionally we should expect results more similar to the tissue sparing seen in fractionated radiotherapy (Hall & Giaccia, 1994; Thames et al., 1986). This is because both allow for one very important thing: cellular repair of damaged DNA and/or other protein structures in the cell. One acute dose will damage many cells but a fractionated dose, even if it targets the same amount of cells, will not kill as many since some of those cells will successfully repair themselves. This cellular repair is the reason that radiotherapy patients can receive 60 Gy of total exposure in multiple fractionated doses and not die when the an 8 Gy single acute dose can kill a human (Hall & Giaccia, 1994; Meirow & Nugent, 2001).

Most radiation studies use acutely delivered radiation doses for ease, simplicity and a desire to assess high energy heavy ion radiation. However, given the fact that tissue begins repair immediately after radiation exposure, delivering the full dose expected of a 3-year Mars mission at one time would not be representative of the reality of GCR radiation.

Previously, several studies assessed chronic low-dose-rate radiation at 1.2 mGy/hour and saw an increase in total body weight, life span, CD4+T cells, CD8 molecule expression and a decrease in CD40+B cells in rodents (Braga-Tanaka et al., 2018; Ina & Sakai, 2005; Ina, Tanooka, Yamada, & Sakai, 2005; Sakai, Nomura, & Ina, 2006). In one study, 7 wk old animals were irradiated for 5 wks and then allowed to live out the remainder of their life without radiation. At 120 wks there were no control mice alive but 33 irradiated mice; leading to the conclusion that radiation improved lifespan. In this study the irradiated animals had a larger percentage of CD8+ cells and a lower percentage of CD40+B cells than control animals (Sakai et al., 2006). In another study animals began radiation at 5 wks old and were irradiated for the remainder of their lifetime leading to an increase in populations of CD4+T cells and CD40+B cells for the first 21 days, during which animals were exposed to radiation, and remained elevated for the remainder of the study (Ina et al., 2005). In another study lifespan was found to be increased in that the 50% survival of non-irradiated animals was 134 days and that of irradiated animals was 502 days (Ina & Sakai, 2005). A review of projects coming out of Japan, where they have chronic irradiation facilities, using chronic dose rates of 0.05, 1 and 20 mGy/day for 400 days resulting in a total of 20, 400 and 8,000 mGy of gamma radiation respectively, revealed that there were changes in all biological endpoints that they studied (Braga-Tanaka et al., 2018). Life span assessment in animals irradiated for 400 days, starting at 8 wks of age, revealed a reduction in life span in males and females exposed to 20 mGy/day and in

females exposed to 1 mGy/day. At 0.05 mGy/day there was no effect on lifespan in either sex (Braga-Tanaka et al., 2018; S. Tanaka et al., 2003). In this experiment they assessed the incidence of neoplasms in these mice at the ends of their lives. Neoplasms were found in over 90% of animals with no differences between irradiated and non-irradiated mice (Braga-Tanaka et al., 2018; Tanaka III et al., 2007; S. Tanaka et al., 2003). In that same lifespan study bodyweight was increased with chronic radiation exposure (Tanaka III et al., 2007). They also found an increase in chromosomal aberrations with total doses of 400 and 8,000 mGy (K. Tanaka et al., 2009). In another of these studies there was no detection of mutation induction in mice exposed to a total of 400 or 20 mGy (Ono et al., 2009). This group also found that mRNA were altered in liver, kidney and testes of male mice exposed to chronic low dose-rate radiation exposure after 400 days of exposure to 20 mGy/day, 1 mGy/day and 0.05 mGy/day (Taki et al., 2009; Uehara et al., 2010). In the liver they found, based on mRNA changes, that there could be altered functions of non-esterified fatty acid levels, body mass obesity and endoplasmic reticulum stress response (Uehara et al., 2010). In the kidneys they found that mitochondrial oxidative phosphorylation was increased in 20 mGy/day and 1 mGy/day. In the testes there was a suppression of DNA metabolism, response to DNA damage and DNA replication in a dose dependent manner (Taki et al., 2009). Liver protein levels after long term chronic radiation exposure were assessed and it was found that rhodanese, located in the mitochondria and involved in sulfur metabolism and detoxification of cyanide, levels were elevated after 1 and 20 mGy/day but not 0.05 mGy/day exposures while levels of antioxidant enzymes remained unchanged (Nakajima, 2008). Four apoptosis-related proteins were elevated even 3 months after 400 days of exposure to chronic low dose rate radiation exposure, three of which were not elevated at the end of exposure, suggesting either long lasting or delayed effects of apoptosis (Nakajima et al., 2017). These

studies present a change in biological response to continuous low-dose-rate radiation exposure that is very different from acute radiation exposure.

Although these studies did not assess bone-specific measures, they attest to the fact that even low doses of radiation can lead to physiological changes. Previously, Yu *et al* assessed bone loss in 14 wk old mice following continuous low-dose-rate radiation exposure from a ^{137}Cs gamma-ray irradiator over 28 days to reach a cumulative dose of 1.7Gy and found no effects of radiation in the either the cortical or cancellous bone of the femur and the cancellous bone of the tibia (Yu et al., 2017). This dose is still much greater than the expected dose on a Mars mission; therefore, further study is needed to understand the effects of low-dose-rate radiation.

1.7 Exercise: Potential Role in Mitigating Space Radiation Impact on Bone

Extreme musculoskeletal losses during spaceflight have been recorded in humans and rodents (Sibonga, 2013; Sibonga et al., 2007). On the International Space Station, the exercise regimens that have been found to be the best method for reducing musculoskeletal losses combine aerobic and resistance exercise (LeBlanc et al., 2000; S. M. Smith et al., 2012). Astronauts routinely exercise up to 1.5 hours per day to reduce the loss of bone, muscle and cardiovascular function. The importance of exercise during spaceflight is paramount. The clear benefits to the musculoskeletal system are undeniable; however, it is important to consider whether or not exercise can play a role in modulating other spaceflight risks, such as radiation.

Aerobic exercise requires an increase in oxygen uptake in the lungs and contracting muscle, producing reactive oxygen species (ROS) and perhaps causing acute oxidative stress (Siegel et al., 2012). Exercise increases key antioxidant enzymes in muscle which can help

sequester reactive oxygen species (ROS). Manganese superoxide dismutase (MnSOD), upregulated by exercise, may provide a mechanism for the exercise reduction of oxidative stress (R. Allen & Tresini, 2000; Ji, 2002). MnSOD is upregulated due to NF-κB signaling (R. Allen & Tresini, 2000; Flohé, Brigelius-Flohé, Saliou, Traber, & Packer, 1997). In rats NF-κB signaling was found to be increased 2 hours following acute exercise and remained elevated for 48 hours. MnSOD mRNA was found to be increased in type 2a muscle from exercised rats and MnSOD protein levels were observed in type 2b muscle after 48 hours. This study indicates that even a small acute bout of exercise may provide sufficient oxidative stress to activate MnSOD and NF-κB signaling (Hollander et al., 2001).

Increases in ROS are likely to be a candidate for damage to non-irradiated tissues in response to radiation (De Lisio et al., 2011). Though radiation can damage DNA and other cellular structures by depositing energy into an organism and generating ROS (Figure 1.4), the formation of ROS is a normal phenomenon in the body due to oxidative metabolism (Cooke et al., 2003; Gomes et al., 2012; Havaki et al., 2015). It is therefore important to consider that there are natural mechanisms within the body to sequester ROS, primarily via antioxidant enzymes (Havaki et al., 2015). Many antioxidants have tested as radio-mitigants; however, these often have side effects or are not effective over the long term (Kondo et al., 2010). Endurance exercise may mitigate damage due to radiation exposure safely and with minimal side effects. ROS formed during exercise activate antioxidant defenses to protect against oxidative stress (De Lisio et al., 2011). One study found that antioxidant defenses, in superoxide dismutase and MnSOD, were increased by 41% and 51%, respectively, in exercising mice exposed to 1Gy of γ radiation compared to non-exercised animals. Additionally, treadmill exercise, up to 18m/min for 45 min,

enhances the response of superoxide dismutase and manganese super oxide dismutase, key antioxidant enzymes, to radiation (De Lisio et al., 2011).

Exercise has very few negative side effects and has a potent anabolic effect on muscle, cardiovascular and bone tissues. One potential deterrence to the use of exercise during cancer treatments is the level of fatigue patients experience. Clinical studies, however, show that judicious use of exercise in radiotherapy populations actually reduces fatigue (Courneya & Friedenreich, 1999; Segal et al., 2009). Further, clinical studies have shown that moderate exercise improves well-being in radiotherapy patients and reduces the recurrence of cancer; however, there is no mechanistic understanding of why this happens (Mock et al., 1997). While these are promising results, they do not provide any understanding of the changes on a tissue or cellular level, nor do they reveal a mechanism for the impact of exercise on irradiated tissue.

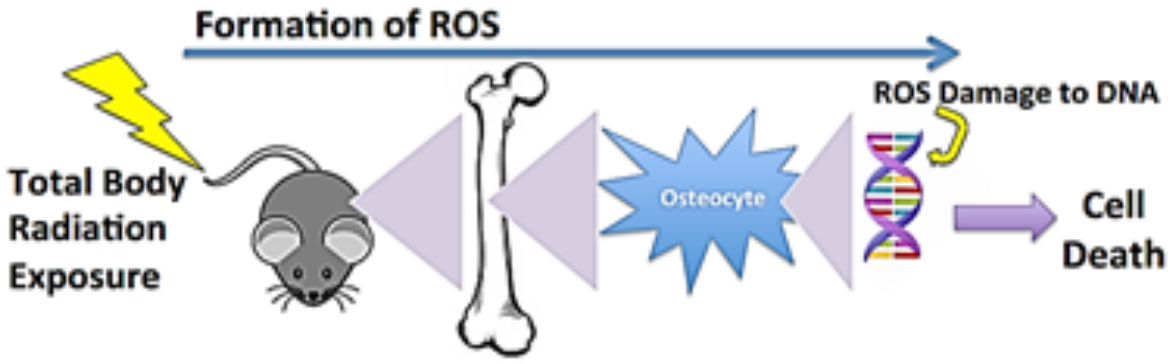

Figure 1.4 ROS activity in the bone. Total body radiation in a mouse can stimulate formation of ROS, causing DNA damage leading to cell death and dysfunction.

In addition to antioxidant properties which have the potential to combat radiation-induced damage, the increased mechanical loading imposed by exercise improves parameters of bone quality and quantity (Hoshi et al., 1998; Ju et al., 2012). In animals previously exposed to a disuse protocol, bone volume was found to recover due to increases in trabecular thickness as a result of a resistance exercise protocol (Ju et al., 2012). Mid-femur ultimate force, ultimate stress and elasticity in three point bending increase with treadmill exercise (Hoshi et al., 1998). Exercise has also been shown to improve bone quantity and quality during disuse in humans and rodents with spaceflight and ground-based analogs (Boudreaux et al., 2014; Cavanagh, Licata, & Rice, 2007; Shirazi-Fard, Alwood, Schreurs, Castillo, & Globus, 2015; Shirazi-Fard et al., 2013; Shirazi-Fard et al., 2014). Shirazi-Fard *et al* found that jump training exercise during recovery following disuse resulted in 10% greater in BMC and 6.6% greater vBMD compared to animals with no exercise in recovery (Shirazi-Fard et al., 2014). External mechanical loading of the tibia performed 5 months after exposure to 0.5 Gy of ^{56}Fe exerts anabolic effects mitigating bone volume losses due to radiation exposure (Shirazi-Fard et al., 2015). Although this mechanical loading is not physiological, as animals were anesthetized during load application and no voluntary muscle contraction was involved, it suggests that osteoblasts' ability to respond to increased mechanical loading is preserved and/or recovered by 5 months after radiation exposure. With the benefits of exercise in disuse being well established, it is important to understand the impact of this effective countermeasure on continuous low-dose-rate radiation, especially with concurrent hindlimb unloading. Unknown is whether radiation impacts on the typical bone formation response to exercise when measured sooner after the exposure.

1.8 Impact of Aging

Most animal studies are conducted on young, growing animals (less than 16 weeks old, for mice). One exception is bone-related studies which typically utilize skeletally mature animals; in mice this is 16 wks of age or greater, so that animals are no longer in the rapid growth stage (Brodt, Ellis, & Silva, 1999; Treuting et al., 2016). The average age of astronauts when they travel to space is ~45 years, which is approximately half of the average lifespan of humans. Many scientific conclusions about spaceflight are drawn using animals that are significantly younger than half of their approximate life span. This indicates that studies of older animals are required to understand the effects of spaceflight on appropriately aged animals. There have been several studies comparing responses to hindlimb unloading (HU) in mature, 6-month-old rats, and aged 30-32 month old rats (Brown & Taylor, 2005; Perrien et al., 2007; Siu, Pistilli, & Alway, 2005). In males, muscle mass losses were 30% greater and muscle force losses were 24-36% greater in old HU animals than adult HU animals (Brown & Taylor, 2005). In males, pro-apoptotic signaling in skeletal muscle mass normalized to body weight was 48% lower in aged animals compared to adult animals (Siu et al., 2005). Cancellous bone volume and microarchitecture in the proximal tibia were diminished by HU only in mature rats but not in old ones. They also found that HU decreased cortical bone mineral density and increased cortical porosity in old rats only (Perrien et al., 2007). These studies were done in males, or an unspecified sex, and, to our knowledge, there are no studies comparing the responses of adult and aged female rodents to HU.

2. IMPACT OF ENDURANCE EXERCISE ON BONE RESPONSE TO CONTINUOUS LOW-DOSE RATE RADIATION DURING HINDLIMB UNLOADING

2.1 Introduction

Bone is sensitive to spaceflight-induced losses in mass and structural integrity. Low bone quality in astronauts upon returning to Earth has been an area of concern for NASA due to an increased risk of fracture on Earth (Sibonga, 2013). While NASA has developed exercise methods for diminishing bone loss during 6 month missions in low Earth orbit, it remains an even more pressing concern for future spaceflight missions due to the fact that future Mars missions will spend a longer time in reduced gravity, be exposed to more radiation, and may not have space to bring exercise equipment. The dangers of low bone mineral density on a Mars mission would likely be greater upon landing where astronauts may fall and sustain injuries to their microgravity weakened bones without the help of the landing crews available on Earth (Sibonga, 2013). Due to the minimal medical capabilities of future extra-planetary missions, a broken bone could pose more serious health risks to the health of the astronaut than if it occurred on Earth; for instance sepsis following a non-union fracture (Alexander, 2016).

Of further concern to NASA are the additional effects of radiation that could worsen the deleterious effects of reduced/zero gravity on the skeletal system. The Earth's Van Allen belts, which create a magnetic field, protect Earth and space station bound humans from the majority of the space radiation, Galactic Cosmic Radiation (GCR). GCR is ionizing radiation from a mixture of species including gamma rays, neutrons, alpha particles, protons and ions as heavy as iron. GCR, though very high in energy, is extremely low dose and constant; therefore, astronauts

will be exposed to a constant low dose of radiation spread over a period of nearly 3 years (Hassler et al., 2014; McGirl et al., 2015). Future missions will expand outside of the safety of the Van Allen belts making radiation an even greater concern for extra-planetary missions. Experiments investigating GCR relevant radiation influence on bone must be done using ground based analogs because it is difficult, dangerous and expensive to conduct experiments outside of low Earth orbit. Therefore, it is imperative to elucidate radiation impacts on physiology through animal studies. To date, many studies involving radiation exposure in animals have consisted of an acute exposure equaling a dose of various radiation ions greater than 1 Gray (Gy). NASA has estimated that astronauts on a Mars mission will be exposed to a dose rate of 0.48 mGy/day on the travel to and from Mars as well as 0.21 mGy/day on the surface of Mars, for an approximate total dose of, 1.01 Sv of radiation from a variety of species over a period of 180 days of cruise time each way and 500 days on the surface of Mars (Hassler et al., 2014; McGirl et al., 2015). In this study we have tested the effects on bone of a radiation field, which provides a continuous low-dose-rate of radiation. To better simulate the spaceflight environment we hindlimb unloaded (HU) animals during the radiation exposure. Previous studies have found complex results on the combined effects of HU and radiation (Shane A Lloyd et al., 2012; Macias et al., 2016; Xu et al., 2014; Yu et al., 2017; Yumoto et al., 2010); however, the majority of these studies suggest that radiation will cause negative effects and that these will be exacerbated by HU. We, therefore, hypothesized that continuous low-dose-rate radiation would result in a decrease parameters of bone quality and quantity and that these will have a combined effect with hindlimb unloading.

One effective countermeasure to microgravity induced bone loss is exercise (Boudreaux et al., 2014; Cavanagh et al., 2007; Shirazi-Fard et al., 2015; Shirazi-Fard et al., 2014). In animals previously exposed to a disuse protocol, bone volume was found to recover due to

increases in trabecular thickness from resistance exercise protocol (Eric R Bandstra et al., 2009). The effects of exercise during continuous low-dose-rate radiation and hindlimb unloading is unknown; we hypothesized that exercise would sufficiently mitigate the decrements in bone in hindlimb unloaded animals exposed to continuous-low-dose-rate radiation.

2.2 Materials & Methods

Experimental design and animals

Female C57bl6/J mice, 17 weeks old at the start of the study, began acclimating to an AIN93-G, a standard chow, diet. Mice were group housed for 2.5 weeks during diet acclimation. Figure 2.1 contains a timeline for your reference. One and a half weeks prior to hindlimb unloading (HU) animals underwent a minor tail ring insertion surgery and were thereafter singly housed for the remaining duration of the experiment. The week following the start of the diet, animals began acclimation to the treadmill by walking along it. Treadmill exercise began at a walking speed and slowly ramped up, over a 1.5 week period, to 51 minutes of running at 12.5 m/min on a 10° incline for a 7 weeks of training. Following 4 weeks of diet acclimation, which overlapped with 3 weeks of exercise training, animals began HU and/or radiation exposure for 4 weeks. Animals in HU were housed within sight of another animal but without the ability to touch, therefore we consider them single housed. Eight groups were examined; sedentary sham (SED+WB+SHAM, n=10), sedentary continuous irradiation (SED+WB+CIRR, n=10), sedentary hindlimb unloaded sham (SED+iHU+SHAM, n=10), sedentary hindlimb unloaded continuous irradiation (SED+iHU+CIRR, n=10), exercise sham (EX+WB+SHAM, n=10), exercise

continuous irradiation (EX+WB+CIRR, n=10), exercise hindlimb unloaded sham (EX+iHU+SHAM, n=10), and exercise hindlimb unloaded continuous irradiation (EX+iHU+CIRR, n=10). We are designating our HU treatment as "iHU", since HU was interrupted for 75 minutes each day of weightbearing, as described below. Sham exposed animals were housed in a room that did not have any radiation dose above background radiation, measured by a dosimeter. Dual x-ray absorptomitry scans were performed 2 days prior to termination and calcein injections were given 2 and 6 days prior to termination. Animals were anesthetized using isoflurane gas and euthanized by both cervical dislocation and thoracotomy. All procedures used in this study were approved by the Institutional Animal Care and Use Committee at Texas A&M University (#2016-0293).

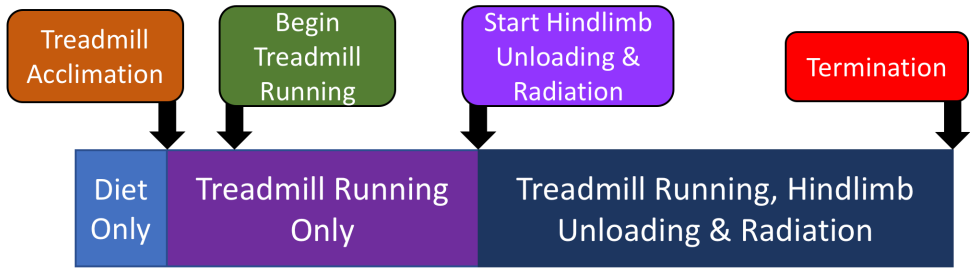

Figure 2.1 Timeline of exercise and hindlimb unloading.

Continuous radiation exposure

A radiation field was created using gamma radiation, because it is the reference radiation. Additionally, as energetic particles, gamma radiation is representative of half of the dose from

heavier ions, which is the result of energetic particles. The orientation of activated Co^{60} wires and design of the radiation field, including the placement of radiation sources and shielding material to contain radiation, was achieved using Monte Carlo simulations conducted earlier (Saucier, 2016). These simulations provided sufficient information to determine the original irradiation dose delivered to the cobalt wires at the Texas A&M Nuclear Science Center, which determined how much radiation they would emit once activated. Animals were housed in a decomissioned x-ray room in our animal facility equipped with lead-shielded walls; animal cages were placed on a 4- tier cart, which could be rolled in and out of the radiation field room The activated Co^{60} wires were encased in copper tubing to prevent corrosion of the wire and contamination from any wire flaking and positioned within a barricade of nuclear shielding-grade concrete blocks, which directed the radiation towards the cart containing animal cages (Figure 2.2 & 2.3). Dose rate was calculated by 20 Luxel+ OSL dosimeters (Landauer) placed at different locations on the cart, therefore moving in and out of the field with the animals and obtaining an accurate measurement of the animals' exposure dose. Dosimeter output matched prior Monte Carlo simulations of the total dose, confirming that the goal dose of 0.175 Gy over 28 days was achieved (Saucier, 2016), yielding a dose rate of 6.25 mGy/day. Active wires decayed less than 6% during the time animal work was completed. Animals remained within the radiation field with the exception of ~ 30 minutes/day out of the field required for health checks and cage changes. Although we determined that the radiation field was consistent in dose regardless of position on the animal cart, no animals remained in the same place on the cart for more than 4 days, at which time cages were rotated to a new position.

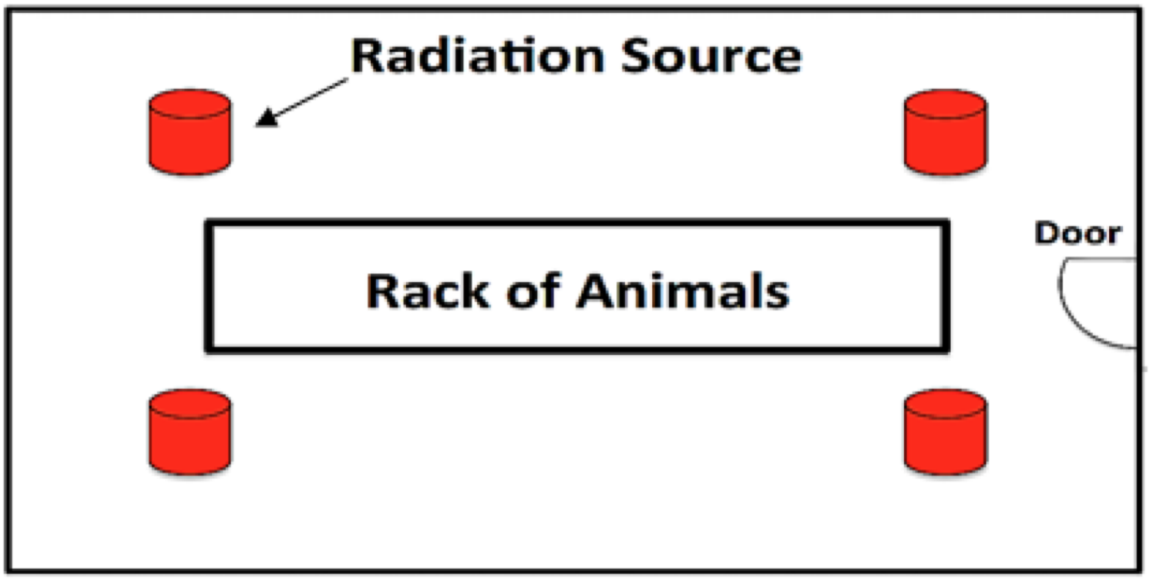

Figure 2.2 Cartoon of radiation field. Pictured is a cartoon representation of the orientation of radiation sources in relation to the cart of animals.

Figure 2.3 Pictured is the radiation field from the perspective of the door. A) Copper tubing which encases the active Co^{60} wires. B) On the left and right are stacks of nuclear shielding grade concrete blocks. C) Cart containing animal cages.

Hindlimb unloading

Hindlimb unloading (HU) was used to simulate zero gravity disuse by suspending animals by their tails so that their back legs were no longer touching the ground. Suspension was achieved by the surgical insertion of a tail ring, comprised of surgical steel wire, between the 4th and 6th caudal vertebra (Ferreira et al., 2011). Tail ring insertion area was allowed to heal for 1.5 weeks prior to the start of HU. Animals, housed two per cage, were allowed to swivel in the center of their half of the cage but could not move laterally into the other mouse's space. Tails were wrapped in gauze so that the tail pointed upward, allowing for improved blood flow to the tail. Animals in HU that were not exercising were also removed from HU during the time period that other animals exercised. The purpose was to assess the antioxidant effects of exercise and not the weight-bearing effects. We will therefore refer to HU in this manuscript as iHU for "interrupted HU" as the animals in this study did not undergo traditional continuous HU. Animals in HU were checked once per day by the facility staff and once per day by investigative staff.

Exercise

Animals began acclimating to treadmill running at 18 wks of age and began treadmill running at 18.5 wks of age. Animals went through a slow incremental increase in treadmill speed and duration over the following week. At age 19.5 wks animals were running on the full protocol until termination at 25 wks of age. Animals exercised on a three days on one day off schedule for the duration of the study. Animals assigned to exercise groups performed treadmill running on a

multi-lane mouse treadmill at 12 m/min for 45 minutes with a 6 minute warm up. EX+WB+CIRR and EX+iHU+CIRR animals were removed from the radiation field for 70 minutes, 51 of which was exercise, to complete the exercise protocol and then immediately returned afterwards. All animals in HU were removed from HU and the radiation field for exercise. Animals in HU but not exercising were also removed from HU during the time period that other animals exercised for the purpose of assessing the antioxidant effects of exercise not the effects of loading. All exercise protocols were completed during the dark hours of a 12:12 light dark cycle.

Dual x-ray absorptometry (DXA)

Densitometry values were assessed using a small animal Lunar PIXImus densitometer (General Electric, Madison, WI). Values of bone mineral density, bone mineral content, lean mass and fat mass were obtained using this measure 2 days prior to termination. Animals were anesthetized using a mixture of isoflourane (Henry Schein Animal Health, Dublin, OH) with oxygen gas during this procedure (≤ 10 minutes total). All mice were placed prone on a specimen tray in the same position so that an ~90° angle was achieved between the upper and lower hindlimb and arms were spread away from the body on a ~45° angle with the head. A whole body region of interest (ROI) that included all but the mouse's head and the tail beyond the animal's feet was used to assess lean mass, fat mass and bone mineral content. BMD was calculated by the PIXImus software (GE Lunar Version 1.42) based on the active bone area in the ROI.

Evaluation of cancellous architecture by micro-computed tomography

Excised left femurs were saved in 4% phosphate buffered formalin for 24 hours and transferred to 70% ethanol at 4°C. Femurs were then shipped to Indiana University of Medicine for micro-computed tomography analyses. To determine cancellous architecture of the femur, the left femur from each animal was subjected to micro-computed tomography (μCT) analyses. μCT scans were taken using a Skyscan 1172 system (Bruker) with an isotropic voxel size of 6μm. Structural parameters of cancellous bone region of interest were measured using standard manufacturer software. For cancellous bone analyses, a 1-mm-long segment of the distal metaphysis secondary spongiosa was defined and the cancellous region within the segment was manually traced. For cortical bone parameters, a single slice located 3 mm proximal to the most distal end of the metaphyseal segment was analyzed to determine cortical bone properties. Key outcomes reported are (for distal femur metaphysis) cancellous bone volume (%BV/TV), trabecular thickness (Tb. Th), trabecular number (Tb. N), and trabecular separation (Tb. Sp); for mid-shaft femur, key outcomes are cortical mid-shaft cross-sectional thickness (Ct.Th) and cortical bone area (Ct. Ar) (Bouxsein et al., 2010).

Evaluation of mechanical strength

All mechanical properties testing was conducted using an Instron 3345 machine (Norwood, MA; 100N load cell; Bluehill v. 2.14.582).

Tibia 3-point bending to failure

Excised left tibia were saved in PBS at -18°C. Femurs were thawed just prior to testing and measured with digital calipers to determine the anterior-posterior and medial-lateral periosteal diameters at the mid-diaphysis. Each bone was positioned with the anterior side resting on two supports, each spaced 10mm apart (Figure 2.4). The upper platen load was applied at the midpoint of the bone and a preload was applied to stabilize the bone. To perform the test, a quasi-static load of 2.54 mm/minute was applied to the upper part of the diaphysis region corresponding with uCT diaphysis scan site (50% total bone length). The test proceeded until fracture occurred. Load cell displacements were monitored and recorded using a linear variable differential transformer. Load-displacement data were analyzed using Matlab (The Mathworks, Inc.; Natick, MA). Stiffness (k, N/mm) was determined by calculating the slope of the load-displacement curve in the elastic region. Ultimate load (N) designated the largest force achieved throughout the test. Data were processed post hoc using a custom-written Matlab program (version 7.12.0, The MathWorks, Inc.) to generate outcomes using force-displacement curves. In addition to outcomes described above, energy absorbed (N·mm) was determined as the area under the entire load-displacement curve.

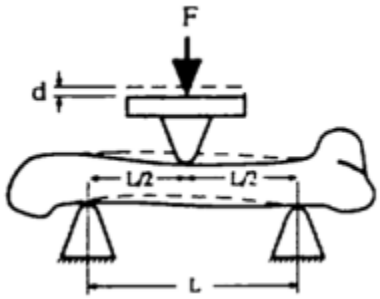

Figure 2.4 Rodent long bone 3-point bending experimental setup [Reprinted with permission from Black, J.M. (2016). *Comparison of the Persisting Effects of Bisphosphonate Treatments Prior to Hindlimb Unloading on Mechanical and Densitometric Properties in the Tibia of Adult Male Rats. 29*. Texas A&M University, MS thesis.].

Femoral neck

Excised right proximal femurs were saved in PBS at -18°C. An axial loading compression test was used to load the femoral neck until failure. Each proximal femur, previously broken in half and the mid-shaft of the femur, was stabilized with the shaft of the femur oriented with the diaphysis portion of the bone firmly inserted into a metal support (Figure 2.5). The load was applied to the tip of the femoral head parallel to the femoral shaft long axis at a rate of 2.54 mm/min. Ultimate load (N) was derived as detailed above. Further measures were not derived due to the inconsistent shape of force displacement curves.

Figure 2.5 Left femoral neck compression test experimental setup (Artwork printed with permission from Jeremy Black).

Histomorphometry

Cortical histomorphometry

Excised, undemineralized distal right tibia, saved at termination in 70% ethanol at 4°C, were dehydrated and embedded in methyl-methacrylate (Sigma-Aldrich M5, 590-9, St. Louis, MO). Serial cross sections (150-200 μm thick) were cut using a diamond wafer low-speed saw (Buehler, Lake Bluff, IL) starting 1mm proximal to the tibia-fibular junction. OsteoMeasure Analysis Software, version 3.3 (Osteo-Metrics, Atlanta, GA) was used to analyze each specimen and determine mineralizing surface/bone surface (MS/BS), mineral apposition rate (MAR), and

bone formation rate (BFR= MS/BS * MAR). Histomorphometric analyses follow the standardizations as defined previously (Dempster et al., 2013). If sections did not have double label present they remained as zeros and in text were identified as missing double label in accordance with published guidelines (Recker et al., 2011).

Cancellous histomorphometry

For these measures, undemineralized right distal femurs, saved at termination in 70% ethanol at 4°C, were serially dehydrated and embedded in methyl methacrylate (Aldrich M5, 590-9, St. Louis, MO, USA). Serial frontal sections were cut 8-µm thick and left unstained for fluorochrome label measurements. Additionally, 4-µm-thick sections were treated with von Kossa stain and tetrachrome counterstain to measure osteoid, osteoid volume, number of osteoclast divided by total area and osteoclast surfaces as a percent of total cancellous surface. The histomorphometric analyses were performed using the OsteoMeasure Analysis System, Version 3.3 (OsteoMetrics, Inc., Atlanta, GA, USA). A defined region of interest was established approximately 500 µm from the growth plate and within the endocortical edges encompassing approximately 1 mm^2 at 20 × magnification. Total bone surface (BS), single-labeled surface, double-labeled surface, and interlabel distances were measured at 200 × magnification while osteoid and osteoclast surfaces were measured at 400 × magnification. All nomenclature for cancellous histomorphometry follows standard usage (Dempster et al., 2013). Two sections from each sample were analyzed and averaged to achieve the reported values. If in both sections there was no double label the value was accepted as zero and in text reported as missing double label in accordance with published guidelines (Recker et al., 2011).

Evaluation of serum bone formation and resorption markers

Measurements of serum C-terminal telopeptide of type 1 collagen (CTX) and procollagen type 1 N-terminal propeptide (P1NP) were obtained by ELISA from cardiac serum collected at termination (Immunodiagnostics, Gaithersburg, MD). Samples were run in duplicate. From there a coefficient of variation was calculated by taking the standard deviation between the two values and dividing them by the mean. When this value was greater than 25% the samples were removed from the study (for CTX n=4 samples removed, for P1NP n=0 samples removed).

Evaluation of 8-hydroxydeoxyguanosine in cancellous bone

Right femurs were fixed in 4% phosphate-buffered formalin for 24 hours at 4°C, then transferred to 70% ethanol at 4°C. Following their return from micro-computed tomography scanning at Indiana University, bones were decalcified in a sodium citrate/formic acid solution for approximately 14 days then stored in 70% ethanol. Sections were then further dehydrated in a Thermo-Scientific STP 120 Spin Tissue Processor, paraffinized via a Thermo Shandon Histocenter 3 Embedding tool, sectioned to approximately 4 μm thickness, mounted on positively charged slides, and immunostained using an avidin-biotin method. Briefly, samples were rehydrated, peroxidase inactivated (3% H_2O_2/methanol), permeabilized (0.5% Triton-X 100 PBS), blocked with species-appropriate serum for 30 min at room temperature (Vectastain Elite ABC; Vector Laboratories, Burlingame, CA, USA) and incubated overnight at 4°C with primary antibodies: polyclonal goat anti-rabbit 8-hydroxydeoxyguanosine (1:1000; Abcam, INC,

Cambridge, UK). On the subsequent day, sections were incubated at room temperature for 45 min with the appropriate species' biotinylated anti-IgG secondary antibody according to manufacturer's specifications. Peroxidase development was performed with an enzyme substrate kit (diaminobenzidine [DAB]; Vector Laboratories). Counterstaining was conducted with 0.2% methyl green counterstain (Vector Laboratories) for 90 s; sections were subsequently dehydrated into organic phase and mounted with xylene-based mounting media (Polysciences, Warrington, PA, USA). Negative controls were completed by omitting the primary antibody. Sections were analyzed by quantifying the proportion of all osteocytes staining positively for the DNA adduct in cancellous bone (~500 μm from the growth plate, an area of approximately 4 mm^2).

Statistical analysis

All data are presented as mean ± standard deviation of the mean (SD) and were evaluated for differences using SPSS (IBM, version 23). Percent change values are expressed in terms of the difference between mean values. Outliers were detected and removed using SPSS program, which identifies outliers first by calculating the interquartile range, multiplying it by 1.5, adding this value to the top of the interquartile range and subtracting this value from the bottom of the interquartile range to obtain the boundaries of acceptable not outlying values. Any value outside this range was deemed an outlier. A three factor ANOVA was used for all normally distributed data in this paper; significant main and interaction effects are reported for these analyses. Post-hoc pairwise comparisons were made using Duncan's test. For groups with data not normally distributed, a Kruskal-Wallis ANOVA was performed with significant

pairwise comparisons reported; main effects for these tests cannot be assessed. Significance was accepted at $p<0.05$.

2.3 Results

iHU and CIRR led to lower body weight

Tail suspended mice exhibited minimal health issues; no porphyrin staining at nose or eyes was observed. In 1 animal, the tail ring insertion site healed such that the tail ring came out of the tail, this animal was removed from the study. Necrotic tail tips, 1 cm, and self-mutilation of the base of the tail were observed extremely infrequently (n=2 animals) and were not severe enough to warrant removal from the study. Body weight was not different at baseline. At termination, body mass was 13% lower in SED+iHU+CIRR compared to SED+WB+CIRR (Figure 2.6). Body weight was generally lower in HU animals.

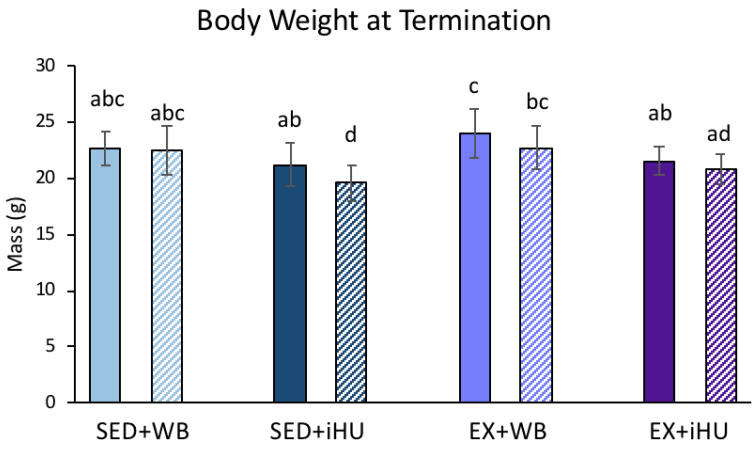

Figure 2.6 Body weight at termination. Data are mean ± standard deviation. Bars sharing the same superscript letter are not statistically different by 3-way ANOVA. Significance was accepted at $p<0.05$. Solid bars represent SHAM animals and hashed bars represent CIRR animals. SED+WB = sedentary with normal weightbearing, SED+iHU = sedentary with hindlimb unloaded, EX+WB = exercise with normal weightbearing, and EX+iHU = exercise with hindlimb unloading.

CIRR and iHU led to changes in body composition

In total body bone mineral density (BMD) at termination there were significant pairwise comparisons between groups, mapped out in Figure 2.7. Total body BMD in SED+iHU+CIRR was 11% lower than SED+WB+CIRR (Table 2.1, graphical representation in Figure 2.7). In lean mass at termination there were significant pairwise comparisons between groups, mapped out in Figure 2.7; lean mass in SED+iHU+CIRR was 14% lower than SED+WB+CIRR. In fat mass at termination there were significant pairwise comparisons between groups, mapped out in Figure 2.7; fat mass in SED+iHU+CIRR was 35-50% lower than in all groups except EX+iHU+CIRR. In summary, total body BMD was lower in most iHU groups; total lean mass was slightly lower

(but only in sedentary mice) and total fat mass was dramatically lower (>35%) with the combination of CIRR and iHU.

Representation of Pairwise Comparisons in DXA

A) Total Body Bone Mineral Density

	SED+WB+SHAM	SED+WB+CIRR	SED+iHU+SHAM	SED+iHU+CIRR	EX+WB+SHAM	EX+WB+CIRR	EX+iHU+SHAM	EX+iHU+CIRR
SED+WB+SHAM	X							
SED+WB+CIRR		X	P=0.005	P=0.048			P=0.046	
SED+iHU+SHAM			X					
SED+iHU+CIRR				X				
EX+WB+SHAM			P=0.007		X			
EX+WB+CIRR			P=0.019			X		
EX+iHU+SHAM							X	
EX+iHU+CIRR								X

B) Total Body Lean Mass

	SED+WB+SHAM	SED+WB+CIRR	SED+iHU+SHAM	SED+iHU+CIRR	EX+WB+SHAM	EX+WB+CIRR	EX+iHU+SHAM	EX+iHU+CIRR
SED+WB+SHAM	X			p=0.007			P=0.025	
SED+WB+CIRR		X		P=0.028				
SED+iHU+SHAM			X					
SED+iHU+CIRR				X				
EX+WB+SHAM				P=0.039	X			
EX+WB+CIRR						X		
EX+iHU+SHAM							X	
EX+iHU+CIRR								X

C) Total Body Fat Mass

	SED+WB+SHAM	SED+WB+CIRR	SED+iHU+SHAM	SED+iHU+CIRR	EX+WB+SHAM	EX+WB+CIRR	EX+iHU+SHAM	EX+iHU+CIRR
SED+WB+SHAM	X			p=0.005				
SED+WB+CIRR		X		P=0.007				
SED+iHU+SHAM			X	P=0.043				
SED+iHU+CIRR				X				
EX+WB+SHAM				p=0.001	X			P=0.022
EX+WB+CIRR				p=0.001		X		
EX+iHU+SHAM				p=0.011			X	
EX+iHU+CIRR								X

Table 2.1 Pairwise comparisons for DXA data. All pairwise comparisons between groups, for not normally distributed data, are represented for BMD (A), lean mass (B) and fat mass (C). These pairwise comparisons are represented as letters above graph bars in Figure 2.7.

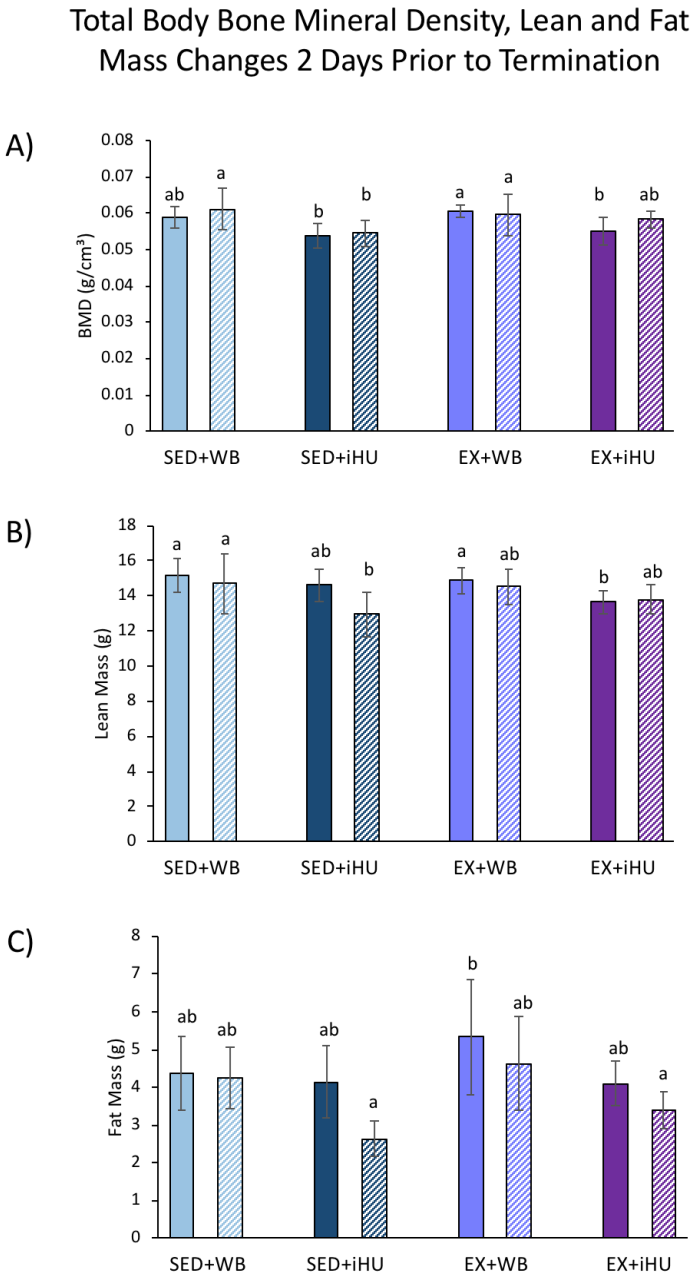

Figure 2.7 DXA data. Data are mean ± standard deviation. A) BMD 2 days prior to termination is represented. B) Lean mass 2 days prior to termination is represented. C) Fat mass 2 days prior to termination is represented. Bars sharing the same superscript letter are not statistically different by non-parametric Kruskal-Wallis ANOVA. Pairwise comparisons are found in Table 2.1 for reference. Significance was accepted at $p<0.05$. Solid bars represent SHAM animals and hashed bars represent CIRR animals. SED+WB = sedentary with normal weightbearing, SED+iHU = sedentary with hindlimb unloaded, EX+WB = exercise with normal weightbearing, and EX+iHU = exercise with hindlimb unloading.

Moderate improvements in cancellous microarchitecture with exercise and interactions between CIRR and iHU response

In the distal femur, %BV/TV was 35% greater in EX+WB+SHAM compared to SED+WB+SHAM (Figure 2.8), indicating a robust effect of exercise. An interaction between CIRR and iHU resulted in SED+iHU+CIRR cancellous BV/TV being 28% lower than in SED+WB+CIRR, indicating that CIRR has a negative impact on iHU animals,; however, this effect was not observed in SED weightbearing animals. Trabecular thickness was 13% greater in EX+WB+SHAM and EX+WB+CIRR than all others. An interaction between CIRR and iHU reflects the observation that trabecular thickness in CIRR-exposed mice is lower (-11%) in WB, but not in EX, mice. Trabecular number was 25% greater in EX+WB+SHAM compared to SED+WB+SHAM. An interaction between CIRR and iHU reflects the observation that trabecular number in CIRR-exposed mice is lower (-8%) in iHU mice compared to SHAM. An interaction between CIRR and EX reflects the observation that trabecular number in EX+iHU+CIRR 21% lower than EX+iHU+SHAM. Trabecular separation was 11% lower in EX+WB+CIRR compared to SED+WB+CIRR. An interaction between CIRR and iHU reflects the observation that trabecular separation was 18% greater in EX+iHU+CIRR than EX+iHU+SHAM. An interaction between CIRR and EX reflects the observation that trabecular separation was 6% lower in EX+WB+CIRR compared to EX+WB+SHAM.

In mid-shaft femur (100% cortical bone site) SED+iHU+CIRR led to much lower (-34%) cross-sectional thickness than in SED+WB+SHAM mice (Figure 2.8, pairwise comparisons available in Table 2.2). Mid-shaft bone area was lower in all iHU groups compared to weightbearing groups. There was no observable impact of CIRR on these outcomes.

In the distal femur cancellous region, bone volume and microarchitecture were improved by exercise as well as diminished by iHU. An interaction effect between CIRR and iHU led to a strong effect of iHU that led to lower bone volume and microarchitecture despite the slight, though not significant, increase found in mice exposed only to CIRR(SED+WB+CIRR). In the cortical mid-shaft femur there was a significant effect of iHU, in almost all situations leading to lower cortical bone thickness and area.

Representation of Pairwise Comparisons in Cortical Mid-shaft Microcomputed Tomography

A) Cross-sectional Thickness

	SED+WB+SHAM	SED+WB+CIRR	SED+iHU+SHAM	SED+iHU+CIRR	EX+WB+SHAM	EX+WB+CIRR	EX+iHU+SHAM	EX+iHU+CIRR
SED+WB+SHAM	X			P<0.0001			P=0.001	P=0.021
SED+WB+CIRR		X		P=0.022				
SED+iHU+SHAM			X					
SED+iHU+CIRR				X				
EX+WB+SHAM					X			
EX+WB+CIRR						X		
EX+iHU+SHAM							X	
EX+iHU+CIRR								X

B) Bone Area

	SED+WB+SHAM	SED+WB+CIRR	SED+iHU+SHAM	SED+iHU+CIRR	EX+WB+SHAM	EX+WB+CIRR	EX+iHU+SHAM	EX+iHU+CIRR
SED+WB+SHAM	X							
SED+WB+CIRR		X	P=0.015	P=0.014			P=0.003	p=0.017
SED+iHU+SHAM			X					
SED+iHU+CIRR				X				
EX+WB+SHAM					X		P=0.026	
EX+WB+CIRR			P=0.021	P=0.02		X	p=0.005	p=0.023
EX+iHU+SHAM							X	
EX+iHU+CIRR								X

Table 2.2 Microcomputed tomography pairwise comparisons. All pairwise comparisons between groups, for not normally distributed data, are represented for cortical mid-shaft cross-sectional thickness (A), cortical mid-shaft bone area (B). These pairwise comparisons are represented as letters above graph bars in Figure 2.8.

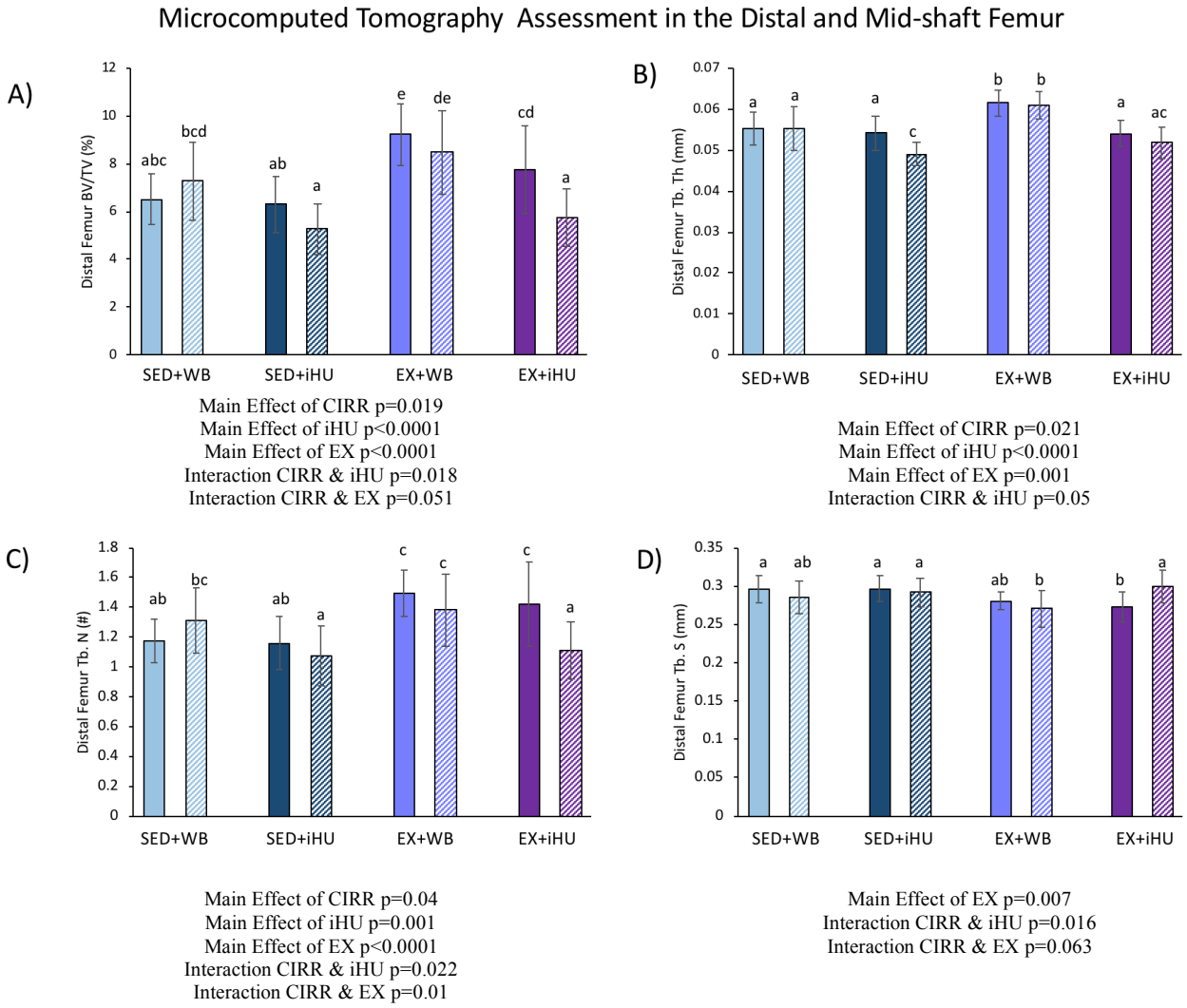

Figure 2.8 Microcomputed tomography on excised mouse femora. Data are mean ± standard deviation. A) Distal femur %BV/TV is represented. B) Distal femur Tb. Th is represented. C) Distal femur Tb. N is represented. D) Distal femur Tb. S is represented. E) Cortical mid-shaft cross-sectional thickness is represented. F) Cortical mid-shaft bone area is represented. Bars sharing the same superscript letter are not statistically different by 3-way ANOVA (A-D) and non-parametric Kruskal-Wallis ANOVA (E-F). Main effects are stated beneath the relevant graph and pairwise comparisons are found in Table 2.2 for reference. Significance was accepted at $p<0.05$. Solid bars represent SHAM animals and hashed bars represent CIRR animals. SED+WB = sedentary with normal weightbearing, SED+iHU = sedentary with hindlimb unloaded, EX+WB = exercise with normal weightbearing, and EX+iHU = exercise with hindlimb unloading.

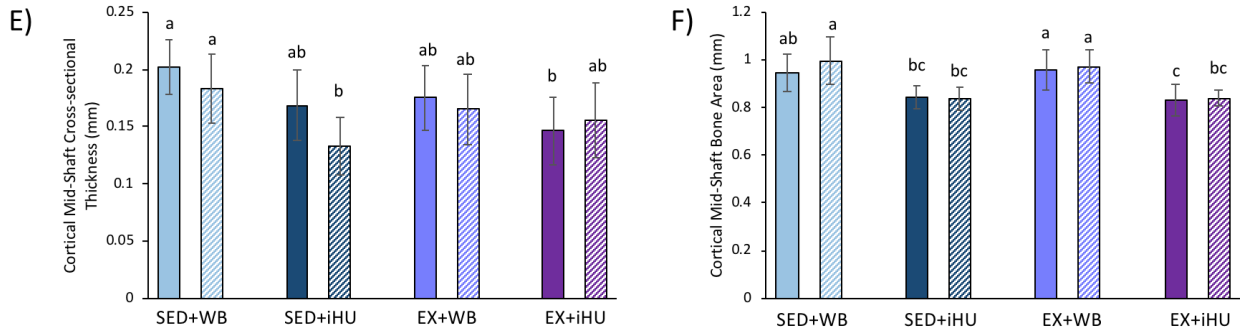

Not normally distributed

Figure 2.8 Continued.

Hindlimb unloading led to reductions in bone strength

Tibial 3-point bending testing revealed, for ultimate load, a main effect of iHU (p=0.006) resulting in a 10% lower ultimate load EX+ iHU+CIRR compared to EX+WB+CIRR (Table 2.3). There were no differences in stiffness among groups. There was a main effect of iHU (p=0.026) and a main effect of CIRR (p=0.021) in yield force; post-hoc comparisons reveal a significantly larger (+15%) yield force in SED+iHU+CIRR compared to SED+iHU+SHAM. Energy to ultimate load was not different among groups. At the femoral neck, the pairwise comparison for ultimate load measured during axial compression was significant between SED+WB+CIRR and SED+iHU+CIRR, with the latter value being 23% lower than the former (Table 2.3). Overall there were reductions in iHU groups compared to WB groups.

		SED+WB+SHAM	SED+WB+CIRR	SED+iHU+SHAM	SED+iHU+CIRR	EX+WB+SHAM	EX+WB+CIRR	EX+iHU+SHAM	EX+iHU+CIRR
MidShaft Tibia	Ultimate Load (N)	11.70 ± 0.99^{abc}	12.30 ± 1.28^{bc}	11.50 ± 0.97^{ab}	12.00 ± 1.11^{abc}	12.20 ± 1.15^{abc}	12.70 ± 1.20^{c}	11.50 ± 1.27^{ab}	11.07 ± 0.77^{a}
	Stiffness (N/mm)	42.40 ± 4.53	46.10 ± 8.43	40.26 ± 9.47	41.60 ± 10.3	42.20 ± 7.00	43.10 ± 9.52	41.40 ± 9.75	42.80 ± 9.31
	Yield Force (N)	10.30 ± 1.18^{ab}	11.60 ± 1.39^{a}	9.83 ± 1.81^{b}	11.30 ± 1.15^{a}	11.50 ± 1.35^{a}	11.70 ± 1.45^{a}	10.50 ± 1.66^{ab}	10.70 ± 1.40^{ab}
	Energy-to-Ultimate (mJ)	3.05 ± 0.36	2.76 ± 0.42	2.74 ± 0.48	2.77 ± 0.32	2.91 ± 0.24	3.03 ± 0.32	2.71 ± 0.40	2.620 ± 0.51
Femoral Neck	Ultimate Load (N)	13.30 ± 2.15^{ab}	15.20 ± 1.79^{a}	13.80 ± 2.98^{ab}	11.64 ± 1.31^{b}	16.50 ± 1.16^{a}	15.00 ± 1.34^{a}	13.10 ± 1.04^{ab}	13.10 ± 1.31^{ab}

Table 2.3 Mechanical testing of the midshaft tibia by 3-point bending and the femoral neck by compression test. Data are mean ± standard deviation. Any group sharing the same letters are not statistically different from one another by 3-way ANOVA (mid-shaft tibia) or by non-parametric Kruskal-Wallis ANOVA (femoral neck). If there were no differences than no letters are provided. Significance was accepted at $p<0.05$. SED = sedentary, EX= exercise, SHAM = sham radiation exposure, CIRR = continuous low-dose-rate radiation exposure, iHU = hindlimb unloading.

CIRR led to greater cortical mineralizing surface when combined with exercise but minimal impact on bone formation indices was detected in cancellous bone

In cancellous bone there were six samples without double label; these were distributed across groups, with no more than 3 in any one group missing double labels. Mineral apposition rate (MAR) for these samples were left as "zero" rather than using an imputed value. On the mid-shaft tibial endocortical surface, there were many missing double labels; however, all groups had at least 5 samples with label except SED+iHU+SHAM, which had only 3. On the tibial periosteal surface, we only report mineralizing surface since all but two animals exhibited missing double labels.

There were no statistical differences in group mean values for histomorphometric measures in the distal femur cancellous bone (Table 2.4). Endocortical MS/BS was consistently greater in CIRR-exposed animals compared to SHAM mice; however, these comparisons reached statistical significance only for in exercising groups. There were no differences among groups for endocortical MAR; however, endocortical BFR was greater in SED+WB+CIRR and EX+WB+CIRR than SED+iHU+SHAM. Periosteal MS/BS was at least 3-fold greater in EX+WB+CIRR than SED+WB+SHAM, SED+WB+CIRR, SED+iHU+SHAM and EX+iHU+SHAM. There were no statistical differences in serum measures of bone formation (P1NP) or bone resorption (CTX) (Table 2.5). Although there were few differences in cellular outcomes, cortical mineralizing surface was greater with CIRR only in exercising animals.

		SED+WB+SHAM	SED+WB+CIRR	SED+iHU+SHAM	SED+iHU+CIRR	EX+WB+SHAM	EX+WB+CIRR	EX+iHU+SHAM	EX+iHU+CIRR
Distal Femur	MS/BS (%)	4.72 ± 1.27	7.45 ± 4.10	3.53 ± 1.85	5.98 ± 2.38	7.14 ± 3.64	6.53 ± 2.78	5.31 ± 3.82	7.46 ± 4.10
	MAR (um/d)	0.31 ± 0.17	0.94 ± 0.80	0.38 ± 0.38	0.52 ± 0.36	1.36 ± 1.20	0.66 ± 0.24	0.59 ± 0.33	0.66 ± 0.37
	BFR ($um^3/um^2/d$)	0.02 ± 0.01	0.08 ± 0.08	0.02 ± 0.02	0.04 ± 0.03	0.08 ± 0.07	0.06 ± 0.06	0.04 ± 0.04	0.08 ± 0.08
	Number of Animals Missing Double Label	1 of 10	1 of 10	3 of 10	0 of 9	0 of 8	0 of 9	0 of 9	1 of 10
	Osteoclast Surface (%)	0.30 ± 0.29	0.45 ± 0.20	0.40 ± 0.40	0.48 ± 0.46	0.41 ± 0.35	0.43 ± 0.28	0.28 ± 0.18	0.49 ± 0.51
	Osteoclast Number/total area (#)	0.74 ± 0.40	1.00 ± 0.49	0.62 ± 0.33	0.77 ± 0.55	1.27 ± 0.89	1.05 ± 0.97	1.57 ± 1.11	0.92 ± 0.74
	Osteoid Surface (%)	1.31 ± 0.78	2.59 ± 2.29	0.83 ± 0.71	1.55 ± 2.00	0.87 ± 0.48	2.38 ± 1.72	1.22 ± 0.68	2.40 ± 1.98
	Osteoid Volume (%)	0.18 ± 0.18	0.70 ± 0.87	0.05 ± 0.08	0.18 ± 0.30	0.08 ± 0.15	0.46 ± 0.45	0.18 ± 0.19	0.35 ± 0.65
	Fraction of Positive Osteocytes for 8OhDG	0.50 ± 0.17	0.63 ± 0.14	0.67 ± 0.16	0.50 ± 0.04	0.64 ± 0.29	0.65 ± 0.17	0.54 ± 0.06	0.54 ± 0.18
Midshaft Tibia	Endocortical MS/BS (%)	18.78 ± 9.45^{a}	30.06 ± 13.76^{ab}	15.93 ± 9.20^{a}	28.77 ± 17.61^{ab}	15.58 ± 9.01^{a}	37.43 ± 11.78^{b}	19.05 ± 9.47^{a}	33.78 ± 28.19^{b}
	Endocortical MAR (um/d)	0.15 ± 0.18	1.72 ± 2.14	0.60 ± 1.24	1.01 ± 1.13	0.34 ± 0.42	1.89 ± 2.42	0.17 ± 0.29	0.49 ± 0.61
	Endocortical BFR ($um^3/um^2/d$)	0.05 ± 0.08^{ab}	0.54 ± 0.68^{b}	0.001 ± 0.002^{a}	0.41 ± 0.48^{ab}	0.14 ± 0.23^{ab}	1.64 ± 2.58^{b}	0.02 ± 0.03^{ab}	0.19 ± 0.32^{ab}
	Number of Animals Missing Double Label	5 of 10	1 of 10	7 of 8	3 of 9	2 of 8	2 of 10	5 of 8	2 of 6
	Periosteal MS/BS (%)	1.29 ± 2.27^{a}	1.27 ± 2.24^{a}	0.82 ± 1.12^{a}	1.95 ± 3.13^{ab}	2.29 ± 2.58^{ab}	6.53 ± 6.53^{b}	1.27 ± 2.66^{a}	1.70 ± 1.63^{ab}

Table 2.4 Histomorphometry on excised distal mouse femora and mid-shaft tibia. In the distal femur mineralizing surface (MS/BS), mineral apposition rate (MAR), bone formation rate (BFR), osteoclast surface and osteoclast number are represented. In the midshaft tibia endocortical MS/BS, MAR and BFR along with periosteal MS/BS are represented. Data are mean ± standard deviation.Any group sharing the same letters are not statistically different from one another by 3-way ANOVA (only endocortical MS/BS) and non-parametric Kruskal-Wallis ANOVA (all other measures). If there were no differences than no letters are provided. Significance was accepted at $p<0.05$. SED = sedentary, EX= exercise, SHAM = sham radiation exposure, CIRR = continuous low-dose-rate radiation exposure, iHU = hindlimb unloading.

There were no statistical differences among groups for the immunohistochemical measurement of cancellous bone osteocytes positive for 8-hydroxydeoxyguanosine, which indicates oxidative damage to DNA.

There were no statistical differences in immunohistochemical measurements of 8-hydroxydeoxyguanosine, measured to determine if there was oxidative stress caused by CIRR, in the cancellous bone.

	SED+WB+SHAM	SED+WB+CIRR	SED+iHU+SHAM	SED+iHU+CIRR	EX+WB+SHAM	EX+WB+CIRR	EX+iHU+SHAM	EX+iHU+CIRR
CTX (ng/mL)	21.60 ± 5.24	2.98 ± 14.23	27.85 ± 12.06	26.36 ± 7.05	26.55 ± 11.5	21.41 ± 5.18	29.19 ± 5.34	20.95 ± 3.43
P1NP (ng/mL)	3.16 ± 1.54	2.59 ± 0.26	3.82 ± 1.72	3.16 ± 0.92	3.10 ± 0.53	3.22 ± 0.68	4.17 ± 2.27	3.44 ± 1.06

Table 2.5 Serum measures of CTX and P1NP on cardiac serum collected on termination day. Data are mean ± standard deviation. SED = sedentary, EX= exercise, SHAM = sham radiation exposure, CIRR = continuous low-dose-rate radiation exposure, iHU = hindlimb unloading. No statistical differences exist for any pairwise comparison

2.4 Discussion

The primary findings of this experiment are, first, the novel continuous low-dose-irradiation (CIRR) led to a response different from acute radiation studies in that there were some declines in body weight, cancellous bone volume and cancellous microarchitecture amongst groups though not all. Interestingly, there were much higher values for endocortical mineralizing surface that reached significance in CIRR- exposed exercising groups; given the

smaller changes in mineral apposition rate and a high degree of variability within each group, this increase in MS/BS did not result in a significant increase in bone formation rate. Second, that interrupted hindlimb unloading (iHU) expectedly led to non-significant losses in total body bone mineral density, trabecular bone volume and significant decrements in cortical bone mass. This represents some losses due to iHU, though not as many as would have been expected with traditional, uninterrupted HU (M. R. Allen & Bloomfield, 2003; S. Bloomfield, Allen, Hogan, & Delp, 2002; Shirazi-Fard et al., 2014). Third, the combined effects of CIRR and iHU produced decrements in distal femur cancellous BV/TV and microarchitecture. The addition of exercise mostly does not mitigate the losses found with the combined effect of CIRR and iHU. Fourth, exercise led to expected increases cancellous bone mass and improvements in cancellous microarchitecture. Together these findings suggest that the complex response to CIRR produces some detriments in bone when combined with iHU, that this response varies based on bone compartment, and that exercise is generally unable to mitigate the negative effects of CIRR combined with iHU.

Previous studies have demonstrated reductions in total body bone mineral density, lean mass and fat mass with hindlimb unloading (Fluckey et al., 2002; B. Smith et al., 2005; Wade et al., 2013). Bone loss, particularly in the cancellous region, has also been well reported in HU with pronounced decrements in cancellous BMD and microarchitecture (Globus & Morey-Holton, 2016; Li et al., 2012; Morey-Holton & Globus, 2002; Shirazi-Fard et al., 2013). A study by Shirazi-Fard*, et al.* found that 28 days of hindlimb unloading led to a decrease in cancellous bone volume, trabecular spacing and number, as well as in cortical bone volume parameters (Shirazi-Fard et al., 2015). Mechanical testing of hindlimb unloaded-bones, done to determine the force required for fracture (among other outcomes), usually reveals a reduction in mechanical

strength of the bone (Shirazi-Fard et al., 2013). Bone loss in the cancellous region of unloaded hindlimbs is demonstrated by reductions in bone mineral density and negative changes in cancellous microarchitecture (Li et al., 2012). Some evidence of unloading effects were seen in this study's iHU groups despite the interrupted weightbearing, as evidenced by mild, though not significant, declines in body weight and total body bone mineral density. In the distal femur cancellous bone we did not find statistically significant changes in bone volume and decrements in microarchitecture, which would be normal with HU. However, in this study we implemented interrupted HU in order to assess the antioxidant effects of exercise not the effect of loading. We did not expect the small amount of loading experienced during HU to minimize the usual losses we have previously found with HU. In as yet unpublished data we show that, in the same strain and age of mouse as used in this study, traditional (uninterrupted) hindlimb unloading results in significant decrements in cancellous bone (BV/TV) and total body bone mineral density. We also show that iHU is not different from an weightbearing control in most bone specific measures but that body weight is lower with iHU.

Previous studies assessing the effects of radiation on bone have demonstrated decrements, no change, and (rarely) improvements in bone following exposure to various doses of acute radiation (J. Alwood et al., 2010; Joshua S Alwood et al., 2012; Eric R Bandstra et al., 2009; Boyle et al., 2003; Green et al., 2012; Havaki et al., 2015; Shane A Lloyd et al., 2012). Those results indicate decrements ranging from 14-41%, compared to controls in bone volume and structural quality following exposure to various doses of radiation ions and doses (J. Alwood et al., 2010; Joshua S Alwood et al., 2012; Eric R Bandstra et al., 2009; Boyle et al., 2003; Green et al., 2012; Shane A Lloyd et al., 2012). When 1 Gy of proton, radiation was delivered in another study there was a 20% loss of cancellous bone volume fraction in the tibia and the femur

and no effect on cortical bone (Shane A Lloyd et al., 2012). In another study, 0.18 Gy ^{56}Fe resulted in lower proximal tibia cancellous bone volume fraction, lower trabecular thickness, greater cortical porosity and lower polar moment of inertia (Eric R Bandstra et al., 2009). While some studies have found no effect of radiation, there is one which actually documented a positive impact on cancellous bone measured nearly a year after exposure to heavy iron. Karim *et al* performed head-only irradiation of mice, leading to a 4.4 cGy of ^{56}Fe radiation dose at the femur, and measured a 51% higher cancellous bone volume in bones 11.5 months following irradiation compared to sham-exposed animals (Karim & Judex, 2014; Yu et al., 2017).

Given that spaceflight travel outside of low Earth orbit for 3 years is expected to deliver no more than 1 Gy of radiation, based on several group's assessments, our low dose of 0.175 Gy over 28 days is highly relevant to the GCR exposure encountered on future missions (Hassler et al., 2014; McGirl et al., 2015). Much of the previous literature examines radiation doses and dose rates higher than those examined in this study (Akkus, Belaney, & Das, 2005; J. Alwood et al., 2010; Willey et al., 2008; Wright et al., 2015). To my knowledge, only one published study has investigated the effects of continuous low-dose-rate gamma exposure on bone outcomes, but at a 10-fold higher total dose and dose rate, than for this present study. This previous work found no significant effect of continuous gamma radiation exposure on cancellous bone volume, even though similar total dose rates (1.7 Gy) delivered acutely usually lead to decrements in bone (Yu et al., 2017). In our study, contrary to our original hypothesis, we found that continuous, low dose-rate gamma radiation exposure alone did not lead to any negative effects on bone. We do not record any strong effects of CIRR on bone outcomes including mechanical properties, suggesting that GCR exposure may not represent a threat to bone integrity or increase fracture risk during long duration spaceflight outside of low earth orbit.

While these outcomes of a mixed, though mild, response to continuous low-dose-rate radiation were unexpected, they also suggest a differential response to low-dose-rate radiation between cortical and cancellous bone. While we were unable to detect differences in histological indices of osteoclasts and osteoblast activity in metaphyseal cancellous bone, which is consistent with a neutral impact on bone, other studies have found that radiation causes an increase in bone resorption and a decrease in bone formation resulting in a net loss of bone (Joshua S Alwood et al., 2015; Boyle et al., 2003; Shane AJ Lloyd et al., 2008; Willey et al., 2008; Wright et al., 2015). At our 28 day time point we were unable to detect cellular changes possibly due to the restabilization of bone modeling in the cancellous bone that takes place within that time period (Shahnazari et al., 2012). We were able to detect an increase in endocortical mineralizing surface in exercising groups exposed to CIRR, which provides encouraging evidence that osteoblasts are able to respond to increased mechanical loading after three weeks of CIRR. This is in line with previously published data documented that, 8 weeks after 5 Gy of ^{137}Cs radiation exposure, there was a 20% increase in MAR and a 30% increase in BFR compared to control therefore it is possible for radiation to cause lead to improvements in indices of bone formation (Green et al., 2012). Taken together these results suggest a complex effect of continuous low-dose-rate radiation. Further study is needed to understand this effect, especially understanding time points earlier during the course of 28 days exposure.

On future long duration missions to Mars and the Moon, astronauts will be exposed to both lack of gravitational loading and GCR; therefore, many studies have focused on the combined effects of disuse and radiation to better predict the biomedical risks of future space travel (Shane A Lloyd et al., 2012; Macias et al., 2016; Xu et al., 2014; Yu et al., 2017; Yumoto et al., 2010). Several previous studies have found an additive effect of radiation exposure and

hindlimb unloading (HU) with higher doses of radiation (Shane A Lloyd et al., 2012; Xu et al., 2014). Xu *et al* found that rats hindlimb suspended after exposure to 4 Gy of X-ray radiation had a synergistic loss of bone due to the combination of disuse and radiation (Xu et al., 2014). Doses of radiation more relevant to long-duration spaceflight (<1 Gy) when combined with disuse have more complex results (J. Alwood et al., 2010; Macias et al., 2016; Yu et al., 2017; Yumoto et al., 2010). Alwood *et al* exhibited a reduction in the compressive yield force in vertebrae of mice exposed to both 0.5 Gy of ^{56}Fe radiation and hindlimb unloading (J. Alwood et al., 2010). However, our group previously found that animals exposed to three fractions of 0.17 Gy ^{28}Si experienced no additive effects of radiation exposure and partial weightbearing on cancellous bone volume (Macias et al., 2016). Interestingly, when a single dose of 0.5 Gy ^{56}Fe is delivered 3 days prior to the end of a 28 day HU period, rapid cancellous bone loss occurs accompanied by a greater increase in osteoclast number as observed in weightbearing animals, suggesting that osteoclasts of HU animals were sensitized to radiation-induced bone loss (Yumoto et al., 2010). This suggests that important effects of radiation exposure occur soon after the time of exposure. Finally, Yu *et al* found that continuous low dose-rate gamma radiation up to a total dose of 1.7 Gy did not exacerbate the effects of hindlimb unloading (Yu et al., 2017). The combined effect of continuous low-dose-rate radiation and iHU seems to be complex and site-specific. Body weight was negatively affected by the combination of CIRR and iHU, an effect which is possibly additive since the SED+iHU+CIRR group was lower than both SED+WB+CIRR and SED+iHU+SHAM. Lean mass, fat mass and cortical cross-sectional area were lower in the SED+iHU+CIRR group, though not significantly affected by either CIRR or iHU alone.

Assessing mechanical properties provides insight into skeletal tissue's resistance to fracture. Femoral neck ultimate load, a mixed bone site with cortical and cancellous bone, was

particularly affected by the combination of CIRR and iHU. Values for this marker of bone strength were lowest in the sedentary mice exposed to both treatments. These results are consistent with some of the literature (J. Alwood et al., 2010; Joshua Stewart Alwood, 2009; Black, 2016). However, CIRR exposure resulted in a higher yield force at mid-shaft tibia, a cortical bone site, in sedentary mice on iHU. This difference in effect is certainly in part due to the difference in the shape of the bone found at each site. Further studies on the impact of CIRR on bone mechanical properties are needed to understand these effects. Overall, our findings suggest that there is evidence for combined effect on mechanical testing parameters resulting in negative effects of continuous low-dose-rate radiation and interrupted hindlimb unloading.

Exercise has been shown to sufficiently mitigate spaceflight-induced bone loss in humans (Cavanagh et al., 2007; Shirazi-Fard et al., 2014; S. M. Smith et al., 2012; S. M. Smith et al., 2008). Additionally, ground-based analogs in humans have demonstrated similar benefits of exercise in ameliorating disuse-induced bone loss (Cavanagh et al., 2007; Iura et al., 2015; S. M. Smith et al., 2012; S. M. Smith et al., 2008). Exercise has been shown to increase bone mass in rodents (Boudreaux et al., 2014; Shimano & Volpon, 2009). Shimano et al found that animals who exercised during recovery from hindlimb unloading had improved bone quality compared to those that were allowed only cage activity (Shimano & Volpon, 2009). Boudreaux et al found that aerobic exercise was sufficient for mitigating bone loss due to disuse (Boudreaux et al., 2014). In 2.5-month-old rats, treadmill exercise resulted in a greater ultimate load at the mid-shaft femur (Raab, Smith, Crenshaw, & Thomas, 1990). As in previous work where improved bone outcomes were found with exercise, we record a mild increase in total body weight and total body fat mass with aerobic exercise. We also observed an increase in cancellous bone volume and improvements in microarchitecture of the distal femur. We also record an increase in

endocortical and periosteal mineralizing surface in groups exposed to CIRR and EX together, but did not detect any other combined effect of CIRR and EX across any other variables. This indicates that CIRR does not impair the ability of osteoblasts to respond to the increased loading of treadmill training. We record that exercise was unable to prevent iHU-induced losses in total body bone mineral density and fat mass, as well as cancellous bone volume and trabecular thickness. We determine that our endurance exercise regimen was not sufficient to prevent iHU losses in bone in these mice. Given that animals in this study took part in interrupted hindlimb unloading (75 minutes of weightbearing on each scheduled exercise day), we speculate that any mitigating effects of exercise in iHU animals are due to the metabolic impacts of exercise, though it is possible that a bone blood flow effect could also have contributed to those positive effects.

Although we have used a completely balanced design with all appropriate controls, the more factors used in one study the more variability the model has, which may have limited our ability to detect some differences. Statistically speaking, we may have seen more pronounced effects of each factor (CIRR, iHU and exercise) if assessed individually. Despite the clear difference in response in cancellous and cortical bone, we were unable to detect cellular alterations in the cancellous bone compartment. It is possible that we could have seen such a response if we had assessed responses at multiple earlier time points during iHU. We were only able to assess female mice in this study; however, it would be beneficial to assess a difference in response to CIRR in males and females. We were limited in the amount of radiation we could deliver at the appropriate dose rate by the amount of time animals could remain in safely in iHU. We believe that with the implantation of two side by side tail rings we could sustain female animals through a longer 6-8 week unloading period. Future studies should focus on safe ways to

implement longer iHU periods to assess a more extended radiation exposure. Finally, in this study we chose to assess the antioxidant/metabolic effects of endurance exercise and did not want these to be confused with the effects of loading induced by weightbearing in the EX+iHU groups. To achieve this, we allowed for weightbearing activity for all iHU animals for the same duration of time that animals exercised so that exercise and their sedentary counterparts had equal amounts of weightbearing during HU. This study design helped to achieve our goals; however, these short periods of weightbearing resulted in less pronounced negative effects of iHU compared to HU.

In conclusion, the novel continuous low-dose-rate gamma radiation exposure studied here is not detrimental to bone. However, we record that the combined effect of CIRR and iHU does produce multiple deficits, which may increase the risk of fracture in astronauts traveling outside of low earth orbit. We did not find that endurance exercise will mitigate the combined negative effect of CIRR and iHU on cancellous bone, but may have mitigate some losses in cortical bone. This poses an additional challenge to space travel outside of low earth orbit in that the current strategies for bone loss prevention aboard ISS (exercise and adequate nutritional intake) may not be effective against the combined impact of GCR and prolonged microgravity exposure.

3. IMPACT OF AGING ON BONE RESPONSE TO CONTINUOUS LOW-DOSE RATE RADIATION DURING HINDLIMB UNLOADING

3.1 Introduction

Bone is sensitive to spaceflight-induced losses in mass and structural integrity. Low bone quality in astronauts upon returning to Earth has been an area of concern for NASA; crew members incur some increased risk of fracture upon return to full gravitational loading on Earth (Sibonga, 2013). While NASA has developed many methods for diminishing bone loss during 6-month missions in low Earth orbit, it remains a pressing concern for future exploration class spaceflight missions. The dangers of low bone mineral density on a Mars mission would be greater upon landing where astronauts may fall and sustain injuries to their microgravity-weakened bones (Sibonga, 2013). Due to the minimal medical capabilities available during extra-planetary missions, a broken bone could be far more detrimental to the health of the astronaut than if it occurred on Earth; e.g., non-union fractures can lead to sepsis, a life-threatening outcome (Alexander, 2016).

Of further concern to NASA are the additional effects of radiation that could worsen the deleterious effects of spaceflight on the skeletal system. The Earth's Van Allen belts, which create a magnetic field, protect Earth and space station-bound humans from the majority of the space radiation, Galactic Cosmic Radiation (GCR). GCR is ionizing radiation from a mixture of species including gamma rays, neutrons, alpha particles, protons and ions as heavy as iron. Exposure to GCR, though very high in energy, is at extremely low doses but constant; therefore, astronauts will be exposed to a nearly continuous low dose of radiation spread over a period of nearly 3 years (Hassler et al., 2014; McGirl et al., 2015). NASA has estimated that astronauts on

a Mars mission will be exposed to a dose rate of 0.21 mGy/day on the surface of Mars (up to 500 days) and a 0.48 mGy/day on the 180-day cruise to Mars from a variety of ion species of radiation (Hassler et al., 2014; McGirl et al., 2015). Both reduced gravity and radiation are stressors that will be encountered by astronauts on these exploration class missions; therefore, these two major stresses should be studied in conjunction since there is evidence of interaction effects (Xu et al., 2014).

Much of the skeletal research conducted in animals to determine spaceflight changes has been conducted on young, rapidly growing rodents or adult animals that have reached peak bone mass (at ~14 months of age in mice). However, many aging studies have determined an age-related decline in bone loss over time, suggesting that responses observed in "adult" animals might not be representative of the "middle-aged" population of humans flying in space, who now average 45- to 50-years-old. There are some published studies which have identified that senescent rodents (22 months of age) do not exhibit the same negative effects of hindlimb unloading as seen in their adult counterparts (Perrien et al., 2007). With the clear difference in response between adult and old animals it is questionable whether a middle-aged animal, one that has some senescent systems but is not a senescent animal, which would be considered an adult by most, would respond the same as an adult animal. Astronauts are of an equivalent age to middle-aged animals this is an important question for future spaceflight endeavors. Therefore, in this study we have sought to compare the response to continuous low-dose-rate radiation and/or hindlimb unloading in both adult and middle-aged animals, ~4 and 11 months of age, respectively, at the start of the study. Our hypothesis was that the response to hindlimb unloading in middle-aged animals would not be as severe compared to adult animals and that continuous

low-dose-rate radiation would have a greater impact on adult animals compared to middle-aged animals.

3.2 Materials & Methods

Experimental design and animals

Female C57bl6/J mice, adult (17 weeks old) and middle-aged (44 weeks old) animals ate a AIN93-G, standard chow diet. Mice were group housed for 2.5 weeks during diet acclimation. One and a half weeks prior to hindlimb unloading (HU) animals underwent a minor tail-ring insertion surgery and were thereafter single housed for the duration of the experiment. Following 4 weeks of diet acclimation, animals began HU and/or radiation exposure for 4 weeks. Animals in HU were housed within sight of another animal but without the ability to touch; therefore, we consider them single housed. Weightbearing controls were single housed in standard shoebox cages. Eight groups were examined: weightbearing adult sham (A+SHAM+WB), weightbearing adult continuous irradiation (A+CIRR+WB), hindlimb unloaded adult sham (A+SHAM+HU), hindlimb unloaded adult continuous irradiation (A+CIRR+HU), weightbearing middle-aged sham (MA+SHAM+WB), weightbearing middle-aged continuous irradiation (MA+CIRR+WB), hindlimb unloaded middle-aged sham (MA+SHAM+HU), and hindlimb unloaded middle-aged continuous irradiation (MA+CIRR+HU). At experiment's end, animals were anesthetized using isoflurane gas and euthanized by both cervical dislocation and thoracotomy. All procedures used in this study were approved by the Institutional Animal Care and Use Committee (IACUC) at Texas A&M University.

Continuous radiation exposure

A radiation field was created using gamma radiation, because it is the reference radiation. Additionally, as energetic particles, gamma radiation is representative of half of the dose from heavier ions, which is the result of energetic particles. The orientation of activated Co^{60} wires and design of the radiation field, including the placement of radiation sources and shielding material to contain radiation, was achieved using Monte Carlo simulations conducted earlier (Saucier, 2016). These simulations provided sufficient information to determine the original irradiation dose delivered to the cobalt wires at the Texas A&M Nuclear Science Center, which determined how much radiation they would emit once activated. Animals were housed in a decomissioned x-ray room in our animal facility equipped with lead-shielded walls; animal cages were placed on a 4- tier cart, which could be rolled in and out of the radiation field room The activated Co^{60} wires were encased in copper tubing to prevent corrosion of the wire and contamination from any wire flaking and positioned within a barricade of nuclear shielding-grade concrete blocks, which directed the radiation towards the cart containing animal cages (Figure 2.2 & 2.3). Dose rate was calculated by 20 Luxel+ OSL dosimeters (Landauer) placed at different locations on the cart, therefore moving in and out of the field with the animals and obtaining an accurate measurement of the animals' exposure dose. Dosimeter output matched prior Monte Carlo simulations of the total dose, confirming that the goal dose of 0.175 Gy over 28 days was achieved (Saucier, 2016), yielding a dose rate of 6.25 mGy/day. Active wires decayed less than 6% during the time animal work was completed. Animals remained within the radiation field with the exception of ~ 30 minutes/day out of the field required for health checks and cage changes. Although we determined that the radiation field was consistent in dose

regardless of position on the animal cart, no animals remained in the same place on the cart for more than 4 days, at which time cages were rotated to a new position.

Hindlimb unloading

Hindlimb unloading (HU) was used to simulate zero gravity disuse by suspending animals by their tails so that their back legs were no longer touching the ground. Suspension was achieved by the surgical insertion of a tail ring, comprised of surgical steel wire, between the 4th and 6th caudal vertebra (Ferreira et al., 2011). Tail ring insertion area was allowed to heal for 1.5 weeks prior to the start of HU. Animals, housed two per cage, were allowed to swivel in the center of their half of the cage but could not move laterally into the other mouse's space. Tails were wrapped in gauze so that the tail pointed upward, allowing for improved blood flow to the tail. Animals in HU were checked once per day by the facility staff and once per day by investigative staff. Adult animals from this chapter are the same as the sedentary animals from chapter 2; therefore, they were exposed to interrupted HU.

Dual x-ray absorptometry (DXA)

Densitometry values were assessed using a small animal Lunar PIXImus densitometer (General Electric, Madison, WI). Values of bone mineral density, bone mineral content, lean mass and fat mass were obtained using this measure 2 days prior to termination. Animals were anesthetized using a mixture of isoflourane (Henry Schein Animal Health, Dublin, OH) with oxygen gas during this procedure (≤ 10 minutes total). All mice were placed prone on a

specimen tray in the same position so that a ~90° angle was achieved between the upper and lower hindlimb and arms were spread away from the body on a ~45° angle with the head. A whole body region of interest (ROI) that included all but the mouse's head and the portion of the tail extending beyond the animal's feet was used to assess lean mass, fat mass and bone mineral content. BMD was calculated by the PIXImus software (GE Lunar Version 1.42) based on the active bone area in the ROI.

Evaluation of cancellous architecture by micro-computed tomography

Excised left femurs were saved in 4% phosphate buffered formalin for 24 hours and transferred to 70% ethanol at 4°C. Femurs were then shipped to Indiana University of Medicine for micro-computed tomography analyses. To determine cancellous architecture of the femur, the left femur from each animal was subjected to micro-computed tomography (μCT) scans using a Skyscan 1172 system (Bruker; Kontich, Belgim) with an isotropic voxel size of 6um. Structural parameters of cancellous bone region of interest were measured using standard manufacturer software. For cancellous bone analyses, a 1-mm-long segment of the distal metaphysis secondary spongiosa starting 500 um proximal to the growth plate was defined and the cancellous region within the segment was manually traced. For cortical bone parameters, a single slice located 3 mm proximal to the most distal end of the metaphyseal segment was analyzed to determine cortical bone properties. Key outcomes reported in both the femur are cancellous bone volume (%BV/TV), trabecular thickness (Tb. Th), trabecular number (Tb. N), trabecular separation (Tb. Sp), cortical mid-shaft cross-sectional thickness (Ct.Th) and cortical bone area (Ct. Ar) (Bouxsein et al., 2010).

Evaluation of mechanical strength

All mechanical properties testing was conducted using an Instron 3345 machine (Norwood, MA; Bluehill v. 2.14.582) equipped with a 100 N load cell.

Tibia 3-point bending

Excised left tibia were saved wrapped in PBS-soaked gauze at -18°C. Just prior to mechanical testing, femurs were thawed and measured with digital calipers to determine the anterior-posterior and medial-lateral periosteal diameters at the mid-diaphysis. Each bone was positioned with the anterior side resting on two supports, each spaced 10mm apart (Figure 2.4). The upper platen load was applied at the midpoint of the bone and a preload was applied to stabilize the bone. To perform the test, a quasi-static load of 2.54 mm/minute was applied to the upper part of the diaphysis region corresponding with uCT diaphysis scan site (50% total bone length). The test proceeded until fracture occurred. Load cell displacements were monitored and recorded using a linear variable differential transformer. Load-displacement data were analyzed using Matlab (The Mathworks, Inc.; Natick, MA). Stiffness (k, N/mm) was determined by calculating the slope of the load-displacement curve in the elastic region. Ultimate load (N) designated the largest force achieved throughout the test. Data were processed post hoc using a custom-written Matlab program (version 7.12.0, The MathWorks, Inc.) to generate outcomes using force-displacement curves. In addition to outcomes described above, energy absorbed (N·mm) was determined as the area under the entire load-displacement curve. From classical

beam bending theory, elastic modulus (E, GPa) was obtained using the equation E = (k·S3) / (48·CSMI·1000), where S = support span distance (10 mm).

Femoral neck

Excised right proximal femurs were saved in PBS-soaked gauze at -18°C. An axial loading compression test was used to load the femoral neck until failure. Each proximal femur (generated after the 3-point bending test to failure), was stabilized with the diaphysis portion of the bone firmly inserted into a metal support and the shaft of the femur oriented vertically (Figure 2.5). The load was applied to the tip of the femoral head parallel to the femoral shaft long axis at a rate of 2.54 mm/min. Ultimate load (N) was derived as detailed above. Stiffness and material properties were not derived due to the inconsistent shape of force displacement curves and variable location of the break point.

Histomorphometry

Cortical histomorphometry

Excised, undemineralized distal right tibia, saved at termination in 70% ethanol at 4°C, were dehydrated and embedded in methyl-methacrylate (Sigma-Aldrich M5, 590-9, St. Louis, MO). Serial cross sections (150-200 μm thick) were cut using a diamond wafer low-speed saw (Buehler, Lake Bluff, IL) starting 1mm proximal to the tibia-fibular junction. OsteoMeasure Analysis Software, version 3.3 (Osteo-Metrics, Atlanta, GA) was used to analyze 1 section from

each animal to determine mineralizing surface/total bone surface (%MS/BS) and mineral apposition rate (MAR, in u/day); bone formation rate (BFR) was calculated as MS/BS * MAR. Histomorphometric analyses and nomenclature follow the standardizations as defined previously (Dempster et al., 2013). If sections did not have double label present they remained as zeros and in text were identified as missing double label in accordance with published guidelines (Recker et al., 2011).

Mid-shaft tibial cortical thickness (Ct. Th) was determined using OsteoMeasure image analysis of a cross section (150-200 μm thick), which is an automated output conducted by calculating the distance between the parameter of the endocortical and periosteal surfaces of the bone.

Cancellous histomorphometry

For these measures, undemineralized right distal femurs saved at termination in 70% ethanol at 4°C were serially dehydrated and embedded in methyl methacrylate (Aldrich M5, 590-9, St. Louis, MO, USA). Serial frontal sections were cut 8-μm thick and left unstained for fluorochrome label measurements. Additionally, 4-μm-thick sections were treated with von Kossa stain and tetrachrome counterstain to measure osteoid surface, osteoid volume, number of osteoclasts divided by total area and osteoclast surfaces as a percent of total cancellous surface. The histomorphometric analyses were performed using the OsteoMeasure Analysis System, Version 3.3 (OsteoMetrics, Inc., Atlanta, GA, USA). A defined region of interest was established approximately 500 μm from the growth plate and within the endocortical edges, encompassing approximately 1 mm^2 at 200 × magnification. Total bone surface (BS), single-labeled surface,

double-labeled surface, and interlabel distances (to compute MAR in um/day) were measured at 200× magnification, while osteoid and osteoclast surfaces were measured at 400× magnification. Two sections from each sample were analyzed and averaged to achieve the reported values. If in both sections there was no double label found, the value for MAR was accepted as zero and in text reported as missing double label in accordance with published guidelines (Recker et al., 2011). All nomenclature for cancellous histomorphometry follows standard usage (Dempster et al., 2013).

Statistical analysis

All data are presented as mean ± standard deviation of the mean (SD) and were evaluated for differences using SPSS (IBM, version 23). Percent change values are expressed in terms of the difference between mean values. Outliers were detected and removed using SPSS program, which identifies outliers first by calculating the interquartile range, multiplying it by 1.5, adding this value to the top of the interquartile range and subtracting this value from the bottom of the interquartile range to obtain the boundaries of acceptable values. Any value outside this range was deemed an outlier. A two factor ANOVA, for CIRR and HU, was used for all normally distributed data in this paper; significant main and interaction effects are reported for these analyses in each age. Post-hoc pairwise comparisons were made using Duncan's test. For groups with data not normally distributed, a Kruskal-Wallis ANOVA was performed with significant pairwise comparisons reported; main effects for these tests cannot be assessed. Significance was accepted at $p<0.05$. The use of an ANCOVA, to covary for body weight, was considered for this data set given the differences in body weight amongst animals; however, when ANCOVAs were

assessed for these data there were no changes in the statistics between the ANOVA and the ANCOVA. Therefore, we chose to use true values and not values adjusted for body weight. To compare the size of each effect in adult and middle-aged animals some measures were transformed. These transformation values are reported in Table 3.5. In Tables 3.2-3.4 a comparison of effect sizes, by partial eta squared of each design parameter, is reported with a moderate effect being considered at a >0.09 level and a large effect being considered at a >0.25 level by Cohn standard.

3.3 Results

Body mass and composition was more affected by HU than CIRR

Body mass at termination was not significantly different amongst groups in the adult animals. By contrast, in the middle-aged mice, body mass was 31% lower in MA+SHAM+HU compared to MA+SHAM+WB, an effect which was conserved in CIRR groups (Figure 3.1). In body mass, the effect sizes for HU were large in middle-aged animals and moderate in adult animals (Table 3.2). Total body bone mineral density (BMD) was 9% lower in A-SHAM-HU animals compared to A+SHAM+WB animals (Figure 3.2). Total body BMD in MA+CIRR+WB group was 12% higher than MA+SHAM+WB (p=0.001; not normally distributed). There was a moderate effect of HU on total body BMD in middle-aged animals and a large effect in adult animals. Total body lean mass was 15% lower in A+CIRR+HU compared to A+CIRR+WB. In middle-aged animals there were no differences in total body lean mass. In total body fat mass the A+CIRR+HU group was 38% lower than A+CIRR+WB (p=0.001; not normally distributed). In

total body fat mass MA+SHAM+HU was 3 times lower than MA+SHAM+WB (p=0.001; not normally distributed). Total body mass, BMD, lean and fat mass were more impacted by HU than CIRR, resulting in losses in most parameters in HU groups. Interactions between CIRR and HU in adult mice led to lower total body lean and fat mass in the CIRR+HU mice compared to CIRR+WB.

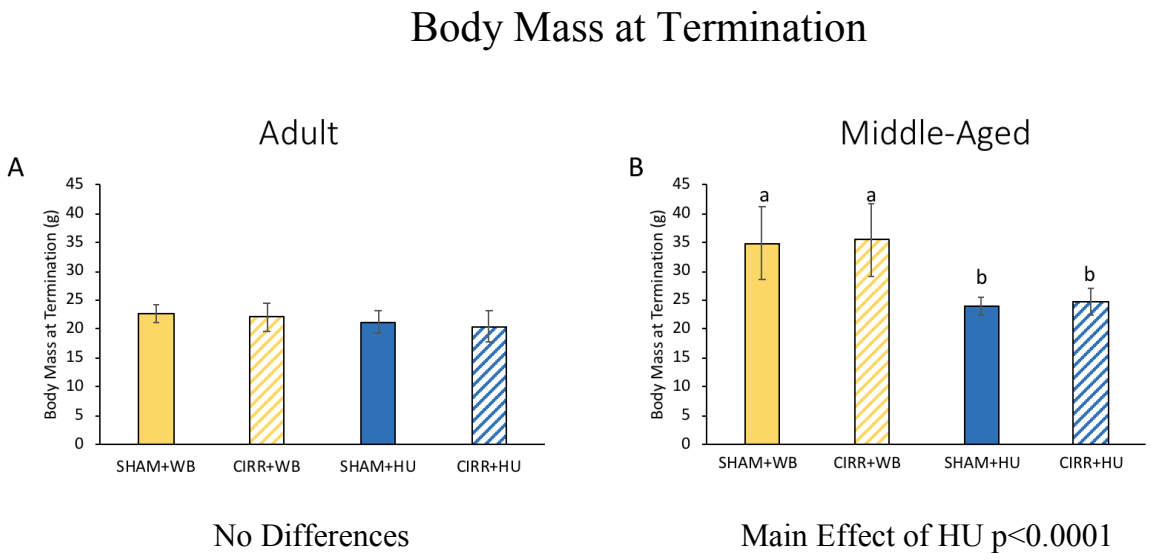

Figure 3.1 Body weight at termination. Data are mean ± standard deviation. In A) adult aged animals age 25 wks and B) middle-aged animals age 52 wks. Bars sharing the same superscript letter are not statistically different by 2-way ANOVA within each age group. Significance was accepted at $p<0.05$. Solid bars represent SHAM animals and hashed bars represent CIRR animals. SHAM-WB = normal weightbearing with no radiation, CIRR-WB = normal weightbearing with continuous low-dose-rate radiation, SHAM-HU = hindlimb unloading with no radiation, and CIRR-HU = hindlimb unloading with continuous low-dose-rate radiation.

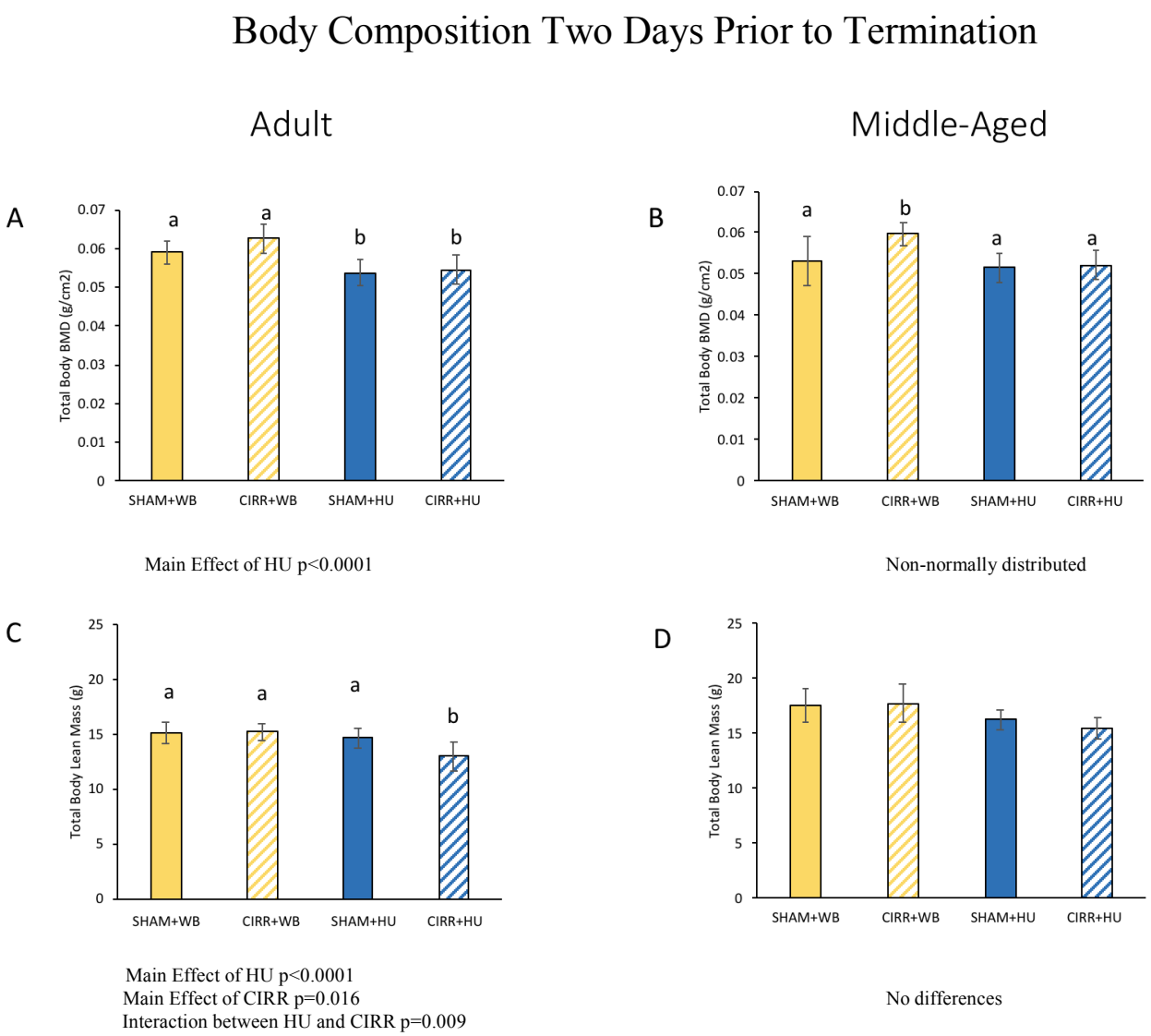

Figure 3.2 Total body bone mineral density (BMD), lean mass and fat mass. Data are mean ± standard deviation. A) adult BMD. B) middle-aged BMD. C) adult lean mass. D) middle-aged lean mass. E) adult fat mass. F) middle-aged fat mass. Bars sharing the same superscript letter are not statistically different by 2-way ANOVA amongst each age for normally distributed data (A, C, D); for non-normally distributed data a 2-way Kruskal-Wallis ANOVA was run (B,E,F). Significance was accepted at $p<0.05$. Solid bars represent SHAM animals and hashed bars represent CIRR animals. SHAM-WB = normal weightbearing with no radiation, CIRR-WB = normal weightbearing with continuous low-dose-rate radiation, SHAM-HU = hindlimb unloading with no radiation, and CIRR-HU = hindlimb unloading with continuous low-dose-rate radiation.

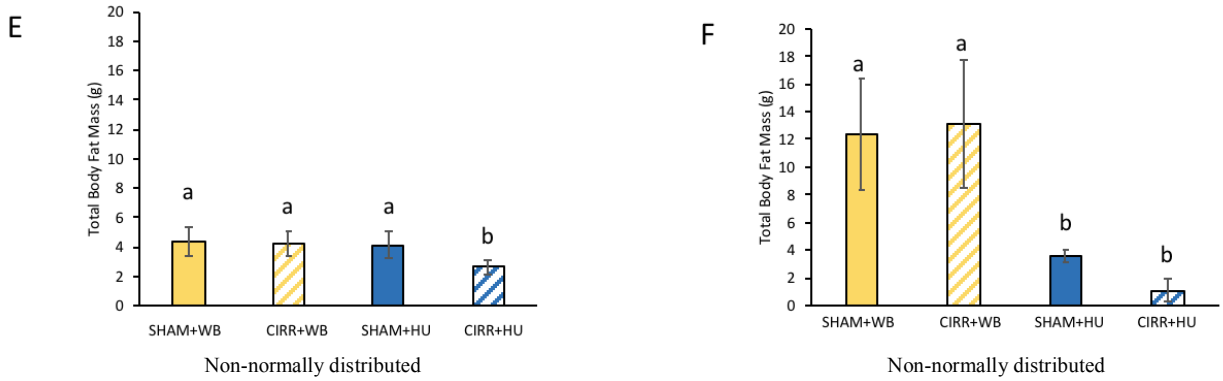

Figure 3.2 Continued.

Alterations in cancellous bone mass and microarchitecture were greater in adult mice than in middle-aged animals

There was a 28% lower bone volume (BV/TV) in A+CIRR+HU compared to A+CIRR+WB (Figure 3.3). There was an 11% lower trabecular thickness (Tb. Th) in A+CIRR+HU compared to A+CIRR+WB. Trabecular number (Tb. N) was an 18% lower in A+CIRR+HU compared to A+CIRR+WB. Therefore, the impact of HU becomes significant only in the presence of CIRR. There were no differences in trabecular spacing amongst groups in adult animals. There were no differences in any measures of cancellous bone volume or microarchitecture among groups of middle-aged animals. By contrast in adults the combination of HU and CIRR resulted in lower BV/TV and decrements in Tb. Th and Tb. N.

In midshaft tibial bone, cortical thickness was 27% lower in A+CIRR+HU compared to A+CIRR+WB though there was no difference between A+SHAM+WB and A+CIRR+HU ($p=0.023$; not normally distributed; Figure 3.4). In middle-aged animals cortical thickness was

13% lower in MA+SHAM+HU and MA+SHAM+CIRR as compared to MA+SHAM+WB. In adult animals there were large effect sizes of both the HU and the CIRR effect, while in middle-aged animals there was only a large effect size due to HU.

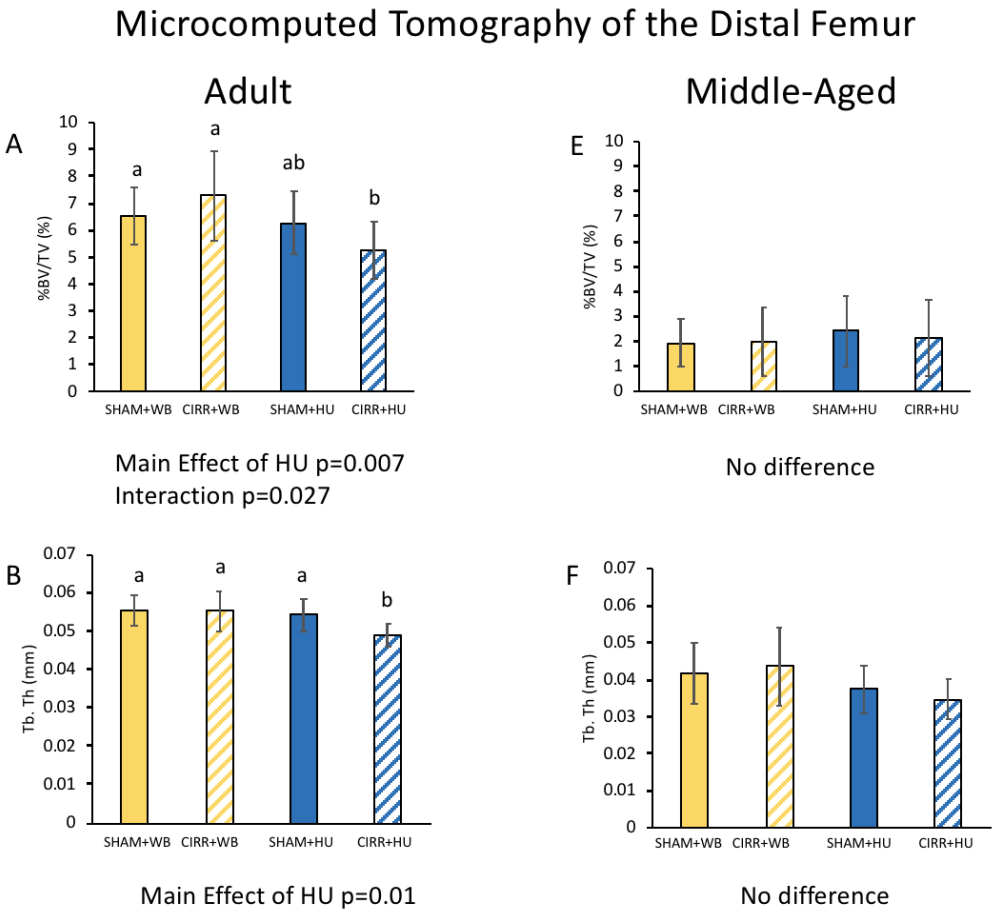

Figure 3.3 Micro-CT of the distal femur in adult and middle-aged animals. Data are mean ± standard deviation. Bone volume (%BV/TV) in adult (A) and middle-aged (E) animals; trabecular thickness (Tb. Th) in adult (B) and middle-aged (F) animals; trabecular number (Tb. N) in adult (C) and middle-aged (G) animals; trabecular spacing (Tb. S) in adult (D) and middle-aged (H) animals. Bars sharing the same superscript letter are not statistically different by 2-way ANOVA amongst each age for normally distributed data (A-D & F-H); for not normally distributed data a 2-way Kruskal-Wallis ANOVA was run (E). Significance was accepted at $p<0.05$. Solid bars represent SHAM animals and hashed bars represent CIRR animals. SHAM-WB = normal weightbearing with no radiation, CIRR-WB = normal weightbearing with continuous low-dose-rate radiation, SHAM-HU = hindlimb unloading with no radiation, and CIRR-HU = hindlimb unloading with continuous low-dose-rate radiation.

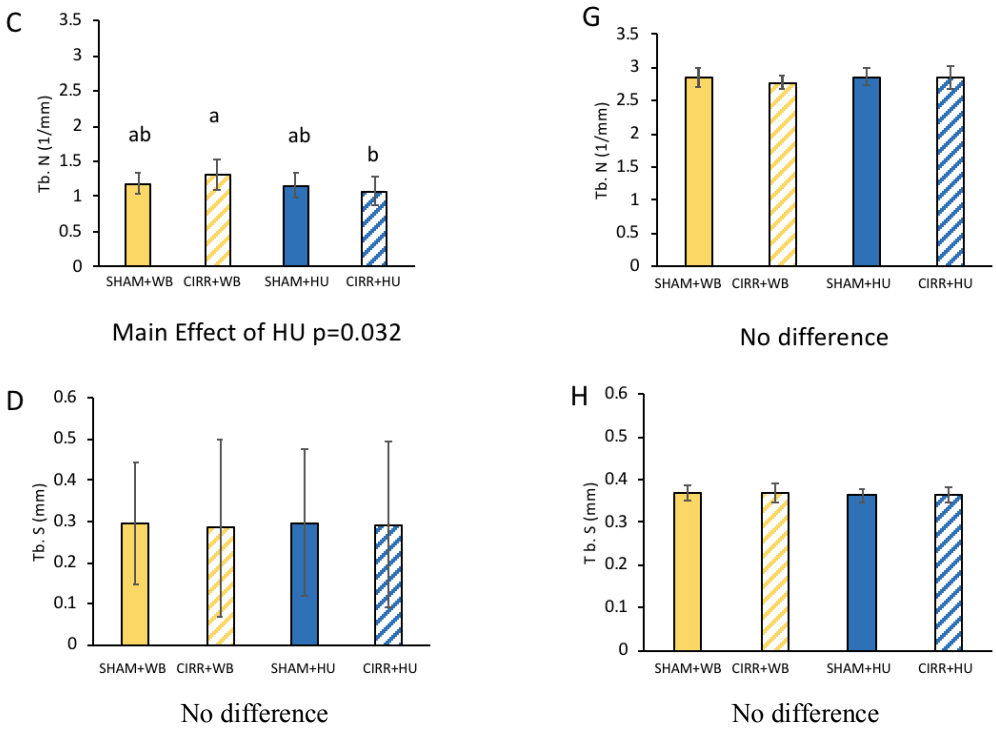

Figure 3.3 Continued.

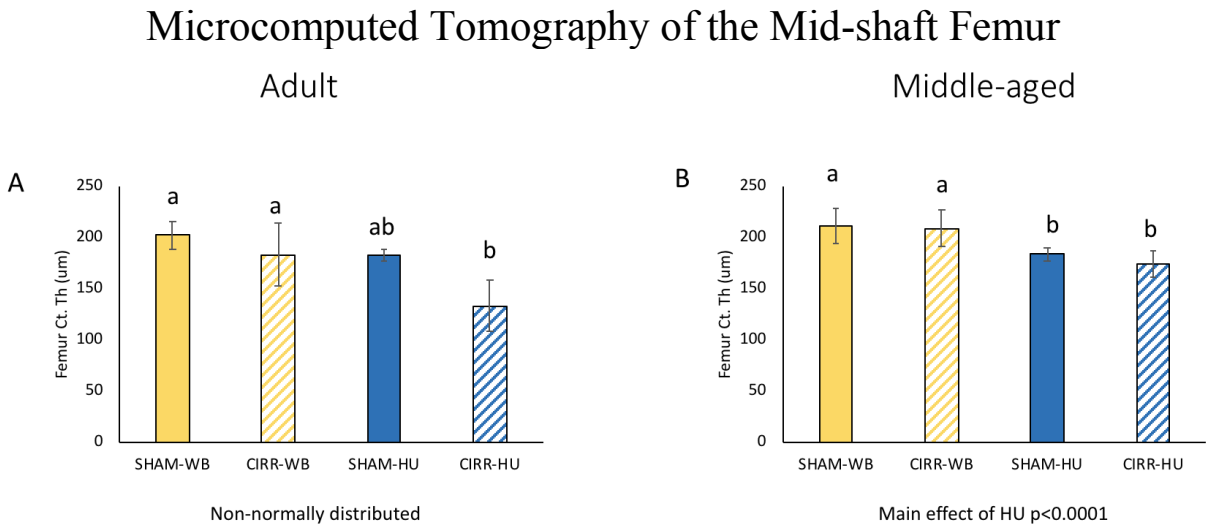

Figure 3.4 Cortical thickness by microcomputed tomography of the mid-shaft femur. Data are mean ± standard deviation. A) Adult animals. B) Middle-aged animals. Bars sharing the same superscript letter are not statistically different by 2-way ANOVA amongst each age for normally distributed data (A); for not normally distributed data a 2-way Kruskal-Wallis ANOVA was run (B). Significance was accepted at $p<0.05$. Solid bars represent SHAM animals and hashed bars represent CIRR animals. SHAM-WB = normal weightbearing with no radiation, CIRR-WB = normal weightbearing with continuous low-dose-rate radiation, SHAM-HU = hindlimb unloading with no radiation, and CIRR-HU = hindlimb unloading with continuous low-dose-rate radiation.

Older animals exhibited greater decrements in bone mechanical properties with CIRR and/or HU

In adult animals, there were no differences in ultimate load, stiffness or energy to ultimate load at the mid-shaft tibia among groups exposed to CIRR and/or HU. By contrast, in middle-aged animals, ultimate load was 13% lower in MA+CIRR+HU compared to MA+SHAM+HU which was 10% lower compared to MA+SHAM+WB (Figure 3.5). Stiffness was 16% lower in MA+SHAM+HU compared to MA+SHAM+WB. There was a 15% lower yield force in A+SHAM+HU compared to A+CIRR+HU. Yield force was 17% lower in

MA+CIRR+HU compared to MA+SHAM+HU, which was 10% lower compared to MA+SHAM+WB. However, only MA+CIRR+HU mice exhibited a lower (-33%) energy to ultimate load; HU exposure alone did not result in a significantly lower value compared to that of WB mice. In a mixed bone site (femoral neck), adult animals exhibited a 23% lower ultimate load in A+CIRR+HU compared to A+CIRR+WB (Figure 3.6, not normally distributed, $p=0.015$). Femoral neck ultimate load was 31% lower in MA+CIRR+HU compared to MA+CIRR+WB. Taken together, these results indicate that bone strength in the cortical bone (tibial diaphysis) was more affected by CIRR and/or HU in middle-aged animals compared to adult animals. There were consistent effects of HU reducing parameters of mechanical strength, with occasional additional impact of CIRR in HU mice. In the femoral neck, a mixed bone site, the CIRR+HU group in adults and middle-aged animals was similarly lower than the CIRR+WB group, though there was no significant difference between the SHAM+WB and SHAM+HU groups at either age.

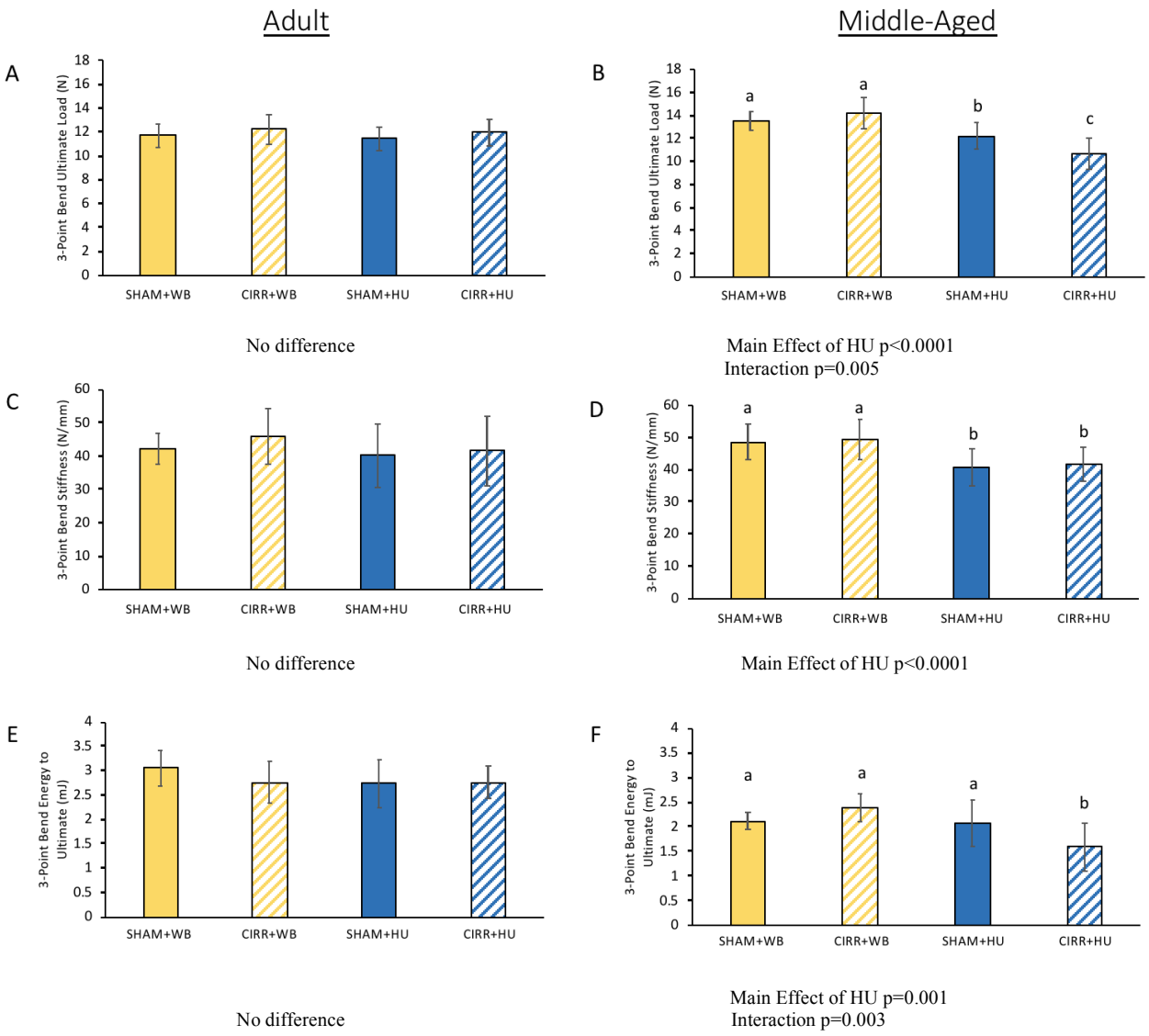

Figure 3.5 Mechanical testing results of a 3-point bend test of the tibia. Data are mean ± standard deviation. Ultimate load in adult animals (A) and middle-aged animals (B), stiffness in adult animals (C) and middle-aged animals (D), energy to ultimate in adult animals (E) and middle-aged animals (F), and yield force in adult animals (G) and middle-aged animals (H). Bars sharing the same superscript letter are not statistically different by 2-way ANOVA amongst each age, all data was normally distributed. Significance was accepted at $p<0.05$. Solid bars represent SHAM animals and hashed bars represent CIRR animals. SHAM-WB = normal weightbearing with no radiation, CIRR-WB = normal weightbearing with continuous low-dose-rate radiation, SHAM-HU = hindlimb unloading with no radiation, and CIRR-HU = hindlimb unloading with continuous low-dose-rate radiation.

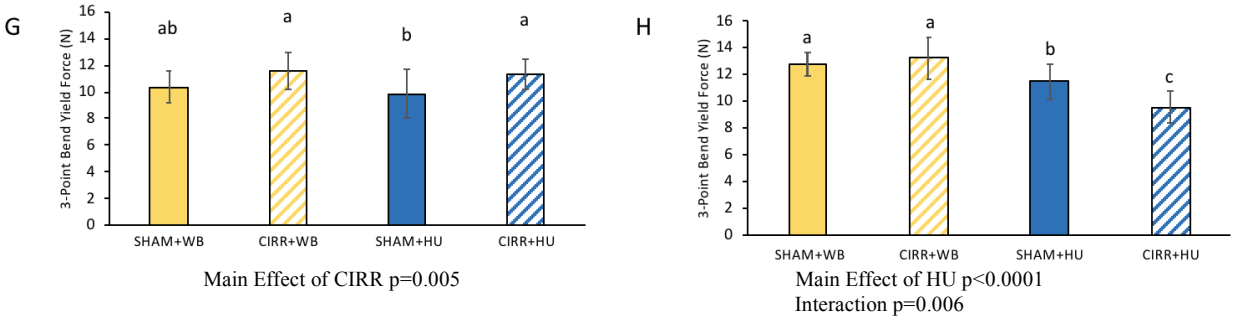

Figure 3.5 Continued.

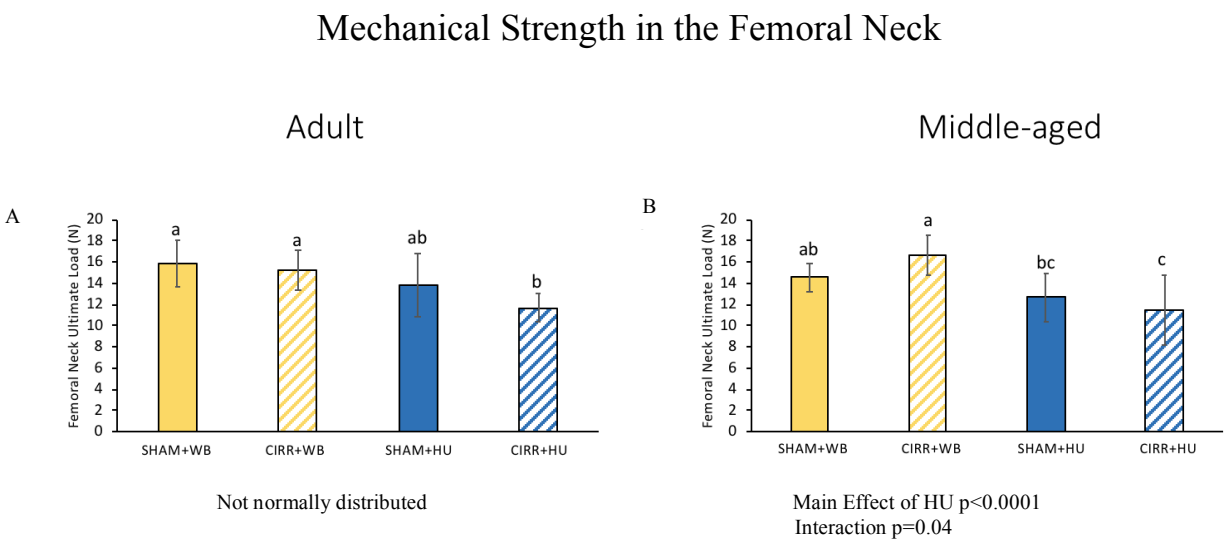

Figure 3.6 Mechanical testing results of an ultimate load test of the femoral neck. Data are mean ± standard deviation. Ultimate load in adult animals (A) and middle-aged animals (B). Bars sharing the same superscript letter are not statistically different by 2-way ANOVA amongst each age, all data was normally distributed. Significance was accepted at $p<0.05$. Solid bars represent SHAM animals and hashed bars represent CIRR animals. SHAM-WB = normal weightbearing with no radiation, CIRR-WB = normal weightbearing with continuous low-dose-rate radiation, SHAM-HU = hindlimb unloading with no radiation, and CIRR-HU = hindlimb unloading with continuous low-dose-rate radiation.

Histomorphometry

In cancellous bone there were seven samples with no double fluorochrome labels, with no more than three specimens missing double labels in any one group. Though there were missing double labels on the endocortical surface, we were able to detect double label in a sufficient number of samples (>3) in every group. We were not able to detect consistent periosteal label in middle-aged animals and double label in only one animal in the whole study on the periosteal surface; therefore, we do not report periosteal data for MS/BS, MAR and BFR in either adult or middle-aged animals.

There were no significant differences in histomorphometric measures of distal femur cancellous bone and the mid-shaft tibia cortical bone in adult or middle-aged animals with CIRR and/or HU (Table 3.1). However, in adults, mineralizing surface on the endocortical surface was two-fold greater in all CIRR animals compared to all SHAM animals, though it was only a trend ($p=0.06$). There were no significant differences in histomorphometric measures on this bone surface in middle-aged animals.

Cortical thickness in the mid-shaft tibia of adult animals was 44% lower in A+CIRR+HU compared to A+CIRR+WB (Figure 3.7). Cortical thickness at the mid-shaft tibia of middle-aged animals was 70% lower in A+CIRR+HU compared to A+CIRR+WB.

Age		Adult				Middle-Aged			
Group		SHAM+WB	CIRR+WB	SHAM+HU	CIRR+HU	SHAM+WB	CIRR+WB	SHAM+HU	CIRR+HU
Distal Femur	MS/BS (%)	4.72 ± 1.27	7.45 ± 4.10	3.53 ± 1.85	5.98 ± 2.38	13.2 ± 8.86	10.2 ± 5.23	9.94 ± 4.97	15.3 ± 8.80
	MAR (um/d)	0.31 ± 0.17	0.94 ± 0.80	0.38 ± 0.38	0.52 ± 0.36	1.14 ± 0.93	0.75 ± 0.36	1.07 ± 0.77	1.25 ± 1.14
	BFR ($um^3/um^2/d$)	0.02 ± 0.01	0.08 ± 0.08	0.02 ± 0.02	0.04 ± 0.03	0.13 ± 0.13	0.09 ± 0.06	0.14 ± 0.14	0.11 ± 0.07
	Number of Animals Missing Double Label	1 of 10	1 of 10	3 of 10	0 of 9	1 of 7	1 of 11	0 of 9	0 of 7
	Osteoclast Surface (%)	0.30 ± 0.29	0.45 ± 0.20	0.40 ± 0.40	0.48 ± 0.46	0.11 ± 0.13	0.17 ± 0.22	0.35 ± 0.35	0.38 ± 0.29
	Osteoid Surface (%)	1.31 ± 0.78	2.59 ± 2.29	0.83 ± 0.71	1.55 ± 2.00	1.71 ± 0.79	2.88 ± 2.28	2.27 ± 2.00	2.67 ± 1.86
Midshaft Tibia	Endocortical MS/BS (%)	17.2 ± 5.92	30.1 ± 13.8	15.9 ± 9.19	28.7 ± 17.6	26.3 ± 14.7	20.0 ± 12.9	26.3 ± 10.3	22.0 ± 8.83
	Endocortical MAR (um/d)	0.15 ± 0.18	1.72 ± 2.14	0.60 ± 1.24	1.01 ± 1.13	3.81 ± 5.67	0.93 ± 0.84	0.87 ± 0.77	1.01 ± 0.88
	Endocortical BFR ($um^3/um^2/d$)	0.04 ± 0.07	0.54 ± 0.68	0.17 ± 0.39	0.41 ± 0.48	1.64 ± 3.21	0.26 ± 0.38	0.28 ± 0.37	0.24 ± 0.23
	Number of Animals Missing Double Label	5 of 11	1 of 9	7 of 10	3 of 9	0 of 10	1 of 10	0 of 9	2 of 9

Table 3.1 Distal femur mineralizing surface (MS/BS), mineral apposition rate (MAR), bone formation rate (BFR), osteoclast surface and osteoid surface. Midshaft tibia MS/BS, MAR and BFR are represented on the endocortical surface only. Data are mean ± standard deviation. There were no differences detected between groups by 2-way ANOVA amongst each age. Significance was accepted at $p<0.05$. Solid bars represent SHAM animals and hashed bars represent CIRR animals. A = Adult, MA = Middle-aged, SHAM-WB = normal weightbearing with no radiation, CIRR-WB = normal weightbearing with continuous low-dose-rate radiation, SHAM-HU = hindlimb unloading with no radiation, and CIRR-HU = hindlimb unloading with continuous low-dose-rate radiation.

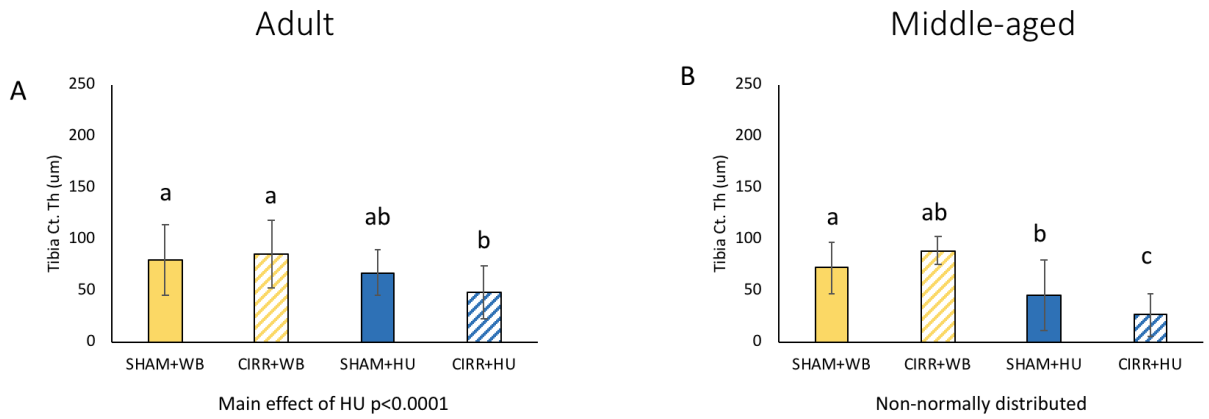

Figure 3.7 Cortical thickness by histological analysis of the mid-shaft tibia. Data are mean ± standard deviation. A) Adult animals. B) Middle-aged animals. Bars sharing the same superscript letter are not statistically different by 2-way ANOVA amongst each age for normally distributed data (B); for not normally distributed data a 2-way Kruskal-Wallis ANOVA was run (A). Significance was accepted at $p<0.05$. Solid bars represent SHAM animals and hashed bars represent CIRR animals. SHAM-WB = normal weightbearing with no radiation, CIRR-WB = normal weightbearing with continuous low-dose-rate radiation, SHAM-HU = hindlimb unloading with no radiation, and CIRR-HU = hindlimb unloading with continuous low-dose-rate radiation.

Measure	Effect	Adult	Middle-Aged
Body Mass	CIRR	0.03	0.00
	HU	0.12	0.59
	CIRR*HU	0.00	0.00
Total Body Bone Mineral Density	CIRR	0.10	0.17
	HU	0.50	0.23
	CIRR*HU	0.05	0.12
Total Body Lean Mass	CIRR	0.15	0.00
	HU	0.35	0.30
	CIRR*HU	0.18	0.03
Total Body Fat Mass	CIRR	No Acceptable Transformation	0.02
	HU		0.25
	CIRR*HU		0.01
Distal Femur Cancellous Bone Volume	CIRR	0.01	0.01
	HU	0.22	0.01
	CIRR*HU	0.14	0.00
Distal Femur Cancellous Trabecular Thickness	CIRR	0.11	0.00
	HU	0.19	0.16
	CIRR*HU	0.10	0.02
Distal Femur Cancellous Trabecular Spacing	CIRR	0.06	0.00
	HU	.02	0.01
	CIRR*HU	0.00	0.00
Distal Femur Cancellous Trabecular Number	CIRR	0.00	0.00
	HU	0.15	0.00
	CIRR*HU	0.10	0.00
Mid-shaft Femur Cortical Thickness	CIRR	0.30	0.06
	HU	0.39	0.58
	CIRR*HU	0.15	0.023
Mid-shaft Tibia Cortical Thickness	CIRR	0.01	0.01
	HU	0.17	0.53
	CIRR*HU	0.05	0.18

Table 3.2 Effect size comparisons for structural data. Comparisons are made between adult and middle-aged animals. Boxes highlighted in yellow represent a moderate effect size (>0.09) and boxes highlighted in green represent a large effect size (>0.25).

Measure	Effect	Adult	Middle-Aged
Three Point Bend Ultimate Load	CIRR	0.06	0.04
	HU	0.17	0.54
	CIRR*HU	0.00	0.20
Three Point Bend Yield Force	CIRR	0.20	0.09
	HU	0.02	0.51
	CIRR*HU	0.00	0.19
Three Point Bend Energy to Ultimate Load	CIRR	0.03	0.02
	HU	0.04	0.26
	CIRR*HU	0.041	0.22
Three Point Bend Stiffness	CIRR	0.03	0.00
	HU	0.04	0.34
	CIRR*HU	0.01	0.00
Femoral Neck Ultimate Load	CIRR	0.11	0.01
	HU	0.34	0.39
	CIRR*HU	0.04	0.13

Table 3.3 Effect size comparisons for mechanical testing data. Comparisons are made between adult and middle-aged animals. Boxes highlighted in yellow represent a moderate effect (>0.09) and boxes highlighted in green represent a large effect (>0.25).

Measure	Effect	Adult	Middle-Aged
Distal Femur Cancellous Mineralizing Surface/Bone Surface	CIRR	0.10	0.01
	HU	0.02	0.01
	CIRR*HU	0.00	0.09
Distal Femur Cancellous Mineral Apposition Rate	CIRR	0.14	0.01
	HU	0.03	0.02
	CIRR*HU	0.07	0.03
Distal Femur Cancellous Bone Formation Rate	CIRR	0.07	0.03
	HU	0.01	0.01
	CIRR*HU	0.07	0.00
Distal Femur Cancellous Osteoid Surface/Bone Surface	CIRR	0.05	0.01
	HU	0.03	0.17
	CIRR*HU	0.00	0.00
Distal Femur Cancellous Osteoclast Surface/Bone Surface	CIRR	0.07	0.00
	HU	0.01	0.19
	CIRR*HU	0.00	0.00
Mid-shaft Tibia Endocortical Mineralizing Surface/Bone Surface	CIRR	0.15	0.04
	HU	0.01	0.00
	CIRR*HU	0.00	0.00
Mid-shaft Tibia Endocortical Mineral Apposition Rate	CIRR	No Acceptable Transformation	0.00
	HU		0.00
	CIRR*HU		0.04
Mid-shaft Tibia Endocortical Bone Formation Rate	CIRR	0.06	0.00
	HU	0.01	0.00
	CIRR*HU	0.00	0.03

Table 3.4 Effect size comparisons for histomorphometric data. Comparisons are made between adult and middle-aged animals. Boxes highlighted in yellow represent a moderate effect (>0.09); there were no variables for either age of mouse exhibiting a large effect (>0.25).

	Adult					Middle-Aged				
Group	SHAM+WB	CIRR+WB	SHAM+HU	CIRR+HU	Transformation Method	SHAM+WB	CIRR+WB	SHAM+HU	CIRR+HU	Transformation Method
Cancellous BV/TV						0.37 ± 0.47	0.37 ± 0.41	0.28 ± 0.19	0.25 ± 0.27	Log
Femur Ct. Th						2.32 ± 0.03[a]	2.32 ± 0.03[a]	2.26 ± 0.02[b]	2.25 ± 0.04[b]	Log
BMD						-1.28 ± 0.05[a]	-1.22 ± 0.02[b]	-1.29 ± 0.03[a]	-1.26 ±0.02[a]	Log
Fat Mass						3.36 ± 0.75[a]	3.15 ± 0.71[ab]	2.17 ± 0.60[bc]	2.85 ± 0.76[c]	Square Root
Cancellous MS/BS	1.51 ± 0.31	1.79 ± 0.77	1.30 ± 0.62	1.72 ± 0.37	Natural Log					
Cancellous BFR	-1.81 ± 0.27	-1.22 ± 0.90	-1.59 ± 0.40	-1.59 ± 0.47	Log					
Cancellous OS/BS	0.02 ± 0.33	0.18 ± 0.57	-0.17 ± 0.42	0.07 ± 0.47	Log					
Cancellous Ocs/BS	0.48 ± 0.26	0.65 ± 0.17	0.55 ± 0.32	0.66 ± 0.31	Square Root	-0.70 ± 0.18	-0.62 ± 0.29	-0.41 ± 0.37	-0.42 ± 0.33	Log
Endocortical MS/BS	4.39 ± 0.92	5.43 ± 1.19	3.81 ± 1.11	4.42 ±2.05	Square Root					
Endocrotical MAR						0.05 ± 0.87	-0.10 ± 0.35	-0.20 ± 0.37	0.05 ± 0.25	Log
Endocortical BFR	-0.96 ± 0.62	-0.55 ± 0.64	-0.76 ± 1.19	-0.52 ±0.70	Log	-0.58 ± 1.08	-0.85 ± 0.60	-0.80 ±0.48	-0.59 ± 0.32	Log

Table 3.5 Means and standard deviations for data transformations in applicable measures. Columns sharing the same superscript letter are not statistically different by 2-way ANOVA. Significance was accepted at $p<0.05$. SHAM-WB = normal weightbearing with no radiation, CIRR-WB = normal weightbearing with continuous low-dose-rate radiation, SHAM-HU = hindlimb unloading with no radiation, and CIRR-HU = hindlimb unloading with continuous low-dose-rate radiation.

3.4 Discussion

The primary findings of this experiment are first, there were few effects of CIRR alone, except that it increased bone mass in middle-aged animals only. There were stronger effects of HU on body mass and cortical bone mass in middle-aged animals. There were strong combined effects of HU on cancellous bone in adult animals but no effects in middle-aged animals. In adult animals there were reductions in mechanical parameters due to HU alone; however, in middle-aged animals there were only reductions in bone mechanical parameters in combination with CIRR and HU. In total these results suggest that the effects of HU are stronger than the effects of CIRR and that adult and middle-aged animals respond to both HU and CIRR differently. Though the effects of HU alone are great, the combination between HU and CIRR was most detrimental to bone structure and mechanical parameters.

Previously, studies in adult animals have shown a reduction in bone mineral density, lean mass and fat mass with hindlimb unloading (Fluckey et al., 2002; B. Smith et al., 2005; Wade et al., 2013). There have been several studies comparing the response to hindlimb unloading (HU) in mature 6-month-old rats to that in senescent 30- to 32-month-old rats (Brown & Taylor, 2005; Perrien et al., 2007; Siu et al., 2005). Perrien *et al.* found that cancellous bone volume and microarchitecture in the proximal tibia were decreased by HU only in mature rats and not in senescent ones. By contrast, HU decreased cortical bone mineral density and increased cortical porosity in senescent rats only (Perrien et al., 2007). Our results in adult animals are consistent with previous studies in some respects, as we found that there was lower total body BMD. Though non-significant losses in bone structure due to HU were found we do not report losses as

extreme as those previously found with adult HU animals. This is in spite of a large effect size of HU in adult animals. This is because the HU described in adult animals only is the same as the sedentary animals from chapter two, therefore, these animals experienced interrupted HU, with 75 minutes of weightbearing per day. We did not find any reductions in bone mineral density in our older middle-aged animals despite dramatically lower body weight and fat mass losses with HU, consistent with previous studies. This is likely because animals at this age have already experienced age-related bone loss and therefore have less bone at baseline left to lose in the event of disuse. The effect size of the HU effect in body mass of middle-aged animals was large while there was only a moderate effect in adult animals. Additionally, we report a differential response to HU amongst adult and middle-aged animals in that there were greater reductions in body weight, fat mass and mechanical properties with HU in middle-aged animals.

Reductions in mechanical property outcomes with HU were greater in middle-aged animals than adult animals in three-point bending to failure, cortical bone only site, evidenced by larger effect sizes in middle-aged animals compared to adult animals. This effect is partially associated with losses in tibia cortical thickness, though both MA+SHAM+HU and MA+CIRR+HU were lower than WB groups. However, in another bone site, a main effect of HU leading to lower femur cortical thickness corresponds with the mechanical testing outcomes in the tibia. Reductions in mechanical properties with HU in middle-aged animals suggest that the bone's ability to resist mechanical failure is reduced and signifies that the bone is less resistant to fracture. Mechanical changes are normally highly correlated with BMD, however; in this situation we do not show that it is based on reductions in mechanical outcomes in middle-aged animals though they had greater cortical bone mass, suggesting that this is a reflection of reduced fracture toughness (Hernandez & van der Meulen, 2017).

Previous studies assessing the effects of acute radiation on bone in adult animals have found decrements in bone volume and structural quality following exposure to various doses of radiation (J. Alwood et al., 2010; Joshua S Alwood et al., 2012; Eric R Bandstra et al., 2009; Boyle et al., 2003; Green et al., 2012; Havaki et al., 2015; Shane A Lloyd et al., 2012). Much of the previous literature examines radiation doses and dose rates higher than those examined in this study (Akkus et al., 2005; J. Alwood et al., 2010; Willey et al., 2008; Wright et al., 2015). Previously, studies have found decrements in bone volume (from 14 to 41%) and structural quality following radiation exposure to various ions and doses (J. Alwood et al., 2010; Joshua S Alwood et al., 2012; Eric R Bandstra et al., 2009; Green et al., 2012; Shane A Lloyd et al., 2012). After exposure to 1 Gy of proton radiation there was a 20% loss of cancellous bone volume fraction in the tibia and femur and no effect on the cortical bone of skeletally mature mice (Shane A Lloyd et al., 2012). Even smaller doses (0.18 Gy of [type of radiation]) delivered to the proximal tibia lead to lower cancellous bone volume fraction and impaired microarchitecture in adult mice (Eric R Bandstra et al., 2009). Finally, some studies have demonstrated no effect of radiation and one found a positive effect of radiation. Head-only irradiation resulted in a 4.4 cGy dose of ^{56}Fe radiation being delivered to the femur in mice leading to a 51% greater cancellous bone volume when measured 11.5 months after radiation exposure (Karim & Judex, 2014). Previous literature suggests a varied response to radiation exposure at different doses, ions and timepoints.

Few studies have investigated the effects of continuous low dose-rate radiation on bone. Given that spaceflight travel outside of low Earth orbit for 3 years is expected to deliver no more than 600 mGy-1 Gy of radiation, our low dose of 0.175 Gy over 28 days is relevant to the GCR

which could be encountered on future missions (Hassler et al., 2014; McGirl et al., 2015). To my knowledge there are no previous studies comparing the effects of continuous low-dose-rate radiation on bone in adult and middle-aged animals. One study has examined the effects of radiation delivered in a similar manner as that of our study, continuously over time. This study delivered a total dose that was 10-fold higher (1.7 Gy) than ours (0.175 Gy) and reported no effects of radiation alone on bone structural outcomes of microcomputed tomography (Yu et al., 2017). In our study we found, similarly, that there were minimal or slightly positive effects of continuous low-dose-rate radiation in this study in our adult mice. Endocortical mineralizing surface was 2-fold greater, though not significantly so, in adult CIRR mice compared to their sham counterparts. Middle-aged animals had improved total body bone mineral density following 28 days of CIRR exposure. Our histomorphometry measures could not detect cell-based alterations in bone formation/resorption indices to explain why this occurred in middle-aged animals; however, it is possible that earlier in the radiation period there was an increase in mineralization, as found later in adult animals. It is also possible that the increases in total body BMD reported in middle-aged animals are reflected in other parts of the skeleton not closely examined in this study. These results suggest that exposure to continuous low-dose-rate gamma radiation alone exerts no detectable negative effects on bone in adult and middle-aged animals.

On future long duration missions astronauts will be exposed to disuse and continuous low-dose-rate radiation (Shane A Lloyd et al., 2012; Macias et al., 2016; Xu et al., 2014; Yumoto et al., 2010). Several previous studies have found an additive effect of radiation exposure and hindlimb unloading (HU) with higher doses of radiation (Shane A Lloyd et al., 2012; Xu et al., 2014). However, with more spaceflight relevant radiation doses, <1 Gy, there are mixed results (J. Alwood et al., 2010; Macias et al., 2016; Yu et al., 2017; Yumoto et al., 2010). Our group

previously found that animals exposed to 3 fractions of 0.17 Gy ^{28}Si found no additive effects of radiation exposure on bone volume in disuse mice. Additionally we found that ultimate load at the femoral neck was significantly affected only by disuse (Macias et al., 2016). Interestingly, when a single dose of 0.5 Gy ^{56}Fe is delivered 3 days prior to the end of a 28 day HU period, rapid cancellous bone loss does occur, likely due to an increase in osteoclast number. This suggests it might be easier to detect the biological effects of radiation if observed closer to the time of exposure rather than after weeks of HU period; a transient increase in osteoclast activity and/or number might be easily missed at later time points.

To my knowledge there is only one other published study investigating the combined effects of continuous low-dose-rate radiation exposure and hindlimb unloading. Continuous low-dose-rate gamma radiation (1.7 Gy) in 16-week-old C57BL/6 females administered simultaneously with HU did not exacerbate the effects of hindlimb suspension, though losses in cortical and cancellous bone typically expected with disuse did occur (Yu et al., 2017). To my knowledge, there are no studies comparing continuous low-dose-rate radiation effects on bone of adult and middle-aged animals also exposed to disuse. In our study, we found that in adult animals the combined effects of CIRR and HU led to significant reductions in total body lean mass, total body fat mass, tibia and femur cortical thickness, femoral neck ultimate loading, cancellous bone volume and decrements in cancellous microarchitecture, consistent with previous studies. However, in middle-aged animals, we record combined effects of CIRR and HU in tibia cortical thickness and several mechanical properties of cortical bone (ultimate load, energy to ultimate and yield force) where there was a reduction beyond MA+SHAM+HU mice. These data suggest that middle-aged animals are protected from the losses due to the combined effects of CIRR and HU on bone mass and femur structure found in adult animals; however, in

absolute terms these older mice may be suffering from lower bone quality leading to reduced fracture resistance in the tibia.

One limitation of this study is that the gamma radiation used in this study, though delivered at the correct dose rate for a Mars mission, represents only a small portion of the expected spectrum of radiation found on a Mars mission. Future studies should attempt to employ a mixed field of radiation which represents multiple parts of the GCR spectrum. This could be achieved by using a mix of sources that emit gamma, alpha and neutron radiation, as all of these are possible to achieve through irradiating specific materials. A final limitation of this study is the use of only female animals. It is possible that there could be sex differences in the response to HU and especially CIRR. Future studies should compare sex specific differences at different ages more appropriate to astronauts. The adult animals from this study are the same mice designated as the sedentary, sham-exposed animals from Chapter 2. Although we report mild losses with HU. they would likely have been greater if HU was not interrupted HU. The difference in age of our animals was problematic in attaining an appropriate interlabel time for fluorochrome label injections. We were able to capture cancellous changes but cortical changes were unable to be adequately assessed. It is possible that using a longer interlabel time for the older animals may have resulted in better results in cortical histomorphometry, though it is equally possible that we would have been unable to capture cancellous changes. Finally, among translational researchers in bone biology it is generally assumed that the bone response to stressors will be similar in any skeletally mature adult animal (at any age older than 4 months) that is not yet in the senescent age range. Our results suggest that this may not be the case and that further studies should consider the utilization of older, “middle-aged” animals.

In conclusion, this study utilizes a unique continuous low dose-rate radiation field which provides an appropriate dose rate for comparison to GCR radiation on a MARS mission. A strength of this study is the comparison between astronaut-aged animals (middle-aged) and the more frequently studied young adult animals. We found that those adult animals experienced expected losses due to HU while middle-aged animals experienced less severe effects of HU. There were minimal effects of CIRR alone and notably an increase in BMD in middle-aged animals and a 2-fold increase in endocortical bone formation rate in adult animals (that did not reach statistical significance). We found that the combined effects of CIRR and HU were the strongest effect in both adult and middle-aged animals. However, there were greater effects in the cancellous bone in adult animals and the cortical bone in middle-aged animals. These results taken together suggest that middle-aged animals are not as negatively affected, in terms of bone structure, by the normally damaging HU and CIRR found in adult animals, but that their bones are more fragile. It is possible that middle-aged animals have already experienced so much age-related bone loss that they do not have as many surfaces on which resorption can happen during HU. It is also possible that, since there were some positive effects of CIRR on BMD, the negative effects of HU and the positive effects of CIRR cancel each other out in middle-aged animals. This study's results illustrate a clear need for further study into the effects of radiation and HU in astronaut-aged animals, as the effects of both stressors vary depending on the age of the animal exposed. If our entire understanding of radiation and HU effects stems from studies conducted in younger animals that have just reached skeletal maturity, it is possible that we may not be capturing results that are relevant to middle-aged astronauts who are long past peak adult bone mass.

4. CONCLUSIONS

In these studies we conclude that continuous low dose-rate radiation has a complex, though not strong, effect by itself but that in combination with HU or iHU results in reduced bone mass and quality. Positive effects of exercise were not hindered by the effects of CIRR. However, exercise was not able to mitigate the combined negative effects of CIRR and iHU. We find that middle-aged animals do not respond the same to the combination of CIRR and HU as adult animals. Our results suggest that middle-aged animals are more resistant to changes from HU and CIRR, likely because they are not rapidly growing and have begun age related bone loss though they are not senescent. In short, we do not find any serious negative effects of CIRR alone but we do record significant impacts when combined with simulated microgravity (hindlimb unloading) which creates concern for bone health in human crew members on spaceflight missions outside of low earth orbit. Further study is also needed to understand a time course of effects in CIRR animals as we were unable to identify a mechanism, possibly because the cellular-mediated changes happen early in the CIRR process.

Our complex results seen with continuous low-dose-rate radiation suggest that we cannot rely on acute radiation studies to accurately represent changes due to prolonged radiation exposure. Therefore, it is important to pursue further investigations to understand the impact of continuous low dose-rate radiation in animals. Although the radiation used in this study was gamma, representing reference radiation and comprising ~50% of the dose from GCR, it is not the only kind of radiation that can be delivered in a continuous manner. It is also possible to deliver alpha particles and neutrons, or perhaps others, in a similar continuous fashion. To do this would be significantly more difficult than creating a gamma radiation field because materials

coming out of a radiation field containing either alpha particles or neutrons are likely to be radioactive and will, therefore, require special disposal and more skilled personnel. Though it is not impossible, it is not surprising that few groups have undertaken such a procedure. These three kinds of radiation should be individually studied for their effects on different tissues, especially bone. Following that, an assessment should be made of a combination of these three different kinds of radiation in a mixed radiation field which proportionally represents the GCR spectrum. Since the GCR spectrum is dominated by alpha particles, ~87%, these should comprise the majority of the field. It is still extremely important to understand the effects of neutrons and gamma radiation, because these are likely to be formed when heavier particles interact with any metallic shielding in the spacecraft.

The assessment of continuous low dose-rate radiation as expressed above would be an excellent start to addressing the real problem of understanding GCR radiation effects. An additional way to understand these effects could be done using particle accelerator facilities, like the NASA Space Radiation Laboratory (NSRL) at Brookhaven National Labs (BNL). Using particle accelerators it is possible to actually assess the appropriate energies expected in space, though the NSRL facility is only able to achieve high enough energies to be relevant behind shielding. The GCR simulator that is proposed to be conducted at BNL's NSRL facility is a good first step but does not address the problem of prolonged exposure. While continuous low-dose-rate radiation is able to deliver the appropriate dose rate, it is not necessarily able to deliver proper energies. One huge limitation that will be experienced at particle accelerators is their inability to deliver the proper dose rate. It would be advisable for a study to be conducted where animals are exposed at the lowest possible achievable dose rate, primarily with major GCR spectrum components, over a period of time (likely representing an entire radiation season at the

facility). This study should be conducted on a large number (hundreds) of animals and tissues should be distributed to trusted scientists for evaluation. A parallel study in continuous low dose-rate radiation could be conducted and the two could be compared. In this way it would be possible to understand how the appropriate dose rates and energies could affect animals. An additional acute radiation group would allow for comparisons to previously published work, allowing for GCR spectrum understanding to utilize the vast data that exists already with previously conducted acute radiation studies.

In this study we only assessed the effects in female animals due to functional and financial restrictions. In future studies it would be wise to assess both males and females in all of the radiation scenarios described above. It is possible that there is a difference in the way that males and females respond to continuous low-dose-rate radiation, as with many other biological responses. One benefit of this study is that we have assessed females; most previously published studies assess males only. Females were chosen because they are generally more robust in handling interventions such as HU and they are better exercisers. Though we chose females for functional reasons, if given the chance, we would have done this study in both males and females.

For this dissertation we used C57Bl6/J mice because they are one of the most common strains of mice and are used in many other radiation studies. However, it would be beneficial to assess the effects of continuous low dose-rate radiation on multiple strains of mice that vary greatly in their radiosensitivity, a measure of their response to acute radiation. Some strains of mice are greatly affected by radiation, while others are not. C57BL6/J mice are relatively radio-resistant on the spectrum of radiosensitivity, though they are not the most radio-resistant. Future experiments assessing the effects of continuous low-dose-rate radiation should examine the

effects of this unique radiation on different strains of mice and compare the effects. It would also be extremely interesting to assess the effects of CIRR in an outbred strain of mice, one that was more heterogeneous and not as inbred as the C57BL6/J mice in the above proposed experiments, because inbred mouse strains do not present as much genetic variability as the human population.

The best possible approach to understanding GCR effects on mammals would be to travel back to the Moon and conduct studies there on GCR effects. The Moon is outside the protection of the Earth's Van Allen Belts and animals on that surface could experience the exact kind of radiation exposure expected on a mission to Mars or beyond. We often view the Moon as an already conquered goal; however, it represents the best option for testing and learning about radiation at a safe distance from our home world. If humans are serious about becoming an interplanetary species, they will spend more time planning missions to understand space close to home before we reach further towards Mars.

REFERENCES

Akkus, O., Belaney, R. M., & Das, P. (2005). Free radical scavenging alleviates the biomechanical impairment of gamma radiation sterilized bone tissue. *Journal of Orthopaedic Research, 23*(4), 838-845.

Alexander, D. J. (2016). Trauma and Surgical Capabilities for Space Exploration *Trauma Team Dynamics* (pp. 253-266): Springer.

Allen, M. R., & Bloomfield, S. A. (2003). Hindlimb unloading has a greater effect on cortical compared with cancellous bone in mature female rats. *Journal of Applied Physiology, 94*(2), 642-650.

Allen, R., & Tresini, M. (2000). Oxidative stress and gene regulation. *Free Radical Biology and Medicine, 28*(3), 463-499.

Alwood, J., Yumoto, K., Mojarrab, R., Limoli, C., Almeida, E., Searby, N., & Globus, R. (2010). Heavy ion irradiation and unloading effects on mouse lumbar vertebral microarchitecture, mechanical properties and tissue stresses. *Bone, 47*(2), 248-255.

Alwood, J. S. (2009). *Radiation and mechanical unloading effects on mouse vertebral bone: Ground-based models of the spaceflight environment*: Stanford University.

Alwood, J. S., Kumar, A., Tran, L. H., Wang, A., Limoli, C. L., & Globus, R. K. (2012). Low-dose, ionizing radiation and age-related changes in skeletal microarchitecture. *Journal of aging research, 2012*.

Alwood, J. S., Shahnazari, M., Chicana, B., Schreurs, A., Kumar, A., Bartolini, A., . . . Globus, R. K. (2015). Ionizing Radiation Stimulates Expression of Pro-Osteoclastogenic Genes in Marrow and Skeletal Tissue. *Journal of Interferon & Cytokine Research*.

Bandstra, E. R. (2008). *The spaceflight environment and the skeletal system.* Clemson University.

Bandstra, E. R., Thompson, R. W., Nelson, G. A., Willey, J. S., Judex, S., Cairns, M. A., . . . Bateman, T. A. (2009). Musculoskeletal changes in mice from 20–50 cGy of simulated galactic cosmic rays. *Radiation research, 172*(1), 21-29.

Baxter, N. N., Habermann, E. B., Tepper, J. E., Durham, S. B., & Virnig, B. A. (2005). Risk of pelvic fractures in older women following pelvic irradiation. *Jama, 294*(20), 2587-2593.

Black, J. M. (2016). *Comparison of the Persisting Effects of Bisphosphonate Treatments Prior to Hindlimb Unloading on Mechanical and Densitometric Properties in the Tibia of Adult Male Rats.* Texas A&M University, MS thesis.

Bloomfield, S., Allen, M., Hogan, H., & Delp, M. (2002). Site-and compartment-specific changes in bone with hindlimb unloading in mature adult rats. *Bone, 31*(1), 149-157.

Bloomfield, S. A., Martinez, D. A., Boudreaux, R. D., & Mantri, A. V. (2016). Microgravity stress: bone and connective tissue. *Comprehensive Physiology*.

Bonewald, L. (2004). Osteocyte biology: its implications for osteoporosis. *Journal of Musculoskeletal and Neuronal Interactions, 4*(1), 101.

Bonewald, L. F. (2011). The amazing osteocyte. *Journal of Bone and Mineral Research, 26*(2), 229-238.

Boudreaux, R., Metzger, C., Macias, B., Shirazi-Fard, Y., Hogan, H., & Bloomfield, S. (2014). Bone loss during partial weight bearing (1/6th gravity) is mitigated by resistance and aerobic exercise in mice. *Acta Astronautica, 99*, 71-77.

Bouxsein, M. L., Boyd, S. K., Christiansen, B. A., Guldberg, R. E., Jepsen, K. J., & Müller, R. (2010). Guidelines for assessment of bone microstructure in rodents using micro–computed tomography. *Journal of Bone and Mineral Research, 25*(7), 1468-1486.

Boyle, W. J., Simonet, W. S., & Lacey, D. L. (2003). Osteoclast differentiation and activation. *Nature, 423*(6937), 337-342.

Braga-Tanaka, I., Tanaka, S., Kohda, A., Takai, D., Nakamura, S., Ono, T., . . . Komura, J.-i. (2018). Experimental studies on the biological effects of chronic low dose-rate radiation exposure in mice: Overview of the studies at Institute for Environmental Sciences. *International journal of radiation biology*(just-accepted), 1-36.

Brenner, D. J., Doll, R., Goodhead, D. T., Hall, E. J., Land, C. E., Little, J. B., . . . Puskin, J. S. (2003). Cancer risks attributable to low doses of ionizing radiation: assessing what we really know. *Proceedings of the National Academy of Sciences, 100*(24), 13761-13766.

Brenner, D. J., Elliston, C. D., Hall, E. J., & Berdon, W. E. (2001). Estimated risks of radiation-induced fatal cancer from pediatric CT. *American journal of roentgenology, 176*(2), 289-296.

Brodt, M. D., Ellis, C. B., & Silva, M. J. (1999). Growing C57Bl/6 mice increase whole bone mechanical properties by increasing geometric and material properties. *Journal of Bone and Mineral Research, 14*(12), 2159-2166.

Brown, M., & Taylor, J. (2005). Prehabilitation and rehabilitation for attenuating hindlimb unweighting effects on skeletal muscle and gait in adult and old rats. *Archives of physical medicine and rehabilitation, 86*(12), 2261-2269.

Burger, E., & Klein-Nulend, J. (1998). Microgravity and bone cell mechanosensitivity. *Bone, 22*(5), 127S-130S.

Burr, D. B., & Allen, M. R. (2013). *Basic and applied bone biology*: Academic Press.

Cavanagh, P. R., Licata, A. A., & Rice, A. J. (2007). Exercise and pharmacological countermeasures for bone loss during longduration space flight. *Gravitational and Space Research, 18*(2).

Cooke, M. S., Evans, M. D., Dizdaroglu, M., & Lunec, J. (2003). Oxidative DNA damage: mechanisms, mutation, and disease. *The FASEB Journal, 17*(10), 1195-1214.

Courneya, K. S., & Friedenreich, C. M. (1999). Physical exercise and quality of life following cancer diagnosis: a literature review. *Annals of Behavioral Medicine, 21*(2), 171-179.

De Lisio, M., Kaczor, J. J., Phan, N., Tarnopolsky, M. A., Boreham, D. R., & Parise, G. (2011). Exercise training enhances the skeletal muscle response to radiation-induced oxidative stress. *Muscle & nerve, 43*(1), 58-64.

Dempster, D. W., Compston, J. E., Drezner, M. K., Glorieux, F. H., Kanis, J. A., Malluche, H., . . . Parfitt, A. M. (2013). Standardized nomenclature, symbols, and units for bone histomorphometry: a 2012 update of the report of the ASBMR Histomorphometry Nomenclature Committee. *Journal of Bone and Mineral Research, 28*(1), 2-17.

Einstein, A. J., Henzlova, M. J., & Rajagopalan, S. (2007). Estimating risk of cancer associated with radiation exposure from 64-slice computed tomography coronary angiography. *Jama, 298*(3), 317-323.

Ferreira, J. A., Crissey, J. M., & Brown, M. (2011). An alternant method to the traditional NASA hindlimb unloading model in mice. *Journal of visualized experiments: JoVE*(49).

Flohé, L., Brigelius-Flohé, R., Saliou, C., Traber, M. G., & Packer, L. (1997). Redox regulation of NF-kappa B activation. *Free Radical Biology and Medicine, 22*(6), 1115-1126.

Fluckey, J., Dupont-Versteegden, E., Montague, D., Knox, M., Tesch, P., Peterson, C., & Gaddy-Kurten, D. (2002). A rat resistance exercise regimen attenuates losses of musculoskeletal mass during hindlimb suspension. *Acta Physiologica, 176*(4), 293-300.

Globus, R. K., & Morey-Holton, E. (2016). Hindlimb unloading: rodent analog for microgravity. *Journal of Applied Physiology, 120*(10), 1196-1206.

Gomes, E. C., Silva, A. N., & Oliveira, M. R. d. (2012). Oxidants, antioxidants, and the beneficial roles of exercise-induced production of reactive species. *Oxidative medicine and cellular longevity, 2012*.

Green, D. E., Adler, B. J., Chan, M. E., & Rubin, C. T. (2012). Devastation of adult stem cell pools by irradiation precedes collapse of trabecular bone quality and quantity. *Journal of Bone and Mineral Research, 27*(4), 749-759.

Hall, E. J., & Giaccia, A. J. (1994). Radiobiology for the Radiobiologist. *Philadelphia, PA: JB Lippencott Company*.

Hallahan, D. E., Spriggs, D. R., Beckett, M. A., Kufe, D. W., & Weichselbaum, R. R. (1989). Increased tumor necrosis factor alpha mRNA after cellular exposure to ionizing radiation. *Proceedings of the National Academy of Sciences, 86*(24), 10104-10107.

Hamilton, S. A., Pecaut, M. J., Gridley, D. S., Travis, N. D., Bandstra, E. R., Willey, J. S., . . . Bateman, T. A. (2006). A murine model for bone loss from therapeutic and space-relevant sources of radiation. *Journal of Applied Physiology, 101*(3), 789-793.

Hassler, D. M., Zeitlin, C., Wimmer-Schweingruber, R. F., Ehresmann, B., Rafkin, S., Eigenbrode, J. L., . . . Böhm, E. (2014). Mars' surface radiation environment measured with the Mars Science Laboratory's Curiosity Rover. *Science, 343*(6169), 1244797.

Havaki, S., Kotsinas, A., Chronopoulos, E., Kletsas, D., Georgakilas, A., & Gorgoulis, V. G. (2015). The role of oxidative DNA damage in radiation induced bystander effect. *Cancer letters, 356*(1), 43-51.

Hayashi, T., Morishita, Y., Kubo, Y., Kusunoki, Y., Hayashi, I., Kasagi, F., . . . Nakachi, K. (2005). Long-term effects of radiation dose on inflammatory markers in atomic bomb survivors. *The American journal of medicine, 118*(1), 83-86.

Hernandez, C. J., & van der Meulen, M. C. (2017). Understanding bone strength is not enough. *Journal of Bone and Mineral Research, 32*(6), 1157-1162.

Hollander, J., Fiebig, R., Gore, M., Ookawara, T., Ohno, H., & Ji, L. (2001). Superoxide dismutase gene expression is activated by a single bout of exercise in rat skeletal muscle. *Pflügers Archiv, 442*(3), 426-434.

Hoshi, A., Watanabe, H., Chiba, M., & Inaba, Y. (1998). Effects of exercise at different ages on bone density and mechanical properties of femoral bone of aged mice. *The Tohoku journal of experimental medicine, 185*(1), 15-24.

Ina, Y., & Sakai, K. (2005). Further study of prolongation of life span associated with immunological modification by chronic low-dose-rate irradiation in MRL-lpr/lpr mice: effects of whole-life irradiation. *Radiation research, 163*(4), 418-423.

Ina, Y., Tanooka, H., Yamada, T., & Sakai, K. (2005). Suppression of thymic lymphoma induction by life-long low-dose-rate irradiation accompanied by immune activation in C57BL/6 mice. *Radiation research, 163*(2), 153-158.

Iura, A., McNerny, E. G., Zhang, Y., Kamiya, N., Tantillo, M., Lynch, M., . . . Mishina, Y. (2015). Mechanical loading synergistically increases trabecular bone volume and improves mechanical properties in the mouse when BMP signaling is specifically ablated in osteoblasts. *PloS one, 10*(10), e0141345.

Ji, L. L. (2002). Exercise-induced modulation of antioxidant defense. *Annals of the New York Academy of Sciences, 959*(1), 82-92.

Ju, Y.-I., Sone, T., Ohnaru, K., Choi, H.-J., & Fukunaga, M. (2012). Differential effects of jump versus running exercise on trabecular architecture during remobilization after suspension-induced osteopenia in growing rats. *Journal of Applied Physiology, 112*(5), 766-772.

Karim, L., & Judex, S. (2014). Low level irradiation in mice can lead to enhanced trabecular bone morphology. *Journal of bone and mineral metabolism, 32*(5), 476-483.

Kondo, H., Yumoto, K., Alwood, J. S., Mojarrab, R., Wang, A., Almeida, E. A., . . . Globus, R. K. (2010). Oxidative stress and gamma radiation-induced cancellous bone loss with musculoskeletal disuse. *Journal of Applied Physiology, 108*(1), 152-161.

Kosniewski, J. L. (2017). *The Efficacy of Bisphosphonate Pre-treatment in Preventing Losses in Densitometric and Mechanical Properties during Hindlimb Unloading and throughout Reambulation in the Distal Femur Metaphysis of Adult Male Rats.*

LeBlanc, A., Schneider, V., Shackelford, L., West, S., Oganov, V., Bakulin, A., & Voronin, L. (2000). Bone mineral and lean tissue loss after long duration space flight. *J Musculoskelet Neuronal Interact, 1*(2), 157-160.

Li, Z., Tan, C., Wu, Y., Ding, Y., Wang, H., Chen, W., . . . Liang, W. (2012). Whole-body vibration and resistance exercise prevent long-term hindlimb unloading-induced bone loss: independent and interactive effects. *European journal of applied physiology, 112*(11), 3743-3753.

Lloyd, S. A., Bandstra, E. R., Travis, N. D., Nelson, G. A., Bourland, J. D., Pecaut, M. J., . . . Bateman, T. A. (2008). Spaceflight-relevant types of ionizing radiation and cortical bone: Potential LET effect? *Advances in Space Research, 42*(12), 1889-1897.

Lloyd, S. A., Bandstra, E. R., Willey, J. S., Riffle, S. E., Tirado-Lee, L., Nelson, G. A., . . . Bateman, T. A. (2012). Effect of proton irradiation followed by hindlimb unloading on bone in mature mice: a model of long-duration spaceflight. *Bone, 51*(4), 756-764.

Lloyd, S. A., Morony, S. E., Ferguson, V. L., Simske, S. J., Stodieck, L. S., Warmington, K. S., . . . Bateman, T. A. (2015). Osteoprotegerin is an effective countermeasure for spaceflight-induced bone loss in mice. *Bone, 81*, 562-572.

Macias, B., Lima, F., Swift, J., Shirazi-Fard, Y., Greene, E., Allen, M., . . . Wang, S. (2016). Simulating the Lunar Environment: Partial Weightbearing and High-LET Radiation-Induce Bone Loss and Increase Sclerostin-Positive Osteocytes. *Radiation research, 186*(3), 254-263.

Manolagas, S. C., & Parfitt, A. M. (2013). For whom the bell tolls: distress signals from long-lived osteocytes and the pathogenesis of metabolic bone diseases. *Bone, 54*(2), 272-278.

McGirl, N., Pawel, A., Schappel, D., Shamblin, J., Younkin, T., & Townsend, L. (2015). *Crew Radiation Exposure Estimates from GCR and SPE Environments During a Hypothetical Mars Mission*.

Meirow, D., & Nugent, D. (2001). The effects of radiotherapy and chemotherapy on female reproduction. *Human reproduction update, 7*(6), 535-543.

Metzger, C. E., Narayanan, A., Zawieja, D. C., & Bloomfield, S. A. (2017). Inflammatory bowel disease in a rodent model alters osteocyte protein levels controlling bone turnover. *Journal of Bone and Mineral Research, 32*(4), 802-813.

Mitchell, M. J., & Logan, P. M. (1998). Radiation-induced changes in bone. *Radiographics, 18*(5), 1125-1136.

Mock, V., Dow, K. H., Meares, C. J., Grimm, P. M., Dienemann, J. A., Haisfield-Wolfe, M. E., . . . Gage, I. (1997). *Effects of exercise on fatigue, physical functioning, and emotional distress during radiation therapy for breast cancer.* Paper presented at the Oncology nursing forum.

Morey-Holton, E. R., & Globus, R. K. (2002). Hindlimb unloading rodent model: technical aspects. *Journal of Applied Physiology, 92*(4), 1367-1377.

Nakajima, T. (2008). Positive and negative regulation of radiation-induced apoptosis by protein kinase C. *Journal of radiation research, 49*(1), 1-8.

Nakajima, T., Wang, B., Ono, T., Uehara, Y., Nakamura, S., Ichinohe, K., . . . Nenoi, M. (2017). Differences in sustained alterations in protein expression between livers of mice exposed to high-dose-rate and low-dose-rate radiation. *Journal of radiation research, 58*(4), 421-429.

Ono, T., Uehara, Y., Okudaira, N., Fujikawa, K., Kagawa, N., Yoshida, M., . . . Oghiso, Y. (2009). Alteration of genome structure induced by very low dose-rate irradiation in mouse tissues. *Data Science Journal, 8*, BR36-BR41.

Perrien, D. S., Akel, N. S., Dupont-Versteegden, E. E., Skinner, R. A., Siegel, E. R., Suva, L. J., & Gaddy, D. (2007). Aging alters the skeletal response to disuse in the rat. *American*

Journal of Physiology-Regulatory, Integrative and Comparative Physiology, 292(2), R988-R996.

Pierce, D. A., & Preston, D. L. (2000). Radiation-related cancer risks at low doses among atomic bomb survivors. *Radiation research, 154*(2), 178-186.

Raab, D. M., Smith, E. L., Crenshaw, T. D., & Thomas, D. P. (1990). Bone mechanical properties after exercise training in young and old rats. *Journal of Applied Physiology, 68*(1), 130-134.

Rabelo, G. D., Beletti, M. E., & Dechichi, P. (2010). Histological analysis of the alterations on cortical bone channels network after radiotherapy: a rabbit study. *Microscopy research and technique, 73*(11), 1015-1018.

Recker, R. R., Kimmel, D., Dempster, D., Weinstein, R., Wronski, T., & Burr, D. B. (2011). Issues in modern bone histomorphometry. *Bone, 49*(5), 955-964.

Robling, A. G., Burr, D. B., & Turner, C. H. (2001). Recovery periods restore mechanosensitivity to dynamically loaded bone. *Journal of Experimental Biology, 204*(19), 3389-3399.

Robling, A. G., Castillo, A. B., & Turner, C. H. (2006). Biomechanical and molecular regulation of bone remodeling. *Annu. Rev. Biomed. Eng., 8*, 455-498.

Robling, A. G., & Turner, C. H. (2002). Mechanotransduction in bone: genetic effects on mechanosensitivity in mice. *Bone, 31*(5), 562-569.

Sakai, K., Nomura, T., & Ina, Y. (2006). Enhancement of bio-protective functions by low dose/dose-rate radiation. *Dose-Response, 4*(4), dose-response. 06-115. Sakai.

Sams, A. (1966). The effect of 2000 r of x-rays on the internal structure of the mouse tibia. *International Journal of Radiation Biology and Related Studies in Physics, Chemistry and Medicine, 11*(1), 51-68.

Saucier, D. H. (2016). *Monte Carlo Irradiation Model For Long-Term Low Dose Environments for Space Life Science Applications.*

Saxena, R., Pan, G., Dohm, E. D., & McDonald, J. M. (2011). Modeled microgravity and hindlimb unloading sensitize osteoclast precursors to RANKL-mediated osteoclastogenesis. *Journal of bone and mineral metabolism, 29*(1), 111-122.

Segal, R. J., Reid, R. D., Courneya, K. S., Sigal, R. J., Kenny, G. P., Prud'Homme, D. G., . . . D'Angelo, M. E. S. (2009). Randomized controlled trial of resistance or aerobic exercise in men receiving radiation therapy for prostate cancer. *Journal of Clinical Oncology, 27*(3), 344-351.

Shahnazari, M., Kurimoto, P., Boudignon, B. M., Orwoll, B. E., Bikle, D. D., & Halloran, B. P. (2012). Simulated spaceflight produces a rapid and sustained loss of osteoprogenitors and an acute but transitory rise of osteoclast precursors in two genetic strains of mice. *American Journal of Physiology-Endocrinology and Metabolism, 303*(11), E1354-E1362.

Shimano, M., & Volpon, J. (2009). Biomechanics and structural adaptations of the rat femur after hindlimb suspension and treadmill running. *Brazilian Journal of Medical and Biological Research, 42*(4), 330-338.

Shirazi-Fard, Y., Alwood, J. S., Schreurs, A.-S., Castillo, A. B., & Globus, R. K. (2015). Mechanical loading causes site-specific anabolic effects on bone following exposure to ionizing radiation. *Bone, 81*, 260-269.

Shirazi-Fard, Y., Anthony, R. A., Kwaczala, A. T., Judex, S., Bloomfield, S. A., & Hogan, H. A. (2013). Previous exposure to simulated microgravity does not exacerbate bone loss during subsequent exposure in the proximal tibia of adult rats. *Bone, 56*(2), 461-473.

Shirazi-Fard, Y., Metzger, C. E., Kwaczala, A. T., Judex, S., Bloomfield, S. A., & Hogan, H. A. (2014). Moderate intensity resistive exercise improves metaphyseal cancellous bone recovery following an initial disuse period, but does not mitigate decrements during a subsequent disuse period in adult rats. *Bone, 66*, 296-305.

Sibonga, J. D. (2013). Spaceflight-induced bone loss: is there an osteoporosis risk? *Current osteoporosis reports, 11*(2), 92-98.

Sibonga, J. D., Evans, H. J., Sung, H., Spector, E., Lang, T., Oganov, V., . . . LeBlanc, A. (2007). Recovery of spaceflight-induced bone loss: bone mineral density after long-duration missions as fitted with an exponential function. *Bone, 41*(6), 973-978.

Siegel, R., DeSantis, C., Virgo, K., Stein, K., Mariotto, A., Smith, T., . . . Fedewa, S. (2012). Cancer treatment and survivorship statistics, 2012. *CA: a cancer journal for clinicians, 62*(4), 220-241.

Simpson, J. (1983). Elemental and isotopic composition of the galactic cosmic rays. *Annual Review of Nuclear and Particle Science, 33*(1), 323-382.

Siu, P. M., Pistilli, E. E., & Alway, S. E. (2005). Apoptotic responses to hindlimb suspension in gastrocnemius muscles from young adult and aged rats. *American Journal of Physiology-Regulatory, Integrative and Comparative Physiology, 289*(4), R1015-R1026.

Smith, B., Lucas, E., Turner, R., Evans, G., Lerner, M., Brackett, D., . . . Arjmandi, B. (2005). Vitamin E provides protection for bone in mature hindlimb unloaded male rats. *Calcified Tissue International, 76*(4), 272-279.

Smith, S. M., Heer, M. A., Shackelford, L. C., Sibonga, J. D., Ploutz-Snyder, L., & Zwart, S. R. (2012). Benefits for bone from resistance exercise and nutrition in long-duration spaceflight: evidence from biochemistry and densitometry. *Journal of Bone and Mineral Research, 27*(9), 1896-1906.

Smith, S. M., Zwart, S. R., Heer, M., Lee, S. M., Baecker, N., Meuche, S., . . . Hargens, A. R. (2008). WISE-2005: supine treadmill exercise within lower body negative pressure and flywheel resistive exercise as a countermeasure to bed rest-induced bone loss in women during 60-day simulated microgravity. *Bone, 42*(3), 572-581.

Spatz, J. M., Wein, M. N., Gooi, J. H., Qu, Y., Garr, J. L., Liu, S., . . . Dedic, C. (2015). The Wnt inhibitor sclerostin is up-regulated by mechanical unloading in osteocytes in vitro. *Journal of Biological Chemistry, 290*(27), 16744-16758.

Taki, K., Wang, B., Nakajima, T., Wu, J., Ono, T., Uehara, Y., . . . Ichinohe, K. (2009). Microarray analysis of differentially expressed genes in the kidneys and testes of mice after long-term irradiation with low-dose-rate γ-rays. *Journal of radiation research, 50*(3), 241-252.

Tanaka III, I., Tanaka, S., Ichinohe, K., Matsushita, S., Matsumoto, T., Otsu, H., . . . Sato, F. (2007). Cause of death and neoplasia in mice continuously exposed to very low dose rates of gamma rays. *Radiation research, 167*(4), 417-437.

Tanaka, K., Kohda, A., Satoh, K., Toyokawa, T., Ichinohe, K., Ohtaki, M., & Oghiso, Y. (2009). Dose-rate effectiveness for unstable-type chromosome aberrations detected in mice after continuous irradiation with low-dose-rate γ rays. *Radiation research, 171*(3), 290-301.

Tanaka, S., Tanaka III, I., Sasagawa, S., Ichinohe, K., Takabatake, T., Matsushita, S., . . . Sato, F. (2003). No lengthening of life span in mice continuously exposed to gamma rays at very low dose rates. *Radiation research, 160*(3), 376-379.

Thames, H. D., Rozell, M. E., Tucker, S. L., Ang, K. K., Fisher, D. R., & Travis, E. L. (1986). Direct analysis of quantal radiation response data. *International journal of radiation biology, 49*(6), 999-1009.

Treuting, P. M., Snyder, J. M., Ikeno, Y., Schofield, P. N., Ward, J. M., & Sundberg, J. P. (2016). The vital role of pathology in improving reproducibility and translational relevance of aging studies in rodents. *Veterinary pathology, 53*(2), 244-249.

Uehara, Y., Ito, Y., Taki, K., Nenoi, M., Ichinohe, K., Nakamura, S., . . . Matsumoto, T. (2010). Gene expression profiles in mouse liver after long-term low-dose-rate irradiation with gamma rays. *Radiation research, 174*(5), 611-617.

Vaughan, J. (1956). The biochemistry and physiology of bone. *by Bourne, GH New York: Academic Press Inc*, 729.

Wade, C. E., Baer, L. A., Wu, X., Silliman, D. T., Walters, T. J., & Wolf, S. E. (2013). Severe burn and disuse in the rat independently adversely impact body composition and adipokines. *Critical Care, 17*(5), R225.

Willems, N. M., Langenbach, G. E., Everts, V., & Zentner, A. (2013). The microstructural and biomechanical development of the condylar bone: a review. *European journal of orthodontics, 36*(4), 479-485.

Willey, J. S., Lloyd, S. A., Nelson, G. A., & Bateman, T. A. (2011). Ionizing radiation and bone loss: space exploration and clinical therapy applications. *Clinical reviews in bone and mineral metabolism, 9*(1), 54-62.

Willey, J. S., Lloyd, S. A., Robbins, M. E., Bourland, J. D., Smith-Sielicki, H., Bowman, L. C., . . . Bateman, T. A. (2008). Early increase in osteoclast number in mice after whole-body irradiation with 2 Gy X rays. *Radiation research, 170*(3), 388-392.

Wright, L. E., Buijs, J. T., Kim, H. S., Coats, L. E., Scheidler, A. M., John, S. K., . . . Sinex, H. J. C. (2015). Single-Limb Irradiation Induces Local and Systemic Bone Loss in a Murine Model. *Journal of Bone and Mineral Research*.

Xu, D., Zhao, X., Li, Y., Ji, Y., Zhang, J., Wang, J., . . . Zhou, G. (2014). The combined effects of X-ray radiation and hindlimb suspension on bone loss. *Journal of radiation research*, rru014.

Yu, K., Doherty, A. H., Genik, P. C., Gookin, S. E., Roteliuk, D. M., Wojda, S. J., . . . Donahue, S. W. (2017). Mimicking the effects of spaceflight on bone: Combined effects of disuse and chronic low-dose rate radiation exposure on bone mass in mice. *Life Sciences in Space Research, 15*, 62-68.

Yuen, E. (2012). Iron overload and radiation exposure cause oxidative damage and reduce bone density. In M. J (Ed.). Journal of Bone and Mineral Research.

Yumoto, K., Globus, R. K., Mojarrab, R., Arakaki, J., Wang, A., Searby, N. D., . . . Limoli, C. L. (2010). Short-term effects of whole-body exposure to 56Fe ions in combination with musculoskeletal disuse on bone cells. *Radiation research, 173*(4), 494-504.

Zerath, E., Holy, X., Roberts, S. G., Andre, C., Renault, S., Hott, M., & Marie, P. J. (2000). Spaceflight inhibits bone formation independent of corticosteroid status in growing rats. *Journal of Bone and Mineral Research, 15*(7), 1310-1320.

APPENDIX A

FIGURES

Examples of Dosimetry Output Information

Participant Number	Name		Dosimeter	Use	Rad. Type	Rad. Quality	Dose Equivalent (mrem) for Periods Shown Below DDE-Deep Dose Equivalent LDE-Lens Dose Equivalent SDE-Shallow Dose Equivalent												Inception Date	Serial Number
	ID Number	Birth Date					Period Shown Below			Quarter to Date			Year to Date			Lifetime to Date				
							DDE	LDE	SDE	DDE	LDE	SDE	DDE	LDE	SDE	DDE	LDE	SDE		
For Monitoring Period:							2016-06-01 to 2016-06-30			QUARTER 2			2016			LIFETIME				
000JF	CONTROL Control Dose Used		Ta Ta	CNTRL			40	40	40											2489636F
06095	AREA 1		Ta	AREA	P		12709	12709	12595	12709	12709	12595	12709	12709	12595	12709	12709	12595	2016/04	2489637F
					P	H	12709	12709	12595											
					N	T	M	M	M											
					N	F	M	M	M											
				NOTE			Dosimeter imaged. Imaging results are inconclusive. Dosimeter reprocessed, second read agrees with reported dose.													
06096	AREA 2		Ta	AREA	P		12158	12250	12250	12158	12250	12250	12158	12250	12250	12158	12250	12250	2016/04	2489638F
					P	H	12158	12250	12250											
					N	T	M	M	M											
					N	F	M	M	M											
				NOTE			Dosimeter imaged. Imaging results are inconclusive. Dosimeter reprocessed, second read agrees with reported dose.													
06097	AREA 3		Ta	AREA	P		12820	12993	12993	12820	12993	12993	12820	12993	12993	12820	12993	12993	2016/04	2489639F
					P	H	12820	12993	12993											
					N	T	M	M	M											
					N	F	M	M	M											
				NOTE			Dosimeter imaged. Imaging results are inconclusive. Dosimeter reprocessed, second read agrees with reported dose.													
06098	AREA 4		Ta	AREA	P		14063	14063	13358	14063	14063	13358	14063	14063	13358	14063	14063	13358	2016/04	2489640F
					P	H	14063	14063	13358											
					N	T	M	M	M											
					N	F	M	M	M											
				NOTE			Dosimeter imaged. Imaging results are inconclusive. Dosimeter reprocessed, second read agrees with reported dose.													

Participant Number	Name		Dosimeter	Use	Rad. Type	Rad. Quality	Dose Equivalent (mrem) for Periods Shown Below DDE-Deep Dose Equivalent LDE-Lens Dose Equivalent SDE-Shallow Dose Equivalent												Inception Date	Serial Number
	ID Number	Birth Date					Period Shown Below			Quarter to Date			Year to Date			Lifetime to Date				
							DDE	LDE	SDE	DDE	LDE	SDE	DDE	LDE	SDE	DDE	LDE	SDE		
For Monitoring Period:							2016-06-01 to 2016-06-30			QUARTER 2			2016			LIFETIME				
06099	AREA 5		Ta	AREA	P		18610	18774	18774	18610	18774	18774	18610	18774	18774	18610	18774	18774	2016/04	2489641F
					P	H	18610	18774	18774											
					N	T	M	M	M											
					N	F	M	M	M											
				NOTE			Dosimeter imaged. Imaging results are inconclusive. Dosimeter reprocessed, second read agrees with reported dose.													
06100	AREA 6		Ta	AREA	P		17154	17172	17172	17154	17172	17172	17154	17172	17172	17154	17172	17172	2016/04	2489642F
					P	H	17154	17172	17172											
					N	T	M	M	M											
					N	F	M	M	M											
				NOTE			Dosimeter imaged. Imaging results are inconclusive. Dosimeter reprocessed, second read agrees with reported dose.													
06101	AREA 7		Ta	AREA	P		17762	17762	17373	17762	17762	17373	17762	17762	17373	17762	17762	17373	2016/04	2489643F
					P	H	17762	17762	17373											
					N	T	M	M	M											
					N	F	M	M	M											
				NOTE			Dosimeter imaged. Imaging results are inconclusive. Dosimeter reprocessed, second read agrees with reported dose.													
06102	AREA 8		Ta	AREA	P		15921	16013	16013	15921	16013	16013	15921	16013	16013	15921	16013	16013	2016/04	2489644F
					P	H	15921	16013	16013											
					N	T	M	M	M											
					N	F	M	M	M											
				NOTE			Dosimeter imaged. Imaging results are inconclusive. Dosimeter reprocessed, second read agrees with reported dose.													
06103	AREA 9		Ta	AREA	P		16000	16000	15904	16000	16000	15904	16000	16000	15904	16000	16000	15904	2016/04	2489645F
					P	H	16000	16000	15904											
					N	T	M	M	M											
					N	F	M	M	M											
				NOTE			Dosimeter imaged. Imaging results are inconclusive. Dosimeter reprocessed, second read agrees with reported dose.													

Appendix Figure 1. Dosimeter outputs are in mrem. There was dosimetry measured at 20 output points around the animal cart. These are then converted to Gy and averaged. Each cohort was found to be within 6% variation of other cohorts.

Participant Number	Name		Dosimeter	Use	Rad. Type	Rad. Quality	Dose Equivalent (mrem) for Periods Shown Below DDE-Deep Dose Equivalent LDE-Lens Dose Equivalent SDE-Shallow Dose Equivalent												Inception Date	Serial Number
	ID Number	Birth Date					Period Shown Below			Quarter to Date			Year to Date			Lifetime to Date				
							DDE	LDE	SDE	DDE	LDE	SDE	DDE	LDE	SDE	DDE	LDE	SDE		
For Monitoring Period:							2016-06-01 to 2016-06-30			QUARTER 2			2016			LIFETIME				
06104	AREA 10		Ta	AREA	P		20577	20577	20419	20577	20577	20419	20577	20577	20419	20577	20577	20419	2016/04	2489646F
					P	H	20577	20577	20419											
					N	T	M	M	M											
					N	F	M	M	M											
				NOTE	Dosimeter imaged. Imaging results are inconclusive. Dosimeter reprocessed, second read agrees with reported dose.															
06105	AREA 11		Ta	AREA	P		17765	17765	17312	17765	17765	17312	17765	17765	17312	17765	17765	17312	2016/04	2489647F
					P	H	17765	17765	17312											
					N	T	M	M	M											
					N	F	M	M	M											
				NOTE	Dosimeter imaged. Imaging results are inconclusive. Dosimeter reprocessed, second read agrees with reported dose.															
06106	AREA 12		Ta	AREA	P		18299	18299	18187	18299	18299	18187	18299	18299	18187	18299	18299	18187	2016/04	2489648F
					P	H	18299	18299	18187											
					N	T	M	M	M											
					N	F	M	M	M											
				NOTE	Dosimeter imaged. Imaging results are inconclusive. Dosimeter reprocessed, second read agrees with reported dose.															
06107	AREA 13		Ta	AREA	P		19161	19206	19206	19161	19206	19206	19161	19206	19206	19161	19206	19206	2016/04	2489649F
					P	H	19161	19206	19206											
					N	T	M	M	M											
					N	F	M	M	M											
				NOTE	Dosimeter imaged. Imaging results are inconclusive. Dosimeter reprocessed, second read agrees with reported dose.															
06108	AREA 14		Ta	AREA	P		19241	19404	19404	19241	19404	19404	19241	19404	19404	19241	19404	19404	2016/04	2489650F
					P	H	19241	19404	19404											
					N	T	M	M	M											
					N	F	M	M	M											
				NOTE	Dosimeter imaged. Imaging results are inconclusive. Dosimeter reprocessed, second read agrees with reported dose.															

Participant Number	Name		Dosimeter	Use	Rad. Type	Rad. Quality	Dose Equivalent (mrem) for Periods Shown Below DDE-Deep Dose Equivalent LDE-Lens Dose Equivalent SDE-Shallow Dose Equivalent												Inception Date	Serial Number
	ID Number	Birth Date					Period Shown Below			Quarter to Date			Year to Date			Lifetime to Date				
							DDE	LDE	SDE	DDE	LDE	SDE	DDE	LDE	SDE	DDE	LDE	SDE		
For Monitoring Period:							2016-06-01 to 2016-06-30			QUARTER 2			2016			LIFETIME				
06109	AREA 15		Ta	AREA	P		18661	18849	18849	18661	18849	18849	18661	18849	18849	18661	18849	18849	2016/04	2489651F
					P	H	18661	18849	18849											
					N	T	M	M	M											
					N	F	M	M	M											
				NOTE	Dosimeter imaged. Imaging results are inconclusive. Dosimeter reprocessed, second read agrees with reported dose.															
06110	AREA 16		Ta	AREA	P		16438	16438	16289	16438	16438	16289	16438	16438	16289	16438	16438	16289	2016/04	2489652F
					P	H	16438	16438	16289											
					N	T	M	M	M											
					N	F	M	M	M											
				NOTE	Dosimeter imaged. Imaging results are inconclusive. Dosimeter reprocessed, second read agrees with reported dose.															
06111	AREA 17		Ta	AREA	P		20845	20845	20390	20845	20845	20390	20845	20845	20390	20845	20845	20390	2016/04	2489653F
					P	H	20845	20845	20390											
					N	T	M	M	M											
					N	F	M	M	M											
				NOTE	Dosimeter imaged. Imaging results are inconclusive. Dosimeter reprocessed, second read agrees with reported dose.															
06112	AREA 18		Ta	AREA	P		16202	16436	16436	16202	16436	16436	16202	16436	16436	16202	16436	16436	2016/04	2489654F
					P	M	16202	16436	16436											
					N	T	M	M	M											
					N	F	M	M	M											
				NOTE	Dosimeter imaged. Imaging results are inconclusive. Dosimeter reprocessed, second read agrees with reported dose.															
06113	AREA 19		Ta	AREA	P		18181	18181	17918	18181	18181	17918	18181	18181	17918	18181	18181	17918	2016/04	2489655F
					P	H	18181	18181	17918											
					N	T	M	M	M											
					N	F	M	M	M											
				NOTE	Dosimeter imaged. Imaging results are inconclusive. Dosimeter reprocessed, second read agrees with reported dose.															

Participant Number	Name		Dosimeter	Use	Rad. Type	Rad. Quality	Dose Equivalent (mrem) for Periods Shown Below DDE-Deep Dose Equivalent LDE-Lens Dose Equivalent SDE-Shallow Dose Equivalent												Inception Date	Serial Number
	ID Number	Birth Date					Period Shown Below			Quarter to Date			Year to Date			Lifetime to Date				
							DDE	LDE	SDE	DDE	LDE	SDE	DDE	LDE	SDE	DDE	LDE	SDE		
For Monitoring Period:							2016-06-01 to 2016-06-30			QUARTER 2			2016			LIFETIME				
06114	AREA 20		Ta	AREA	P		17805	17963	17963	17805	17963	17963	17805	17963	17963	17805	17963	17963	2016/04	2489656F
					P	H	17805	17963	17963											
					N	T	M	M	M											
					N	F	M	M	M											
				NOTE	Dosimeter imaged. Imaging results are inconclusive. Dosimeter reprocessed, second read agrees with reported dose.															

Appendix Figure 1 continued. Dosimeter outputs are in mrem. There was dosimetry measured at 20 output points around the animal cart. These are then converted to Gy and averaged. Each cohort was found to be within 6% variation of other cohorts.